

REPUBLIQUE ALGERIENNE DEMOCRATIQUE ET POPULAIRE

Ministère de l'Enseignement Supérieur et de la Recherche Scientifique



Université Hadj Lakhdar - BATNA 1
Faculté des Sciences de la Matière
Département de Physique



THÈSE

Présentée en vue de l'obtention du
Diplôme de Doctorat

par :

Benaissa Sabrina

Thème :

Combustion du biogaz de décharge dans une turbine à gaz

Domaine : Sciences de la Matière
Filière : Physique
Spécialité : Physique énergétique
Intitulé de la Formation : Physique énergétique appliquée

Soutenue le 30 /01/ 2022

Devant le jury :

Président :	Soudani Azeddine	Professeur	Université de Batna 1
Rapporteur :	Adouane Belkacem	Professeur	Université de Batna 1
Examineurs :	Mameri Abdelbaki	Professeur	Université Larbi Ben M'hidi O.E.B
	Brima Abdelhafid	Professeur	Université de Batna 2
	Aouachria Zeroual	Professeur	Université de Batna 1

Democratic and Popular Republic of Algeria
Ministry of Higher Education and Scientific Research



University El-Hadj Lakhdar - BATNA 1
Faculty of Science of matter
Department of Physics



THESE

Submitted in order to obtain
Doctorate Diploma

by :

Benaissa Sabrina

Theme :

Combustion of landfill gas in a gas turbine

Domain : Science of matter
Sector : Physics
Speciality : Energetic Physics
Title of Training : Applied Energetic Physics

Defended on 30 /01 / 2022

In front of the jury :

Président :	Soudani Azeddine	Professor	University of Batna 1
Supervisor:	Adouane Belkacem	Professor	University of Batna 1
Examiners:	Mameri Abdelbaki	Professor	Université Larbi Ben M'hidi O.E.B
	Brima Abdelhafid	Professor	University of Batna 2
	Aouachria Zeroual	Professor	University of Batna 1

Dedicated to my Family.

ACKNOWLEDGEMENTS

From the bottom of my heart, all thanks are to the Lord for His guidance and support, for granting me the opportunity to accomplish this doctorate.

I sincerely thank my guide and supervisor, **Professor Belkacem Adouane** for his invaluable suggestions and guidance throughout this research. Thank you for being patient and helping me improve. Thank you for the opportunities you provided, and for having faith in me. I'll be eternally grateful to you for everything you've taught me.

I express my sincere thanks to **Pr. Z. Aouachria, Dr. J. Leicher, Dr. A. Mohammad, Dr. S. Mughees Ali, Dr. A. Aeatabani, Pr. A. Mameri, Pr. A. Hadeif, and Dr. S. Rashwan**, for their constant support and the valuable suggestions, they offered me to improve the worth of my work. Technical and non-technical discussions with them always provide me motivations to excel myself in the scientific details in general and in the combustion field in specific.

I gracefully appreciate the juries who attended thesis defense physically which was quite moral boosting during these extraordinary COVID-19 situation. Their critical examination and insightful comments were highly invaluable to make the present thesis more worthy for readers.

I would like to show gratitude to all my friends especially, **A. Sonia, D. Rania** and **A. Habiba** for their encouraging words, thank you for being there by my side every time. You are truly loyal friends, I wish you every success as I wished it to myself, my dear friends. My thanks are also due to the Senior Lab Technician **Mr. Zohir**, for his kind cooperation and support.

Finally, I am grateful to all of *my family members* for their unwavering support and belief in me at every stage of my studies, especially to my **Mom** and **Dad** who were, and continue to be, an inspiration for their ability to grant me prospects and self-belief, including to my beloved **grandma** for her encouragement.

Thank you all. Thank you all.

Benaissa Sabrina

الملخص

الهدف من هذه الأطروحة هو دراسة تأثير مختلف الخصائص الحرارية الفيزيائية لوقود الغاز الحيوي ممزوج بالهيدروجين على خصائص احتراقه. يتم تمثيل الغاز الحيوي النقي بمزيج 60% (حجمي) CH_4 و 40% (حجمي) CO_2 . كمية الهيدروجين المضافة R_H تتغير من حيث الحجم من 0% إلى 50%. تتناول هذه الأطروحة عملين مختلفين مهمين جداً لنفس الخليط، وسيتم تلخيصهما كالتالي:

1- تمت دراسة المجال الحسابي ثلاثي الأبعاد باستخدام نموذج الاحتراق غير المخلوط (الانتشار) بقوة احتراق 60 كيلو وات. تم استخدام نموذج اللهب الرفائقي الثابت (steady laminar flamelet). تم الاعتماد في المحاكاة على نموذج المضطرب القياسي ($k - \epsilon$) الشهير ونموذج الإشعاع (P-1). يتم تحليل تأثير الهيدروجين المضاف ونسبة التكافؤ الاجمالية (ϕ) مع أرقام دوامة مختلفة (SN) على عملية اللهب المستقر وتوزيع درجة الحرارة وانبعاثات أكسيد النيتروجين والتركيزات المولية. لمحاكاة الاحتراق، تم استخدام آلية تفاعل الحركية المفصلة (GRI mech 3.0).

تشير النتائج إلى أن الهيدروجين المضاف، وتغير نسبة التكافؤ، وعدد الدوامات، أثرت بشكل كبير على البنية الكلية للهب. في الواقع، إن الهيدروجين المضاف سيزيد من درجة حرارة اللهب. حيث يؤدي انخفاض نسبة التكافؤ مع ارتفاع أرقام الدوامات إلى تقليلها. ومع ذلك، تم تقليل الحد الأقصى للانبعاثات NO في مخرج غرفة الاحتراق بنسبة 43 و 78 (@ ppm 15% من حجم O_2) لكل من الغاز الحيوي والغاز الحيوي المخصب ب 50% من H_2 ، على التوالي، وذلك بسبب انخفاض في درجة حرارة اللهب. درجة حرارة اللهب وانبعاثات أكسيد النيتروجين عند $\phi = 0.2$ مع معدل مرتفع من الهيدروجين (50% H_2) قريبة من نتائج الغاز الحيوي النقي، (0% H_2)، بنفس نسبة التكافؤ (ϕ). تظهر النتائج أن انبعاثات ثاني أكسيد الكربون واحادي أكسيد الكربون تتناقص مع زيادة معدل الهيدروجين وتقليل نسبة التكافؤ؛ بسبب انخفاض كمية الكربون، وتأثير التبريد الناتج من الهواء الثانوي، وزيادة تركيز الهيدروكسيد.

2- تم استخدام الرموز الشائعة PREMIX ذات البعد الواحد و SENKIN ذات البعد الصفري لتشغيل عمليات المحاكاة العددية باستخدام (GRI mech 3.0). تعتبر الشروط الأولية المستخدمة في هذه الدراسة ذات أهمية عملية وتتعلق بظروف المحرك. تحتوي آلية التفاعل التفصيلية المطورة للميثان، على تفاعلات وبيانات حركية لجميع التركيبات المدروسة. يتم فحص خصائص الاحتراق عند درجات الحرارة العالية بمساعدة الرسومات البيانية لكل من سرعة اللهب ودرجة حرارة اللهب والأنواع تراكيز المولية والحرارة المحررة. بينما تمت دراسة خصائص الأكسدة عند درجات الحرارة المنخفضة بمساعدة تحليل تأخير الاشتعال. تتم مقارنة سرعة اللهب للغاز الحيوي النقي ($R_H = 0.0$) في الظروف المحيطة المحسوبة باستعمال هذه الآلية مع البيانات التجريبية تم الحصول عليها من الأدبيات وتم التحقق من صحتها بنجاح. يتم بعد ذلك توسيع عمليات المحاكاة لتشمل خليط الهيدروجين $R_H = 0.0 - 0.5$ ، من خلال مجموعة من نسب التكافؤ، $\phi = 0.7 - 1.4$ ، ضغط المزيج الغير محترق $P = 0.1 - 7.0$ ميجا باسكال، درجات الحرارة المزيج الغير محترق $T = 300 - 600$ K. تم ربط سرعة اللهب للغاز الحيوي + خليط الهيدروجين مع الهواء بالتغيرات في معدل الهيدروجين، ونسبة التكافؤ، ودرجة حرارة الغاز الغير محترق، وضغط الغاز الغير محترق.

تشير النتائج إلى أن إضافة الهيدروجين إلى الغاز الحيوي يعزز سرعة اللهب وكذلك تأخير الاشتعال. انخفاض سرعة اللهب الرقائقي الناتج عن زيادة ضغط الغاز الغير محترق هو دالة خطية لخليط الهيدروجين مع الغاز الحيوي. بالإضافة إلى ذلك، يتم إجراء الحساسية لتحديد تأثير الهيدروجين المضاف للغاز الحيوي، باستخدام معامل حساسية سرعة اللهب الصفحية، (σ). سيؤدي فهم خصائص الاحتراق لهذه المخاليط إلى الموافقة على قابلية التنفيذ والاستعمال، والخليط المناسب من الغاز الحيوي والهيدروجين، وتعزيز وتحسين التصميم.

الكلمات المفتاحية: مكب النفايات، الغاز الحيوي + وقود الهيدروجين، المحرك التوربين الغازي، نماذج اللهب، الانبعاثات.

Abstract

The objective of the thesis was to study the effects of various thermo-physical properties of biogas fuel blended with hydrogen on its combustion characteristics. The pure biogas is represented with a blend of 60% (volumetric) CH₄ and 40% (volumetric) CO₂. The amount of hydrogen enrichment R_H is varied from 0% to 50% by volume. This thesis deals with two different works that are very important to the same mixture, which we will summarize below:

- 1- Three-dimensional computational domain studied using the non-premixed (Diffusion) combustion model with the combustor power of 60 kW. The steady laminar flamelet model is used. The famous $k-\epsilon$ standard turbulent model, and (P-1) radiation model are adopted in simulation. The effect of hydrogen enrichment and global equivalence ratio (ϕ) with different swirl numbers (SN) on a stable flame operation, temperature distribution, emissions of NO, and species concentrations are analyzed. For combustion simulation, the detailed kinetics reaction mechanism (GRI mech 3.0) is used.

The results indicate, that hydrogen enrichment, the variation of the equivalence ratio, and the swirl numbers, significantly impacted the flame macrostructure. Indeed, hydrogen enrichment will increase the flame temperature. Where the decrease of the equivalence ratio with high swirl numbers will decrease it. However, the NO maximum emissions in the outlet chamber have been dropped by 43 and 78 (ppm @15 % vol. O₂) for the biogas and biogas-50% H₂, respectively, due to the reduction in flame temperature. The flame temperature and NO emissions at $\phi = 0.2$ with a high rate of hydrogen (50% H₂) are close to the results of pure biogas, (0% H₂), at the same equivalence ratio (ϕ). The results display that CO and CO₂ emissions decrease with increasing hydrogen mixing and decreasing the equivalence ratio; due to a decrease in the amount of carbon, the cooling effect of secondary air, and an increase in the OH concentration.

- 2- The common one-dimensional PREMIX and zero-dimensional SENKIN codes are used to run the numerical simulations using the (GRI mech 3.0). The initial conditions used in this study are of practical importance and related to the engine conditions. The detailed reaction mechanism, developed for methane, contains reactions and kinetic data for all the considered compositions. The

high-temperature combustion characteristics are investigated with the help of flame speed, flame temperature, species, and heat release profiles. Whereas low-temperature oxidation characteristics are studied with the help of ignition delay analysis. The flame speed for pure biogas ($R_H = 0.0$) at ambient conditions computed from this mechanism is compared with experimental data from the literature and validated successfully. The simulations are then extended to include hydrogen mixing $R_H = 0.0- 0.5$, through a range of equivalence ratios, $\phi = 0.7 -1.4$, unburned pressures $P = 0.1- 7.0$ MPa, unburned temperatures $T = 300-600$ K. The flame speed of biogas + hydrogen and air mixtures has been correlated for variations in the hydrogen diluent, the equivalence ratio, unburnt gas temperature, and unburned pressures.

The results suggest that adding hydrogen to biogas enhances flame speed as well as ignition delay. The laminar flame speed decreases, caused by an increase in unburned pressure, is a linear function of hydrogen mixing to biogas. In addition, a sensitivity is conducted to quantify the impact of hydrogen supplied to biogas, using the coefficient of sensitivity of laminar flame speed, (σ). The comprehension of the combustion properties of these mixtures will lead to feasibility conformity, appropriate mixtures of biogas and hydrogen, and enhancement of design.

Keywords: Landfill, Biogas + hydrogen Fuel, Gas turbine engine, flame models, Emissions.

Résumé

L'objectif de cette thèse est de comprendre les effets de diverses propriétés thermo-physiques du biogaz carburant mélangé avec l'hydrogène sur ses caractéristiques de combustion. Le biogaz pur est représenté avec un mélange de 60% (volumétrique) de CH_4 et 40% (volumétrique) de CO_2 . La quantité d'enrichissement en hydrogène (R_H) est variée de 0% à 50% en volume. Cette thèse traite deux travaux différents qui sont très importants pour le même mélange que nous résumerons ci-dessous :

1- Un calcul tri-dimensionnel, utilisant le modèle de combustion non-prémélangé avec la puissance de combustion de 60 kW. Le modèle de flammelette laminaire stationnaire est utilisé. Le modèle standard k- ϵ turbulent et le modèle de rayonnement P-1 sont adoptés dans la simulation. L'effet de l'enrichissement en hydrogène et de la richesse du mélange, (ϕ), avec différents nombres de tourbillons "Swirl" (SN) sur la stabilité de la flamme, la distribution de la température, les émissions de NO et les concentrations d'espèces sont analysés. Le mécanisme cinétique de réaction détaillé, (GRI mech 3.0) est utilisé pour la simulation de la combustion.

Les résultats indiquent que l'enrichissement de l'hydrogène, la variation de la richesse, et les nombres de swirl affectent de manière significative la macrostructure de la flamme. En effet, l'enrichissement en hydrogène, augmente la température de la flamme. La diminution de la richesse avec des nombres de swirl élevés la diminuera. Cependant, les émissions maximales (NO) à la sortie de la chambre ont été réduites de 43 ppm corrigées 15 % en volume d' O_2 pour le biogaz et de 78 ppm corrigées 15 % en volume d' O_2 pour le biogaz + 50 % H_2 . Cela est dû à la réduction de la température de la flamme. La température de la flamme et les émissions de NO à $\phi = 0,2$ avec une teneur élevée en hydrogène, (50% H_2), sont proches des résultats du biogaz pur (0% H_2) à la même richesse. Les résultats montrent que les émissions de CO et de CO_2 diminuent avec l'augmentation de l'addition de l'hydrogène et la diminution de la richesse ; en raison d'une diminution de la quantité de carbone, de l'effet de refroidissement et d'une augmentation de la concentration des radicaux OH.

2- Les codes PREMIX unidimensionnel et SENKIN zéro dimension sont utilisés pour exécuter les simulations numériques à l'aide du (GRI mech 3.0). Les conditions initiales utilisées dans cette étude sont d'importance pratique et liées aux conditions du moteur. Le mécanisme réactionnel détaillé, développé pour

le méthane, contient des réactions et des données cinétiques pour toutes les compositions considérées. Les propriétés de combustion à des températures élevées sont vérifiées à l'aide de la vitesse de la flamme, la température de la flamme, les espèces, et les caractéristiques de dégagement de chaleur. Alors que les propriétés de la combustion à basse température ont été étudiées à l'aide d'une analyse du retard d'allumage. La vitesse de flamme pour le biogaz pur ($R_H = 0,0$) aux conditions ambiantes calculée à partir de ce mécanisme est validée par rapport aux données expérimentales de la littérature. Les simulations sont ensuite étendues pour inclure l'ajout d'hydrogène $R_H = 0.0-0.5$ avec une richesse $\phi = 0.7-1.4$, les températures initiales $T = 300-600$ K et les pressions initiales $P = 0.1-7.0$ MPa. La vitesse de flamme des mélanges air biogaz-hydrogène a été corrélée pour les variations en hydrogène, la richesse, la température des gaz imbrûlés et les pressions initiales.

Les résultats indiquent que l'addition d'hydrogène au biogaz augmente la vitesse de la flamme et retarde l'allumage. La quantité de réduction de la vitesse laminaire de la flamme due à l'augmentation de pression initiale est une fonction linéaire de l'addition d'hydrogène au biogaz. De plus, une analyse de sensibilité a été examinée pour mesurer l'effet de l'hydrogène ajouté au biogaz en utilisant le coefficient de sensibilité à la vitesse de flamme laminaire (σ). La compréhension des propriétés de combustion de ces mélanges conduira à la conformité de faisabilité, à des mélanges appropriés de biogaz et d'hydrogène et à l'amélioration de la conception.

TABLE OF CONTENTS

المُلخَص	I
ABSTRACT	III
RESUME	V
TABLE OF CONTENTS.....	VII
LIST OF TABLES	XI
LIST OF FIGURES	XII
NOTATIONS	XV
1 INTRODUCTION	1
1.1 Overview	1
1.2 Objectives	3
1.3 Organization of Thesis	5
2 THEORY AND LITERATURE REVIEW	7
2.1 Introduction.....	7
2.2 Combustion.....	7
2.3 Classification of Flames	8
2.3.1 Non-premixed flame	8
2.3.2 Premixed flame	9
2.4 Laminar Premixed Flame speed.....	10
2.4.1 Laminar flame speed approaches	11
2.5 Laminar Premixed Flame Structure	12
2.6 Laminar flame speed correlations	13
2.7 Combustion Thermodynamics	13
2.7.1 Mixtures Properties	13
2.7.2 Combustion Stoichiometry	15
2.7.3 Heating Values.....	15

2.7.4	Adiabatic Flame temperature.....	16
2.8	Combustion applications	16
2.8.1	Definition of Engine.....	16
2.8.2	Combustor components.....	18
2.8.3	Gas Turbine combustor	20
2.9	Emissions.....	21
2.10	Classification of Fuels	23
2.11	Gaseous fuels	23
2.11.1	Natural Gas	24
2.11.2	Biogas.....	25
2.11.3	Hydrogen	28
2.11.4	Fuel variability in the IC Engines and Gas Turbines	29
2.11.5	Application of biogas in IC engines and GT Engines.....	30
2.11.6	Earlier studies on combustion instability in gas turbine	32
2.12	Motivation.....	33
2.13	Conclusion	35
3	NUMERICAL MODELLING	36
3.1	Introduction.....	36
3.2	Governing equations	36
3.2.1	Continuity equation.....	36
3.2.2	Momentum equation	36
3.2.3	Turbulent kinetic energy (k)	37
3.2.4	Dissipation of kinetic energy (ϵ).....	37
3.2.5	The energy equation.....	37
3.2.6	The radiation flux equation (q_r)	38
3.2.7	Mixture fraction f	38
3.3	Chemical Reaction	38

3.4	Can-Type Combustor Computational Domain	40
3.5	Boundary Conditions and Meshing for Non-Premixed Model.....	41
3.5.1	Studies on Can-Type Combustion with the same modelling Approach	42
3.5.2	Studies using the same modelling approach other than Can-type combustors.....	42
3.5.3	About the model limitations	43
3.6	Boundary conditions, solver details	43
3.7	Grid independence study	45
3.8	Computational method Biogas+hydrogen combustion characteristics	46
3.9	Laminar flame velocity correlations.....	47
3.10	Conclusion.....	50
4	RESULTS AND DISCUSSION.....	51
4.1	Introduction.....	51
4.2	Gas Turbine Computation Validation	51
4.3	Flame temperature contours	54
4.4	Effects of H ₂ enrichment, and equivalence ratio on temperature	58
4.5	Effects of H ₂ addition, and equivalence ratio on NO emissions.....	61
4.6	Effects of H ₂ addition on CO and CO ₂ emissions.....	65
4.7	Effects of the equivalence ratio on CH ₄ , H ₂ , OH, and O ₂	66
4.8	Hydrogen Biogas Combustion Characteristics Computation Data Validation.....	69
4.8.1	Computation Validation of Ignition Delay.....	69
4.8.2	Laminar flame velocity at ambient conditions.....	70
4.9	Ignition delay	72
4.10	Laminar flame velocity at ambient condition	77
4.11	Laminar flame velocity at elevated unburned pressure.....	80
4.12	Laminar flame velocity at the elevated unburned temperature.....	84

4.13	Flame structure of biogas/hydrogen-air mixtures at elevated unburned temperatures	85
4.14	Laminar flame velocity at elevated pressures and temperatures combined ..	90
4.15	Conclusion	91
5	CONCLUSIONS	93
5.1	Summary.....	93
5.2	Scope for Future Work	95
	REFERENCES	96

LIST OF TABLES

Table 1-1: Impact of hydrogen mixings to fuels in internal combustion engines (ICs) and gas turbines (GTs).....	2
Table 2-1 Laminar flame speed at atmospheric conditions for a stoichiometric mixture of different fuels with air	10
Table 2-2 the flammability limits (HFL and UFL) for different fuels at ambient conditions.....	14
Table 2-3 Lower and higher and heating values for different fuels	16
Table 2-4 Fossil Fuel Emission Levels	24
Table 2-5 Composition of natural gas and biogas produced from different sources ..	26
Table 2-6 Wobbe index ranges at normal condition	30
Table 2-7 Use of biogas on internal combustion engines for the spark ignition (SI) .	31
Table 2-8 Biogas applications in compression ignition engine	31
Table 2-9 Application of biogas in gas turbines	32
Table 2-10 Comparison biogas with other common gaseous fuels characteristics.....	34
Table 3-1 Can-type gas turbine operational conditions with fuels compositions at 300K atmospheric pressure	44
Table 3-2 Mesh statistics	46
Table 3-3 Summary of the correlations and their coefficients for biogas+hydrogen blends.....	50
Table 4-1 The detail conditions (fuel, boundary, and operating conditions).....	52
Table 4-2 the operating conditions of Ghenai	53
Table 4-3 NO maximum emissions in the outlet chamber (ppm @15 vol.% O ₂)	63

LIST OF FIGURES

Figure 2-1 Fire triangle.....	7
Figure 2-2 Examples of Combustion for Premixed and Non-Premixed	8
Figure 2-3 Schematic diagram of a one-dimensional planar and an unstretched flame front.	12
Figure 2-4 Classification of heat engines.	17
Figure 2-5 A conventional combustor's main components	18
Figure 2-6 Combustor Zones	19
Figure 2-7 Types of gas turbine combustors: (a) can, (b) annular, and (c) can-annular[63].....	20
Figure 3-1 Three-dimensional can-type computational domain of combustion chamber with the mesh, (a) Combustion chamber details with dimensions, (b) air-fuel inlet, (c) combustor chamber, (d) combustor chamber outlet.....	41
Figure 3-2 Grid independence study for three different mesh sizes along axial direction; (a) mean temperature profile, (b) mean NO emissions, (c) mean CO ₂ mole fraction profile, (d) mean CO mole fraction profile, (e) mean CH ₄ mole fraction profile, (f) mean H ₂ mole fraction profile, and (g) mean H ₂ O mole fraction profile.	46
Figure 4-1 Validation of the static temperature profiles of Natural gas as compared to the work done by Ghenai et al. [136]	52
Figure 4-2 Validation of the static temperature contours of methane as compared to the work done by Ghenai: (a) Present work, (b) Ghenai Data	53
Figure 4-3 A sequence of images describing the biogas flame temperature distributions [K] (above) and NO emissions (below), with different rates of hydrogen concentration by Vol%	55
Figure 4-4 Comparison of flames temperature distributions and NO emissions, with different values of equivalence ratio: $\phi=0.3-0.5$ (CF: conical flame shape), $\phi=0.2$ (VF: "V" shaped flame)	56
Figure 4-5 Flame temperature distributions cross-sections, for 50% H ₂ hydrogen rate.	57
Figure 4-6 Velocity streamlines for 40% H ₂ hydrogen rate, with different values of equivalence ratio: $\phi=0.5-0.2$ and different values of swirl number: 0.74-1.19	58

Figure 4-7 Axials temperature profiles for different hydrogen concentrations (a) $\phi=0.5$, (b) $\phi=0.2$, and (c) at different ϕ s for biogas and 40% H ₂ -Biogas (d) mixture fraction for 40% H ₂ at different ϕ s/ SN	60
Figure 4-8 Maximum static temperature profiles (a) at different ϕ s (b) at different hydrogen concentrations (H ₂ %)	61
Figure 4-9 Axial NO emissions profiles at different hydrogen concentrations (a) $\phi=0.5$, (b) $\phi=0.2$	62
Figure 4-10 Maximum NO emissions profiles at different hydrogen concentrations (a) at different ϕ s (b) at different hydrogen concentrations (H ₂ %) and (c) different (H ₂ %) at Z=0.45m.....	64
Figure 4-11 Axial NO mole fraction profiles (a) NO thermal and (b) NO prompt (c) comparison the reaction of NO thermal	65
Figure 4-12 Axial concentration of CO ₂ and CO profiles (a,b) at different H ₂ %, and $\phi=0.5$ (c,b) at 40 H ₂ % and different ϕ s.....	66
Figure 4-13 Axial mole fractions profiles at different ϕ s, and 40 H ₂ % of (a) CH ₄ mole fraction(b) O ₂ mole fraction (c) OH mole fraction, and (d) H ₂ mole fraction.....	69
Figure 4-14 Comparison of ignition delay prediction with experiments for stoichiometric CH ₄ /CO ₂ -air mixture at unburned pressure of 0.1 MPa. Symbols: experiments; lines: computations	70
Figure 4-15 Laminar flame speed vs equivalence ratio for hydrogen added biogas air mixtures at STP	71
Figure 4-16 Variation of average thermal diffusivity (α_o), ($HRRo$) and α_oHRRo vs equivalence ratio for (a) $R_H = 0$ (b) $R_H = 0.4$	72
Figure 4-17 The biogas+hydrogen ignition delay time at (a) 4 MPa and (b) 7 MPa..	73
Figure 4-18 Comparison of variation in mole fraction of H-radical (X_H) with normalized induction time (t/τ_i) with increase in hydrogen percentage in biogas/hydrogen-air mixture at initial P = 4 MPa and T = 1000 K.....	74
Figure 4-19 Comparison of variation in mole fraction of H-radical (X_H) with normalized induction time (t/τ) with increase in hydrogen percentage in biogas/hydrogen-air mixture at initial P = 4.0 MPa and T = 1800 K.....	75
Figure 4-20 Variation of ignition delay with an increase in hydrogen fraction added to biogas-air mixture at stoichiometric conditions against the unburned pressure (a) T = 1250 K (b) T = 1500 K.....	76

Figure 4-21 Variation of laminar flame velocity (S_u), normalized laminar flame velocity (left axis, filled symbols, and continuous lines), adiabatic flame temperature (T_{ad}) and the normalized flame temperatures (right axis, open symbols, and dash lines) of biogas-air mixtures 78

Figure 4-22 Variation of heat release rate profile (HRR) and thermal diffusivity (α) along with the flame thickness for two equivalence ratios ($\Phi = 1.0$ and 1.2) at $R_H = 0.5$ for ambient conditions ($P = 0.1$ MPa and $T = 300$ K)..... 79

Figure 4-23 The laminar flame velocity with increase in hydrogen fraction added to biogas-air mixtures for various elevated pressures (a) $P = 0.1$ MPa (b) $P = 1.0$ MPa (c) $P = 4.0$ MPa (d) $P = 7.0$ MPa and $T = 300$ K. Symbols: computations; lines: correlations 80

Figure 4-24 The laminar flame velocity of hydrogen added biogas air mixtures for various elevated pressures (a) $R_H = 0.0$ (b) $R_H = 0.4$ at 300 K. Symbols: present computation; lines: present correlation 81

Figure 4-25 Variation of pressure exponent (β) against equivalence ratio for various biogas/hydrogen-air mixtures 82

Figure 4-26 Comparison of sensitivity coefficient (σ) of important reaction pathways for hydrogen added to biogas-air stoichiometric mixtures at $T = 300$ K and (a) $P = 0.1$ MPa (b) $P = 1.0$ MPa, respectively 83

Figure 4-27 The laminar flame velocity of (biogas/hydrogen)air mixtures at elevated temperatures for (a) $R_H = 0.0$ (b) $R_H = 0.4$ at 0.1 MPa. Symbols: computations; lines: correlations..... 84

Figure 4-28 Variation of temperature exponent (α) against equivalence ratio for various biogas/hydrogen-air mixtures 85

Figure 4-29 Heat release rates of biogas/hydrogen-air mixtures against the non-dimensional temperature..... 87

Figure 4-30 Mole fractions of major species against the non-dimensional temperature 88

Figure 4-31 Minor species variation with the non-dimensional temperature..... 89

Figure 4-32 Variation of the laminar flame velocity of biogas/air mixtures at elevated pressure, 4.0 MPa, and fuel temperature, 450 K, for different hydrogen mixings. Symbols: computations; lines: correlations 91

NOTATIONS

		Greek letters
C	linear-anisotropic phase function coefficient	α Temperature exponent
C_i	Species concentration	$\tilde{\alpha}$ absorption coefficient
C_p	specific heat	$\acute{\alpha}$ molar fraction of carbon dioxide
$C_{1\epsilon}, C_{2\epsilon}, C_\mu$	constants in turbulence model equations	β Pressure exponent
D	mass diffusivity of species	β various minimum oxygen requirements of the fuel species
E	total energy	γ mole fraction of the hydrogen
f	mixture fraction	ξ hydrogen mole fraction of products
\tilde{f}	mean mixture fraction	η the medium refractive index
f''	mixture fraction variance	δ delta function
G	the medium refractive index	δ_l Flame thickness
HHV	higher heating value	δ_R Reaction zone thickness
k	turbulent kinetic energy	δ_{PH} Preheat zone thickness
k'	thermal conductivity	ρ density
LHV	lower heating value	ν the kinematic viscosity
m	mass flow rate	μ dynamic viscosity
P	burner power	μ_t the turbulent viscosity
p	pressure	τ stress tensor
P_{rt}	turbulent Prandtl number	ε dissipation of the turbulent kinetic energy
P_k	the production of the turbulence kinetic energy	ϕ global equivalence ratio
Q	volume flows	θ constant of Stefan-Boltzmann($5.67 \times 10^{-8} \text{ W/m}^2\text{-K}^4$)
q_r	radiation flux	σ Sensitivity coefficient

R	outer radius of the annulus	σ_k	the turbulent Prandtl numbers for k
Re	Reynolds number	σ_ε	the turbulent Prandtl numbers for ε .
R_H	hydrogen fraction in the fuel	σ_s	the scattering coefficient
S_G	user-defined radiation source		
S_h	term source includes the heat of chemical reactions, radiation and any other volumetric heat sources.		
SN	Swirl number		
S_u	Laminar flame velocity		
t	Time		
T	Temperature		
T_u	Reference temperature		
u, v, w	velocity magnitude		
WI	Wobbe Index		
Z	the elemental mass fraction for element 'i'		

CHAPTER 1

1 INTRODUCTION

1.1 Overview

Due to increased demand for energy, and the general strategy to reduce fossil fuels consumption (e.g., natural gas, petroleum, coal) [1,2] the alternative fuels found paramount interest. The understanding of combustion, oxidation characteristics, and applicability of these alternative fuels in existing combustion systems such as internal combustion engines (ICEs) and gas turbine engines (GTs) received significant attention worldwide in recent decades. Among these alternative fuels, biogas has been valued as a promising substitute due to its lower processing cost and slightly higher density compared to natural gas. Biogas is a renewable gaseous fuel that will play a pivotal role in protecting the environment [3]. It is a type of biofuel formed from the anaerobic degradation of organic waste. The main compositions of biogas fuel are methane (60%) and carbon dioxide (40%). It is comparable to natural gas, which constitutes methane around 99%. Biogas is easily transportable due to its physical properties, which are similar to those of other conventional resources, fossil fuels such as natural gas (NG) [4]. However, in the initial condition, the biogas has a lower low-calorific-value (LCV) of 17 MJ/kg, as compared to natural gas (50 MJ/kg) and hydrogen (120 MJ/kg) [5]. This is due to the presence of carbon dioxide (CO_2 acting as a diluent) in the biogas compositions. Therefore, the usage of 100% biogas in the burners (CI engines or gas turbines) is limited by the potential flame instabilities, narrow flame flammability range, low-temperature flames, and reduced burning velocity, etc. It is undoubtedly beneficial if the biogas is mixed with hydrogen because hydrogen has some favorable combustible properties such as its strong reactivity, very low ignition delay, high flame speed, and higher combustion density, low-to-no emission, stability [6,7]. It is known that the utilization of 100% hydrogen in IC engines or gas turbines has numerous problems related to safety and storage [8]. To overcome these problems, many researchers suggest adding hydrogen in large quantities to alternative fuels as hydrogen-air mixed with methane [9–16], liquefied petroleum gas [17], n-butane [18], n-decane [19], etc. Several studies investigated experimentally and numerically the impact of hydrogen mixings to fuels in internal combustion engines (ICs) and gas turbines (GTs),

as presented in Table (1-1). According to these studies, the hydrogen in (ICs) and (GTs) has excellent characteristics in combustive properties, such as reducing NO_x emissions and high-velocity engine operation. The hydrogen-thermodynamic features and heat transfer allow operating under the lean mixture conditions enabling higher efficiency and output power.

Table 1-1: Impact of hydrogen mixings to fuels in internal combustion engines (ICs) and gas turbines (GTs)

<i>Year</i>	<i>Authors</i>	<i>Application</i>	<i>Type of study</i>	<i>Findings</i>
2008	C D Rakopoulos et al. [20]	spark ignition (SI) engine	Experimental study	<ul style="list-style-type: none"> - Hydrogen enrichment in biogas can increase the second-law efficiency of engine operation (from 40.85 % to 42.41%) by reducing the combustion-generated irreversibility (from 18.25 % to 17.18 %) - The increases in H₂ addition in biogas led to increased combustion temperatures and decreased combustion duration, thus reducing the combustion irreversibility.
2006	GL Juste et al. [21]	industrial gas turbine combustor	Experimental study	<ul style="list-style-type: none"> - By injecting small amounts of hydrogen-air mixture into the lean primary zone, it is possible to reduce the level of nitrogen oxides (NO_x)
2010	K.K. Gupta et al. [22]			<ul style="list-style-type: none"> - Increasing the primary air in gas turbine combustor is an effective way to reduce NO_x emissions
1997	Noriyuki Kobayashi et al. [23]	gas-turbine system	Experimental study	<ul style="list-style-type: none"> - The effects of swirl number and equivalence ratio in gas turbines have been examined, and the NO_x emission is highly dependent on the swirl number and the equivalence ratio. - Swirl was effective in decreasing nitrogen oxide emissions.
2014	A. Aziz Hairuddin et al. [24]	Diesel compression ignition engines	Review experimental study and Numerical methods	<ul style="list-style-type: none"> - Hydrogen addition becomes a natural choice to improve diesel engine performance and emissions.
2015	Hayder A. Alrazen et al. [25]			<ul style="list-style-type: none"> - Hydrogen addition would affect emissions; as a decrease in non-combustible hydrocarbons, carbon dioxide (CO₂), carbon monoxide (CO), and particulate matter (PM) emissions, there is also an increase in the (NO_x) when enriching H₂. However, it can be controlled by exhaust gas recirculation (EGR) and by controlled injections.

The hydrogen-enriched to hydrocarbon-air mixture enhances combustion intensity, especially by increasing the flammability limits (FL) for lean mixtures, which are the key characteristics of the fuel mixture to use in gas turbines and in the internal

combustion engines. Despite the advantages of using hydrogen as an additive fuel for biogas, there are still some problems and issues not addressed in the literature, which are:

- 1- What is the optimum operability condition for the use of biogas +hydrogen blends in the gas turbine combustion using non-premixed combustion (diffusion combustion)?
- 2- Are biogas +hydrogen blends as fuel suitable to use in this gas turbine combustion?
- 3- What are the advantages and disadvantages of these fuels? Regarding flame stabilization and emissions.

After knowing the answers to these questions, there are other questions to be asked, answered, and discussed:

- 1- What about using these fuels in internal combustion with premixed combustion?
- 2- What is the effect of thermophysical properties of biogas +hydrogen blends on their ignition delay time and flame speed?
- 3- Is it possible to obtain an analytical correlation for biogas /H₂-air regarding flame speed without referring to the repeated use of experiments?

The main objectives related to these questions are explained in detail in the next section (1.2)

1.2 Objectives

The overall objective of this research is to thoroughly investigate the combustion characteristics of biogas fuel blended with hydrogen at various compositions, in the combustor.

The specific objectives are as follows:

NON -Premixed combustion:

- ✚ This study deals with identifying the optimum range of hydrogen and equivalence ratio for a reduction in NO_x emissions for a can-type gas turbine combustor chamber.

- ✚ to evaluate the influence of hydrogen addition and equivalence ratio on temperature and species distributions, flame temperature contours, species, and emissions within gas turbine combustor

Premixed combustion:

- ✚ Development of laminar flame speed analytical correlation data for hydrogen/biogas-air mixture under engine relevant conditions.
- ✚ The explanation of variation in laminar flame speed values with unburned pressure and temperature through temperature and pressure exponent factors (α and β) for lean to rich regimes.
- ✚ Identification of simplified reaction pathway (that is, $\text{OH} + \text{H}_2 = \text{H} + \text{H}_2\text{O}$) which is important only in the cases in which hydrogen is added in the mixture.
- ✚ Identification of third body reaction pathway ($\text{H} + \text{CH}_3 (+\text{M}) = \text{CH}_4 + \text{M}$) leading to a reduction in overall mixture reactivity with the increase in unburned pressure.
- ✚ Quantification of the effects of unburned pressure and unburned temperature on ignition delay timing for hydrogen/biogas-air mixtures.
- ✚ Effect of hydrogen mixing on the flame structure of laminar premixed biogas/hydrogen flames in terms of comparison of heat release rate, major and minor species concentration.

In bringing out these aspects, it is believed that the current study has provided some crucial new information on the combustion characteristics of premixed and non-premixed combustion biogas/hydrogen-air mixtures.

Many different combustion models and reaction mechanisms have been used in the literature. It is observed that the GRI (detailed chemical reaction mechanism: mech 3.0) is a popular choice for biogas+hydrogen combustion and has been widely chosen for the biogas+hydrogen combustion mixture [26–28] successfully in the past. GRI mech 3.0 contains 53 species and 325 reactions. Most importantly, it contains the constituent elements of the interactions of biogas (CH_4 , CO_2), where also, it was included a detailed combustion H_2 mechanism.

1.3 Organization of Thesis

This thesis consists of five parts, the first being the introduction chapter. A summary of the importance of different fuels is given in this chapter (biogas and biogas fuel blended with hydrogen), and the impact of hydrogen mixings to fuels in internal combustion engines (ICs) and gas turbines (GTs). We also touched on the main objectives that were studied and discussed in this thesis.

The second chapter focuses on literary analysis pertinent to the present topic. The review discusses various theoretical, numerical, and experimental investigations on the combustion characteristics of biogas fuel blended with hydrogen at various compositions, as well as how the current study can fill in gaps in the literature.

The third chapter explains the numerical model that was used to simulate the biogas-H₂ combustion characteristic. The numerical domain, computational domain, governing equations, boundary conditions, multi-species and kinetic model, and radiation model used in this study are all described in detail in this chapter. The solution procedure is also described in this chapter. Finally, a systematic presentation of the development of laminar flame speed analytical correlation data for hydrogen/biogas-air mixtures under engine-related conditions is presented.

The fourth chapter discusses the results of the biogas-H₂ air combustion mixture. First, numerical investigations are performed to study the combustion characteristics of biogas fuel blended with hydrogen at various compositions under non-premixed swirling flame mode in a can-type gas turbine combustor. A numerical approach using the non-premixed combustion model, turbulent standard ($k-\epsilon$) model, and P-1 radiation model is adopted and simulated with the combustor power of 60 kW. The steady laminar flamelet model is used to analyze the effect of hydrogen enrichment and global equivalence ratio with different swirl numbers on a stable flame operation, temperature distribution and contours, velocity streamlines contours, emissions of NO, and species concentrations. Second, computational research on the combustion characteristics of biogas+hydrogen blends under several thermo-physical conditions relevant for real combustion applications. The numerical simulations were conducted using 0-D SENKIN, and 1-D PREMIX programs, while the GRI Mech 3.0 was used to model chemical kinetics. Both the high and the low-temperature combustion characteristics were studied for pure and hydrogen blended biogas-air mixtures. The low-temperature

oxidation characteristics were studied using ignition delay analysis. While, the high-temperature oxidation characteristics were studied using flame temperature (T_{ad}), laminar flame velocity (S_u), heat release rate, and species concentrations (C_i) profiles.

A general summary of the numerical work performed in this analysis is presented in the fifth and final chapter, where the most important findings of this research are presented. A brief presentation of the scope for prospective research work in this area follows.

CHAPTER 2

2 THEORY AND LITERATURE REVIEW

2.1 Introduction

This chapter provides a summary of the research studies relating to combustion, flame, fuel, and the effect of enriched hydrogen on hydrocarbon-air mixtures, as well as biogas mixtures and their effect on improving combustion characteristics. The motivations are also covered, with the main objectives of this work being mentioned.

2.2 Combustion

Combustion is one of the most established and widely used thermochemical technologies. It is a scientific term for burning. The combustion is an essential process in most people's daily life. For example, when you drive a car, use a gas stove, or create a pleasant atmosphere by burning a candle. Additionally, most power is generated by fossil fuel burning. It is an important process in the industry, especially in mineral production [29–31]. Combustion can be described as the rapid oxidation of a fuel that produces heat and light [32]. In other words, combustion is the process of converting the energy contained in the fuel's chemical bonds into heat. Combustion occurs when three basic elements are present: fuel, oxidizing agent (oxygen), and heat, and thus a flame (fire) is generated.



Figure 2-1 Fire triangle

This flame can be defined as a thin combustion zone, in which an intensive chemical reaction propagates via an unburned fuel- air mixture. This thin reaction zone or combustion zone releases the heat at that zone, which causes the surrounding gas to rise

in temperature and pressure. The combustion can happen in both flame (visible: like stove flames) or non-flame (invisible: like the combustion of the hydrogen) mode.

2.3 Classification of Flames

Fuel and oxidizer (air or oxygen) are mixed and burned, resulting in a flame. Generally, there are two fundamental types of flame:

- Premixed flame or premixed combustion
- Non-premixed flame or non-premixed combustion, and it's called also diffusion flame or diffusion combustion.
- Each of these types is further subdivided depending on whether the fluid flow is laminar or turbulent [32,33]. This is illustrated in figure 2-2.

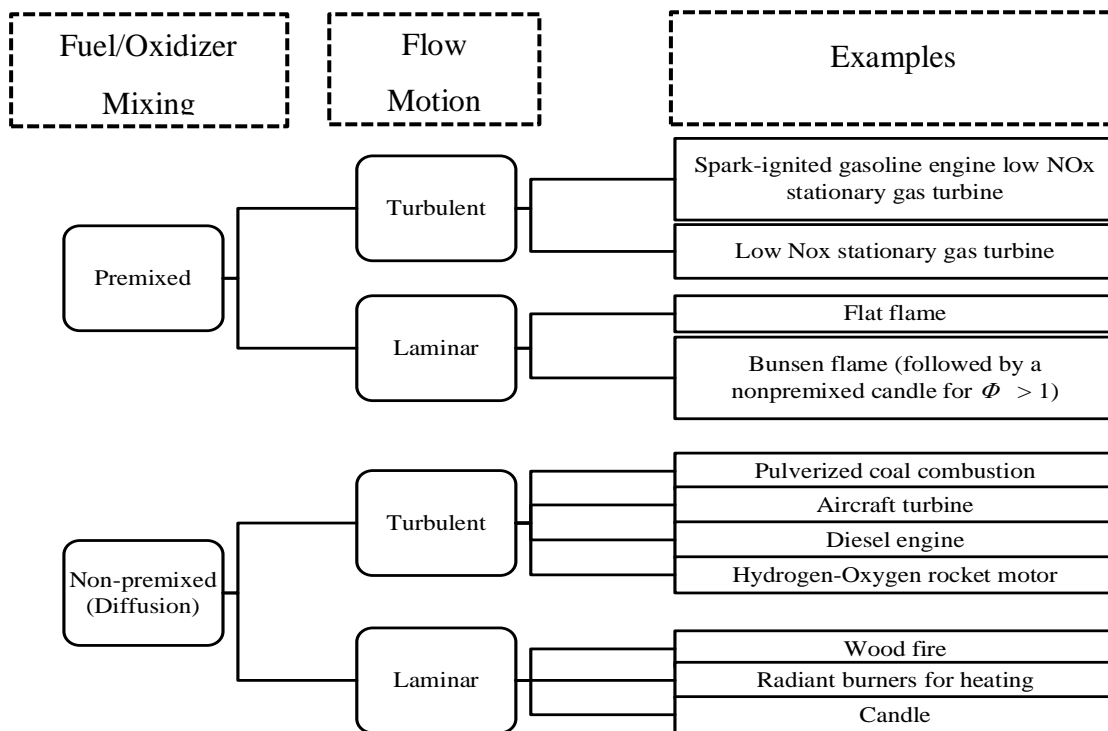


Figure 2-2 Examples of Combustion for Premixed and Non-Premixed

2.3.1 Non-premixed flame

Reactants are added separately in the reaction zone in non-premixed flames (also known as diffusion flames) since fuel and oxidizer are transported into the reaction zone mainly by diffusion. The maximum temperature of burnt gases is determined by the temperature of fuel and oxidizer burning in stoichiometric proportions and is difficult to control [34].

- Steady Laminar Flamelet Model

The steady laminar flamelet models (SLFM) principle is based on the premise that a turbulent flow's flame can be considered as an ensemble of small laminar diffusion flames known as flamelets. These flamelets are obtained through experiments or calculations. In simple configurations, they are expected to have the same structure like laminar flames [35].

2.3.2 Premixed flame

In the premixed combustion process, the reactants (fuel/oxidizer) are assumed to be thoroughly mixed before entering the reaction zone. Premixed flames propagate towards the fresh gases by diffusion, the heat released by the reaction preheats the reactants until the reaction starts, it can refer that the reaction rates increase exponentially with temperature. For the determination of laminar flame speed, flames considered will be limited to laminar premixed flames.

Fully premixed flames and partially-premixed flames are the two types of premixed flames, as mentioned below:

2.3.2.1 Fully Premixed flame

In this type of flame, the reactants (fuel and oxidizer) are completely mixed before reaching the reaction zone, also this flame is identified as the flame front. The location of the reaction zone inside the flames is not defined by the diffusion of reactants. However, they occur as a result of the balancing of the local convective velocity of the reactants with the rate of consumption of the reactants, also recognized as the flame speed. Also as a note, lower flame temperatures are achievable in this type of flame.

2.3.2.2 Partially-Premixed Flame

The premixed and non-premixed flame regimes mentioned previously are idealized situations. Fuel and oxidizers cannot be completely premixed in real-world applications. In certain cases, incomplete premixing is created on purpose to save fuel or reduce pollutant emissions. For example in spark-ignited internal combustion engines, the fuel injection is tuned to create a quasi-stoichiometric mixture near the spark to promote ignition, but a lean mixture in the rest of the cylinder to promote combustion. Fuel and oxidizer should meet in non-premixed flames to burn and maintain flame stability, resulting in partially premixed zones. The so-called triple flame, which happens when reactants are partially premixed before the flame [34].

2.4 Laminar Premixed Flame speed

The laminar flame speed (S_u) is traditionally defined as the velocity that a laminar, steady, one-dimensional, stretch/free, adiabatic flame, and planar flame front travels to the unburned gas in a direction normal to the flame surface, which is a physicochemical property of a premixed, flammable mixture due to the combined effect of three mixtures, reactivity, diffusivity, and exothermicity [30,36]. For combustion models, such as engine simulations and the validation of chemical kinetic mechanisms, an understanding of flame speed is required. It provides a measure of the overall reactivity of fuel-air mixtures, which aids in determining heat release rates and validating reaction mechanisms and kinetic models. The laminar flame speed (LFS) of the fuel-air mixtures is related directly to overall mixture reactivity and flame thickness[36]. Flame stabilization, flame blowout, flame flashback, and flame extinction are all examples of combustion phenomena that can be described using laminar flame speed [37,38]. Laminar flame speed is used in combustion systems like industrial furnaces, internal combustion engines (ICEs), gas turbine combustors (GTCs), and rocket engines (REs) [39–41]. Laminar flame speed or laminar burning velocity depends only on the fuel, oxidizer, and transport properties such as thermal conductivity, viscosity, and molecular diffusivity. Table 2-1 shows a list of the laminar flame speed at the atmospheric conditions ($T= 300\text{k}$ and $P= 1\text{atm}$) for a stoichiometric mixture of different fuels [42]. It can be seen that the speeds range from (35 to 43 cm/sec) for most fuels, except for hydrogen, which is about 5 times larger than the other fuels.

Table 2-1 Laminar flame speed at atmospheric conditions for a stoichiometric mixture of different fuels with air

<i>Fuel</i>	<i>Formula</i>	<i>Flame speed [cm/sec]</i>
Methane	CH ₄	40
Hydrogen	H ₂	213
Ethane	C ₂ H ₆	42
Propane	C ₃ H ₈	40
n-butane	n-C ₄ H ₁₀	41
n-pentane	n-C ₅ H ₁₂	38
n-heptane	n-C ₇ H ₁₆	37
Iso-octane	iso-C ₈ H ₁₈	35
Methanol	CH ₃ OH	43
Ethanol	C ₂ H ₅ OH	40
DME	CH ₃ OCH ₃	43

2.4.1 Laminar flame speed approaches

In the literature, laminar flame speed is also referred to as flame speed, burning velocity, adiabatic burning velocity, or burning velocity. Laminar flame velocity has been a topic of interest to many academics. Some researchers studied the subject theoretically, while others attempted to understand physics through a variety of experimental approaches. In this section, emphasis will be placed on the theoretical approaches. Theoretically, there are three approaches to laminar flame speed:

➤ Thermal theory

Mallard and Le Chatelier [38] were the first to investigate the problem of determining a mixture's laminar flame speed. They divided the premixed flame into two zones. Reaction zone where the reaction occurs and a preheat zone where these high temperatures products transfer heat to the unburnt mixture. It simply means the hot products from the reaction zone transfer heat to unburnt gas by diffusion such that unburnt reactants reach an ignition temperature where they ignite and burn. In the reaction zone, after self-ignition, the chemical enthalpy is converted to sensible enthalpy.

➤ Comprehensive Theory

Zeldovich *et al.*[38] improved the classical thermal theory using the two different zones approach. In this case, they considered the effects of both molecular and thermal diffusions at the same time.

➤ Diffusion Theory

Tanford *et al.*[43] proposed the diffusion theory. They proposed that active radical like (hydrogen, oxygen...etc) diffusion regulates the combustion process and, as a result, hence laminar flame speed.

These three theoretical approaches highlight the relationship between laminar flame speed, and various variables such as thermal conductivity, diffusivity, reaction rate... etc.

❖ Factors influencing laminar flame speed

The factors affecting the laminar flame speed are the equivalence ratio, fuel/air mixture composition, temperature and pressure.

2.5 Laminar Premixed Flame Structure

The knowledge of the flame front structure of the laminar premixed flame helps to know the definition of laminar flame speed. Once the problem of "flammability" and the "ignition" is solved, the flame appears. A flame can be thought of as a propagating combustion wave through a flammable mixture. The laminar flame and its flame thickness is described as (δ_L), in which the fuel and oxidizer are premixed, is the most basic for the premixed model. Fristrom and Westernberg [28] researched the composition of the flame in great detail, claiming that it is divided into four sections: unburned, preheat, reaction, and burned gas, as shown in figure 2-3. At first, a fresh unburned mixture is delivered to the flame zone in ambient conditions. The preheat zone is the region where the mixture gets its temperature rise mainly by thermal conduction and a slight rate of convection getting from the reaction zone (note that the radiative heat transfer in this zone is negligible) with its flame thickness (δ_{PH}). The reaction zone is the region zone where combustion reactions occur with its flame thickness (δ_R); once the ignition temperature (T_i) is reached, each element of gas begins a chemical reaction, producing more heat until the equilibrium temperature (T_f) or often called the burned gas temperature (T_b) is reached. The gases that emerge from this region join the burned gas zone, where their temperature and concentration are maintained [44].

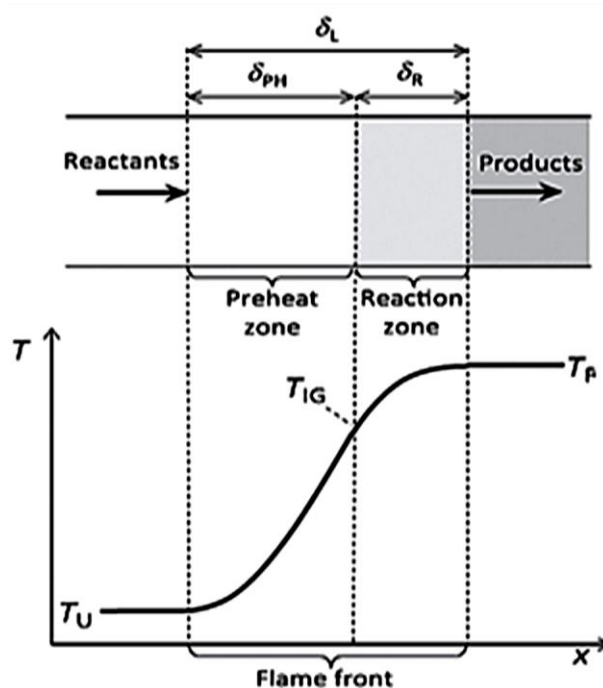


Figure 2-3 Schematic diagram of a one-dimensional planar and an unstretched flame front.

The flame thickness is also related to the laminar flame speed. The following relationship combines the laminar flame speed (S_u) and flame thickness(δ) is obtained [36]:

$$S_u = \left(\frac{\lambda}{\delta_{PH}} \right) = \left(\frac{\lambda}{\delta_R} \right) = \left(2 \frac{\lambda}{\delta_L} \right) \quad (2-1)$$

With λ is the thermal diffusivity.

2.6 Laminar flame speed correlations

Laminar flame speed depends on four basic elements: equivalence ratio (ϕ), unburned temperature (T), unburned pressure (P) of the fuel-air mixture, and dilution concentrations. Through the study of the relations between these important elements, it can reach co-relations that allow finding results without resorting to empirical studies every time. Metghalchi and Keck [45] suggested the most common correlation between equivalence ratio, unburned temperature, and pressure, it represented in the equation below:

$$S_u = S_{u0}(\phi) \left(\frac{T}{T_u} \right)^\alpha \left(\frac{P}{P_u} \right)^\beta \quad (2-2)$$

Where S_{u0} is the laminar flame speed parameter which is determined at reference conditions of temperature (T_u) and pressure (P_u), and it is in terms of equivalence ratios(ϕ). both power exponent coefficients (α and β) are dependent on the equivalence ratios and they were determined from the laminar flame speed. More details have added in the next chapter (section 3.11)

2.7 Combustion Thermodynamics

2.7.1 Mixtures Properties

Thermodynamic properties are represented in terms of the mass or the moles [46]. In terms of the thermal properties of a pure substance, enthalpy, internal energy, and specific heat are determined. The combustion system is composed of several gases, which is the consequence of a combination of the characteristics of all of the constituent gases as the thermodynamic properties of a mixture. The ideal gas law will be adopted for gaseous mixtures so that the ideal gas relation can be introduced to each component of gas. The mass-weighted average of species properties is used to calculate the mixture's fluid viscosities from Sutherland's law, the specific heat (C_p)/enthalpy(h)/

entropy(s) from NASA polynomials, and thermal conductivity (k) from kinetic theory. Thus, Sutherland's model, NASA piecewise polynomials, and kinetic theory relations are used to calculate these properties for each species [47].

➤ Flammability limits of the mixture

A flammable mixture is one in which the fuel is mixed with a sufficient amount of oxygen and ignited at a specific temperature. There are two types of flammability limits [48]:

- a. Upper flammability limit (UFL): When the fuel density inflammable mixture is too high.
- b. Lower flammability limit (LFL): When the fuel density is insufficient to produce a spark.

The table 2-2 shows an overview of the flammability limits (UFL and LFL) for different fuels at ambient conditions, which may vary slightly depending on the source due to the lack of test devices and standard conditions[48–50].

Table 2-2 the flammability limits (UFL and LFL) for different fuels at ambient conditions

<i>Fuel</i>	<i>UFL [VOL. %]</i>	<i>LFL [VOL. %]</i>
<i>Petrol</i>	7.6	1.4
<i>Natural Gas</i>	≈ 13.5	≈ 4.8
<i>CH₄</i>	15.0 - 16.0	4.8 – 5.0
<i>C₂H₆</i>	11.2 – 12.5	2.2 — 3.0
<i>C₃H₈</i>	9.5 — 10.0	2.1
<i>n-C₄H₁₀</i>	8.5	1.5
<i>n-C₅H₁₂</i>	7.8	1.4
<i>n-C₆H₁₄</i>	7.0	1.25
<i>n-C₇H₁₆</i>	6.0	1.0
<i>n-C₈H₁₈</i>	3.2	0.95
<i>H₂</i>	74.5 – 76.0	4.0 – 6.5
<i>CO</i>	70.0 — 75.0	12.5 — 15.0

The ignitability of an air-fuel mixture is primarily defined through its autoignition temperature and the minimum ignition energy

➤ Minimum Ignition Energy (E_{min})

The minimum ignition energy is the least amount of energy required to heat a small volume of mixture to start to ignite the system [33,51].

➤ Autoignition Temperature (AIT)

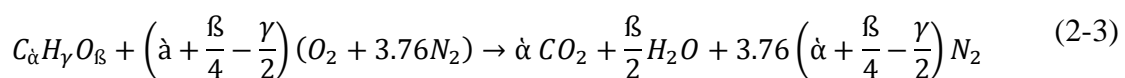
The autoignition temperature is commonly defined as the lowest temperature at which a given mixture must be heated in order to spontaneously combust in the absence of an ignition source [52].

➤ Ignition Delay Time

The time between fuel injection into the combustion chamber and the start of ignition is identified as ignition delay [53,54]. The start of fuel injection is typically described as the moment the injector needle lifts off, while the start of combustion is more difficult to pinpoint. The combustion start can be identified by a sudden shift in the cylinder pressure gradient, light emission, the temperature increases due to the combustion. Ignition delay has a direct effect on the heat release rate, as well as an indirect effect on exhaust gas emissions and engine noise [55].

2.7.2 Combustion Stoichiometry

The stoichiometric air (or it is called theoretical air) is the minimum amount of air required for the complete combustion of a fuel. For example: If all of the carbon (C) in the fuel is converted to CO₂, all of the hydrogen (H) is converted to H₂O, and all of the sulphur (if any) is converted to SO₂, the combustion process is complete. Thus, a complete combustion process in which the fuel is completely burned with stoichiometric air. This process is called theoretical (or stoichiometric) combustion. The stoichiometric equation for combustion of a general hydrocarbon fuel with air can be expressed as [48]:



Where α , β , and γ are the number of carbons, hydrogen, and oxygen atoms in the hydrocarbon or hydrocarbon mixture.

2.7.3 Heating Values

Heating Value (also known as the heat of combustion, and calorific value) of a fuel (MJ/kg) is defined as the maximum quantity of heat that is generated by the combustion of fuel-air at standard conditions (T= 298 k or 25°C and, P= 101.3kPa). The amount of heat released during fuel combustion depends on the water phase of the products. If the water in the gas phase is found in the products, then the value of the total heat release is called the lower (Net) heating value [LHV]. For water in the condensed form,

additional heat energy (which is equal to the latent heat of vaporization) is extracted. Then the total energy release is called higher (Gross or upper) heating value [HHV] [46]. Table 2-3 shows the lower/higher heating value for different fuels. The highest heating value (HHV or LHV) is hydrogen, compared to other fuels, hydrogen is the highest among the hydrocarbon fuels.

Table 2-3 Lower and higher and heating values for different fuels

<i>Fuels</i>	<i>State at ambient conditions (temperature and pressure)</i>	<i>HHV (MJ/kg)</i>	<i>LHV (MJ/kg)</i>
<i>Hydrogen</i>	Gas	141.9	119.9
<i>Methane</i>	Gas	55.5	50
<i>Ethane</i>	Gas	51.9	47.8
<i>Gasoline</i>	Liquid	47.5	44.5
<i>Diesel</i>	Liquid	44.8	42.5
<i>Methanol</i>	Liquid	20	18.1

2.7.4 Adiabatic Flame temperature

The adiabatic flame temperature (adiabatic combustion) [T_{ad}] occurs when the combustion chamber is isolated (no heat loss in the surrounding areas), the temperature of the products reaches a maximum [46,56]. It is worth noting that when complete combustion happens with the theoretical amount of air (at stoichiometric), the adiabatic flame temperature reaches its maximum value. As a result, the adiabatic flame temperature is a critical factor in the design of combustion chambers, burners, engines, nozzles, gas turbines. The maximum temperature can be adjusted by adjusting the amount of excess air used as a coolant.

2.8 Combustion applications

Combustion is applied in our daily life in several devices, including:

- Burners: Stoves, Furnaces, Boilers, Gasifier, etc.
- IC engine: Petrol and diesel engines
- Gas turbine combustor: Power plant steam turbine, air-craft gas turbine combustor, etc.

In this section, it will focus on IC engines and Gas turbine combustor, where some studies have been applied to them.

2.8.1 Definition of Engine

An engine is a device that converts one type of energy into another. However, when converting energy into another form, the conversion efficiency is critical. Because most

engines convert thermal energy into mechanical work, they are referred to as 'heat engines'. A heat engine is a device that converts a fuel's chemical energy into thermal energy and then uses that thermal energy to do useful work. therefore, thermal energy is thus transferred to mechanical energy in a 'heat engine'[57]. There are two types of heat engines, which are depicted in Figure 2-4 along with the devices that power them.

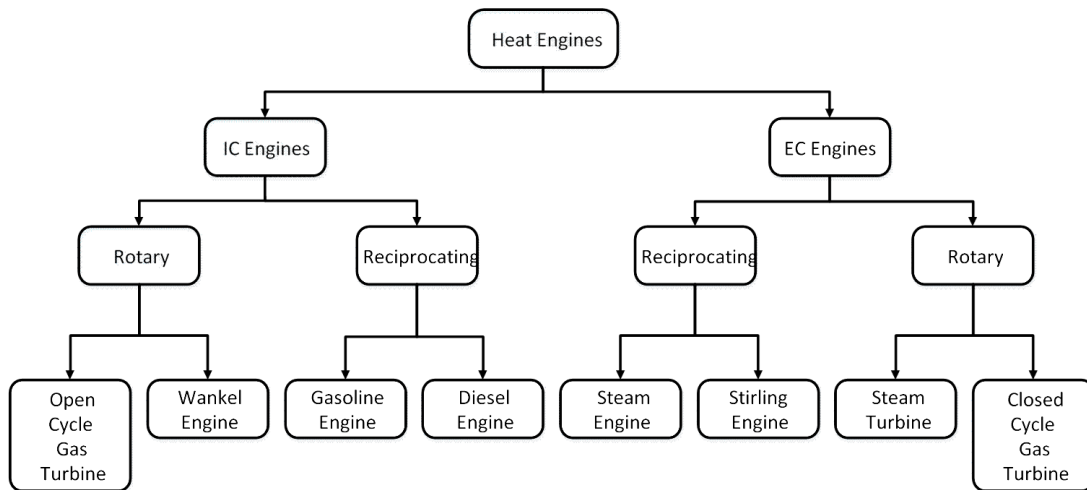


Figure 2-4 Classification of heat engines.

- *External Combustion Engines*

External combustion engines (ECEs) are those in which combustion occurs outside of the engine. The term "external combustion engine" refers to any engine that receives heat from a source other than the fluid that powers the engine. For example, A boiling water reactor would use a flame (heat) to convert water into steam. The resulting steam moves the turbines, which, in turn, generates power.

- *Internal Combustion Engines*

Internal combustion engines (ICEs) and 'jet engines' are machines that convert combustion heat into kinetic energy or mechanical. ICEs are classified into two types: spark-ignition (SI) engines and compression-ignition (CI) engines, which correspond to gasoline and diesel engines, respectively. SI engines (Petrol engines) are commonly used to power passenger cars and motorcycles. CI engines (Diesel engines), on the other hand, are primarily used in ships, trucks, and off-road vehicles, etc..., due to their greater energy efficiency and power density when compared to gasoline engines[58].

- *Gas turbines*

The gas turbine (GT) is similar to the internal combustion engine in that it is not typically a "heat engine"[59]. The gas turbine, also called a combustion turbine, is a power plant that, despite its size and weight, produces a large amount of energy. Gas turbines are now available that run on different fuels, including natural gas, pure methane, biomass gases (biogas or syngas), diesel fuel, low Btu gases, raw gases, evaporated fuel oils[60].

2.8.2 Combustor components

The combustion chamber consists of many components [61], which are the case, diffuser, liner, snout, dome/swirler, fuel injector, igniter, and combustion zones, they have been described in figure 2-5.

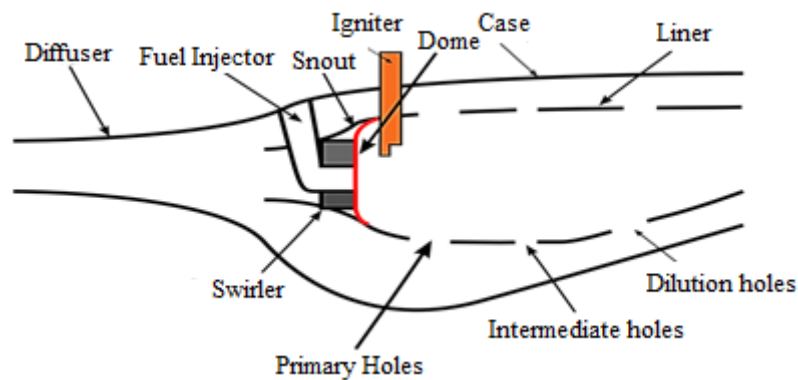


Figure 2-5 A conventional combustor's main components

- Swirler

Airflow in the primary zone is critical for flame stabilization in the combustion chamber. In order to stabilize the flame, all combustors create a toroidal flow reversal to recirculate hot combustion products into the entering of the mixtures of air and fuel. Introducing swirlers is one of the most important ways of generating recirculation. Swirler performance is determined by the parameter swirl number (SN).

The swirl number (SN) is a dimensionless parameter; the ratio of the tangential momentum flux over the axial momentum flux. It is used to study the effect of the airflow swirling inlet on the flame combustion characteristics[62]:

$$SN = \frac{G_{tg}}{R G_{ax}} = \frac{\int_0^R \rho u w r^2 dr}{R \int_0^R \rho u^2} r dr \quad (2-4)$$

Where G_{tg} is the axial flux of the tangential momentum, and G_{ax} is the axial flux of the axial momentum, R is the outer radius of the annulus, u , and w are the axial and tangential velocity at the radial position r .

➤ Combustor Zones

The classic combustion device has a very high ratio of air to fuel. At such air-to-fuel ratios, it is clear that no fossil fuel can initiate or sustain combustion. This requires the combustor to be divided into zones, which results in stable combustion. In general, a combustor is divided into three major zones.

- Primary zone: this is an area in which only a few airs are drawn (usually 15-20 percent of the total combustor flow)[51]. The swirler circulates the air, which is thoroughly mixed with the fully atomized fuel before being ignited.
- Intermediate zone: Combustion may be rich or incomplete in the primary zone at times. Furthermore, the temperature in the initial zone can sometimes reach the stoichiometric flame temperature of the fuel. This entails employing an area (Intermediate zone) in the liner that draws in sufficient air to complete combustion and partially reduces temperatures, where low emissions are desirable.
- A dilution zone: This is a region in which the temperature of the combustion products is reduced and mixing of the resulting gases to establish a temperature that supports the integrity of the turbine blades.

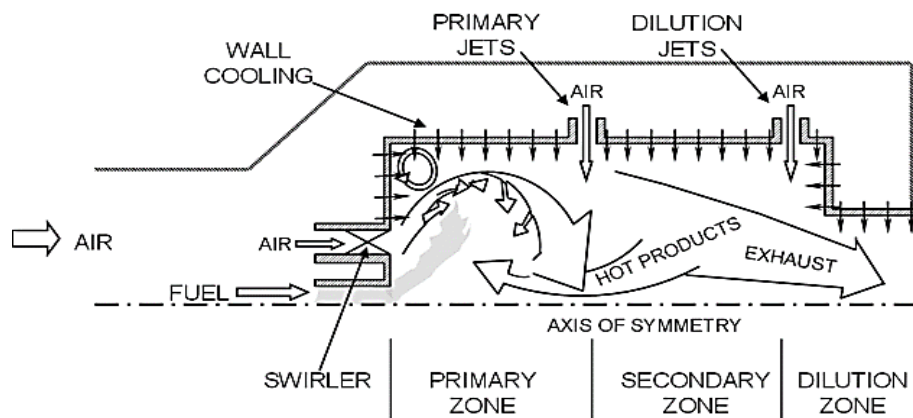


Figure 2-6 Combustor Zones

2.8.3 Gas Turbine combustor

A combustion chamber is a component of an internal combustion engine where fuel and compressed air are combined and burned before being used, to drive the turbine with the high-temperature exhaust gas. In a gas turbine, the combustion chamber has named a combustor. There are three types of combustor: can-type, annular-type, and can-annular type, which are briefly listed below.

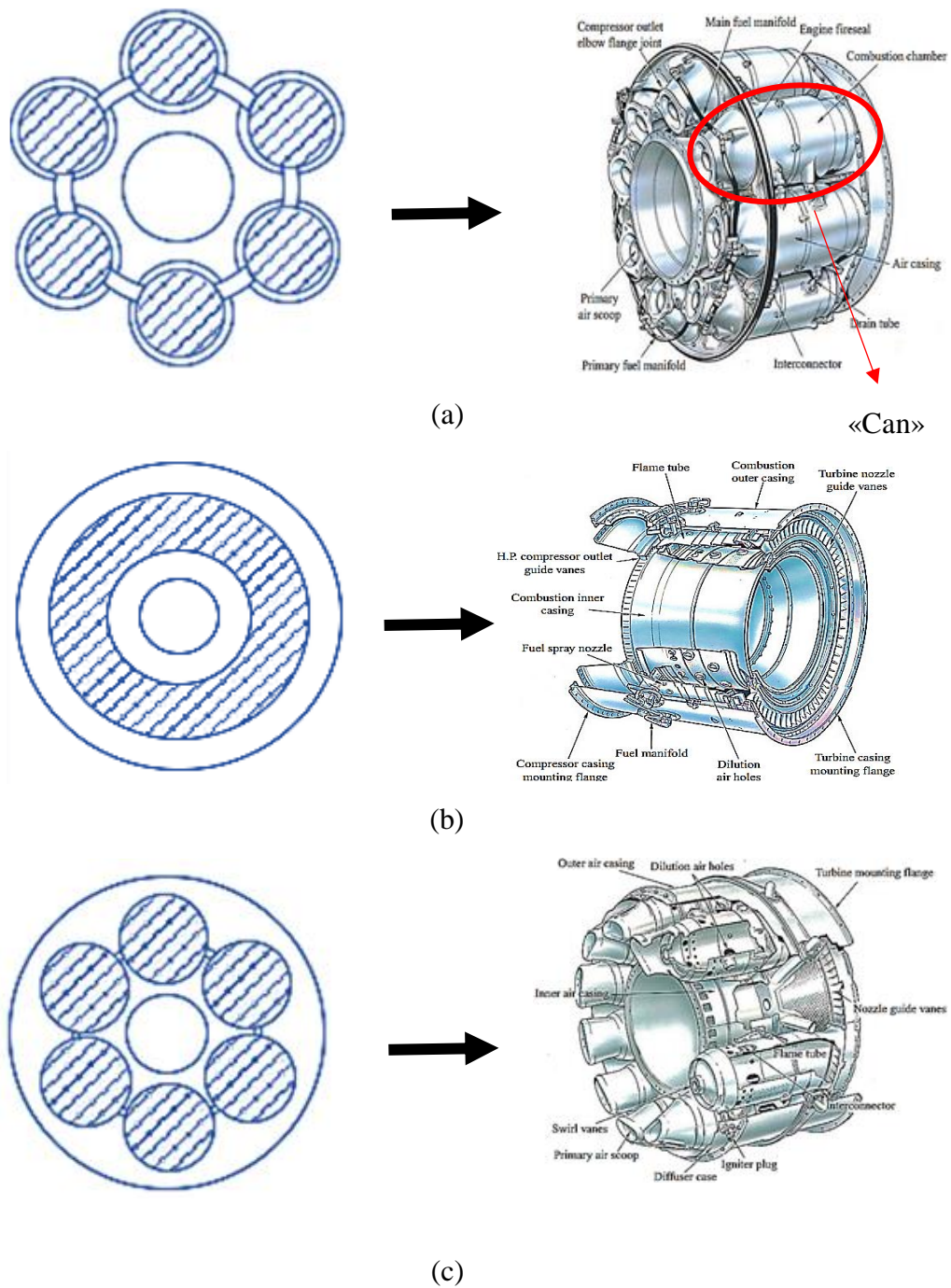


Figure 2-7 Types of gas turbine combustors: (a) can, (b) annular, and (c) can-annular[63]

- Can type: The earliest type, consisting of individual cans. Fuel injectors, liners, interconnectors, and casing are all unique to each “can.” A can-type combustor is depicted in Fig. 3-1(a) [63].
- Annular type: As shown in Fig. 3-1(b), this is a modern combustor. Annular combustors are characterized by different combustion areas, a continuous liner, and a ring-shaped casing (the annulus). Annular designs allow for more effective combustion, with nearly all of the fuel being consumed [63].
- Can-annular type: This is a hybrid of the two types above, with discrete combustion zones enclosed in separate liners with their fuel injectors and a common air casing shared by all combustion zones. The combustion efficiency of can-annular designs is lower, but their modular nature makes them easy to repair or replace. Figure 3-1(c) depicts a combustor of the can-annular type [63].

2.9 Emissions

One of the main factors of the study designs of modern engines and gas turbines is to reduce emissions. In general, there are five main types of emissions: unburned hydrocarbons (UHC), carbon dioxide (CO₂), carbon monoxide (CO), nitrogen oxides (NO_x), and smoke/soot.

▪ Unburned Hydrocarbons

Unburned hydrocarbons produced from fuel unburned resulting from incomplete combustion caused by local extinction. Flame extinction occurs when the flame front reacts with cold tube walls or when there are gaps in the combustor or when the temperature is low, reaction time becomes larger than mixing time, putting the flame front under strain.

▪ Carbon Dioxide and Carbon Monoxide

Carbon monoxide (CO) is a key component in the oxidation of hydrocarbons. Fuel will be broken down into CO during the combustion process before being oxidized into carbon dioxide (CO₂). The carbon monoxide, on the other hand, oxidizes slowly. Carbon dioxide is a harmful pollutant that occurs in the global warming process. nearly stoichiometric mixtures, and due to the high combustion temperatures, carbon dioxide is separated and thus a large amount of carbon monoxide is formed. As a result, CO

concentrations can drop fast as a function of temperature as long as the carbon dioxide has enough time to oxidize and create carbon dioxide[64].

- Oxides of Nitrogen

This is a pollutant that contributes to the removal of ozone from the stratosphere, resulting in an increase in ultraviolet (UV) radiation on the earth's surface. Nitrogen oxides (NO_x) are composed of NO, N₂O and NO₂. Most combustion chambers produce the amount of NO more than NO₂ because NO₂ is formed from NO in non-premixed combustion systems' low-temperature mixing regions. NO is produced by four primary mechanisms: Thermal NO_x (ie, Zeldovich), nonthermal mechanisms or Prompt NO_x, Fuel NO_x, and nitrous oxides [33].

- a. Thermal NO_x: it typically has a high concentration, at temperatures higher than 1750 K. This type has three formation reactions:



Thermal NO_x, also known as Zeldovich NO_x, is formed when high temperatures dissociate N₂, O₂ and reform them as NO. Thermal NO formation is thermochemically preferred at high temperatures of combustion products. The term "thermal" is used because the first reaction, which is the rate-limiting step in NO formation, has very high activation energy because of the strong triple bond in the nitrogen (N₂) molecule.

- b. Prompt NO_x: a nonthermal mechanism, this conversion takes place at low temperatures (lower than 1800 K) and high pressures, long before thermal NO has formed, and usually ahead of the flame front.

This mechanism is important in fuel-rich conditions and is formed in relatively low temperatures « about 1000 K ».

- c. Fuel NO_x: This kind of mechanism is linked to the presence of N₂ in fuels.

Generally, gaseous fuels such as natural gas, are devoid of nitrogen associated with the fuel, it is frequently present in liquid and solid fuels.

- d. Nitrous oxides (N_2O): N_2O is important in high pressure and high-temperature conditions. This mechanism is activated when (O atoms) attack molecular nitrogen(N_2).

When a third N molecule is present, the process produces N_2O , which interacts with O atoms to make NO. N_2O emissions are insignificant, but they can act as a mediator to NO_x emissions.

2.10 Classification of Fuels

Combustion processes and distribution methods, based on the state of matter of fuel, making the fuel phase at standard conditions a rational basis for classification.

- a) Solid Fuel: Most solid fuel consists of volatile matter, moisture, ash, and fixed carbon. The ultimate analysis of solid fuels defines the relative amounts of these constituents on a mass basis. The final analysis may be assumed on a dry basis. Examples: wood, coal, biomass.... Hydrocarbon solid fuel: $C_aH_bO_g$ with ($a > b$)
- b) Liquid Fuel: Most liquid fuels are blends of various hydrocarbons. Liquid fuel is commonly treated as a single hydrocarbon with a basic common formula C_xH_y but it can be a mixture of different hydrocarbons. Examples include gasoline, oil, diesel, etc. Liquid hydrocarbon fuels: $C_aH_bO_g$ with ($a < b$)
- c) Gaseous Fuel: a mixture of gaseous. Example: LPG gas, Biogas, Syngas, CNG gas, etc.

2.11 Gaseous fuels

As mentioned in the combustion part, gas/liquid fuels, mix easily with air and can be used more in internal combustion engines (ICEs) or gas turbines (GTs) even though there can be a slight loss in the power output when transported. Fuels are commonly classified as standard or non-standard, i.e. conventional or alternative fuels. Natural gas, petroleum products, and coal are examples of conventional fuels. Historically, alternative fuels were defined as any other hydrocarbon that could be used as a fuel. Biofuels (biodiesel, ethanol, methanol), biogas, hydrogen, and biomass sources are just a few examples of well-known alternative fuels. For a variety of reasons, there has been a great deal of interest in the use of alternative fuels. Discovering a domestic source of fuels is a security thing and economics for several countries that are reliant on foreign sources of energy. Another important reason is that some of these alternative fuels can

help reduce emissions and in the short and long term. Biogas and hydrogen are two prominent alternative fuels that may play a significant role in the future energy mix. In response to the growing interest in hydrogen, many original equipment manufacturers (OEMs) have recently proposed solutions for its use in gas turbines. The following parts provide a brief overview of the fuels discussed in this study.

2.11.1 Natural Gas

Natural gas, also known as (fossil gas) is a natural hydrocarbon gas mixture primarily composed of methane. Methane is a highly flammable gas that burns easily and almost completely. It produces very little emissions in the atmosphere. Natural gas is non-corrosive and non-toxic, has a high ignition temperature, and a narrow flammability range, making it an intrinsically safe fossil fuel as opposed to other fuel sources[65]. Natural gas is the next alternative, and it already meets roughly 23.8% of the primary energy consumption in the world, and 25% in Organisation for Economic Co-operation and Development (OECD) member countries. To be considered as an energy source, natural gas must be compared to other fossil fuel sources such as petroleum and coal. This comparison must be based on the level of emissions from these sources; typical values are shown in Table 2-4.

Table 2-4 Fossil Fuel Emission Levels

Pollutants	Coal	Oil	Natural Gas
<i>Carbon dioxide</i>	208,000	164,000	117,000
<i>Carbon monoxide</i>	208	33	40
<i>Sulfur dioxide</i>	2591	1122	1
<i>Nitrogen oxide</i>	457	448	92
<i>Particulates</i>	2744	84	7
<i>Mercury</i>	0.016	0.007	0.000

However, it also emits a significant amount of carbon dioxide, which contributes to global warming, as well as nitrogen oxides, which cause acid rain and smog, much like other carbon-based fossil fuels. Therefore, another percentage of fuel is added to the hydrogen to improve the mixture and reduce emissions. Natural gas has long been the preferred fuel in gas turbine combustors, and this energy conversion technology processes greatly improves this fuel and its combustion properties.

2.11.2 Biogas

Biogas is precious renewable energy, an alternative to global energy requirements and at the same time a reduction of emissions of waste and greenhouse gases (GHGs) and a secondary supplier of biodegradable organic materials for energy usage [66]. Biogas is a gas that is formed when organic matter is biologically broken down without oxygen. Biogas is a form of biofuel that comes from biological materials. Biogas is generated by fermentation or anaerobic digestion of biomass, sewage, manure, municipal waste, vegetable material, Green waste, energy plants, and other biodegradable substances. The major components of this form of biogas are methane and carbon dioxide [67]. Biogas is a low-cost fuel that can be utilized for any heating purpose, including cooking, in any region. It can also be utilized in modern waste management facilities to control any kind of heat engine, which can produce mechanical or electrical power[66].

2.11.2.1 Biogas production

Biogas is generated via anaerobic digestion, waste methanation, landfills, industrial composting, and biomass gasification (thermos-chemicals production), anaerobic co-digestion of animal farm manure, digestion facilities for the agro-food sector under thermophilic (55 °C) as well as in mesophilic (35 °C). Biogas that are rich in methane (CH₄), with greater heating values ranging from 15 to 30 MJ/Nm³ were created by this activity [68,69].

2.11.2.2 Biogas composition

The content of biogas varies according to the type of feedstock and the operating conditions of the digester. Generally, biogas is composed of (50–75 percent) CH₄ and (25–50 percent) CO₂, as well as other trace elements such as water vapor (H₂O), nitrogen (N₂), oxygen (O₂), ammonia (NH₃), hydrogen sulfide (H₂S), methyl siloxanes, halogenated volatile organic compounds (VOCs), carbon monoxide (CO), and hydrocarbons [70,71]. The principal components of biogas are methane, and carbon dioxide. Biogas composition varies due to differences in biodegradable compounds and their amounts present in organic wastes as landfill, agricultural waste, sewage sludge, and industrial wastes/wastewaters. Biogas pollutants cause corrosion and failure of process equipment and pipeline systems, as well as have negative health and environmental consequences[72]. Furthermore, the presence of such impurities will reduce the final CH₄ content of biogas, decreasing its calorific value when burned. As

a result, for both economic and environmental reasons, biogas must be cleaned up or even upgraded. Bio-methane (CH₄-rich biogas) of high quality can be obtained after biogas upgrading and used as a natural gas substitute [73]. Typical natural gas (GN) compositions, biogas, and the negative effect of biogas pollutants can be found in Table 2-5.

Table 2-5 Composition of natural gas and biogas produced from different sources

<i>Compounds</i>	<i>Natural gas</i>	<i>Biogas source</i>			<i>The negative effect of biogas contaminants</i>
		<i>Landfill gas</i>	<i>Anaerobic digestion at WWTP</i>	<i>Agricultural wastes</i>	
CH ₄ (%)	85-92	35-65	60-70	55-75	
CO ₂ (%)	0.2-1.5	25-40	30-40	35-40	• Decrease in heating value
H ₂ S (ppmv)	1-6	20-500	0-34000	30-7200	• Odor • Corrosion in equipment and gas transportation systems • Immediate hazard to human health at concentrations >100 ppmv • SO _x emission during combustion
NH ₃ (ppmv)	-	<5	<100	70-150	• NO _x emission during combustion
N ₂ and O ₂ (%)	<0.5	15	0-8	1-2	• Decrease in heating value
Siloxanes (mg m ⁻³)	-	7-24	n.a.	n.a.	• Corrosion of equipment and gas transportation systems

Only methane (CH₄) contributes to the calorific value of biogas. As an example, at standard temperature and pressure, 1 m³ of raw biogas including 60% CH₄ has a calorific value of 21.5 MJ/m³ (5.97 kWh electricity equivalent), compared to pure CH₄ at standard temperature and pressure 35.8 MJ/m³ (9.94 kWh electricity equivalent)[66]. CO₂ is a refractory gas that affects biogas density and heat values, although it is not corrosive or poisonous as a sulfide of hydrogen. The latter is harmful and hazardous to the environment and corrosive to the metal components of compressors, pumps,

engines, gas storage tanks, and valves, as well as reducing the equipment's lifetime [74,75]. Contaminants in biogas must be removed before they can be used. The biogas treatment consists of two primary steps: purification (removal of dangerous and toxic substances such as H₂S, NH₃, N₂, Si, O₂, H, CO, and VOC) and improvement (adjusting the carbon dioxide content, to increase the calorific value of the biogas to an optimum level). The ultimate product is biomethane, mainly made up of CH₄ (95%–99%) and CO₂ (1%–5%) [76]. A number of biogas upgrading technologies have emerged in recent years, with the main distinction being the nature of the process.

2.11.2.3 Biogas applications

Biogas has three primary applications:

- Electricity generation
- Vehicle fuel
- Production of heat and steam

Biogas can be also used in a variety of applications, including [77,78]:

- Internal Combustion Engine
- Gas Turbine Engine (Large)
- Microturbine Engine (Small)
- Stirling Heat Engine
- Boiler (Steam) Systems
- Hot Water Systems
- Process Heaters (Furnaces)
- Space or Air Heaters
- Gas Fired Chiller
- Absorption Chiller
- Combined Heat and Power (CHP)
- Fuel Cells

2.11.2.4 Advantages of biogas

- ✚ Renewable energy source.
- ✚ Less pollution: Biogas is considered to be a less polluting fuel. It also helps to reduce deforestation and any kind of indoor air pollution.
- ✚ Reduces landfills.

- ✚ Use of cheaper technology: the technology utilized to produce biogas is improving, so the applications of biogas are also increasing. Biogas can be utilized for heating as well as for electricity production.
- ✚ Gaining a large number of jobs.
- ✚ Capital investment is minimal: setting up a biogas plant requires little capital investment and is easy when built on a small scale. The waste material produced by livestock on farms can be used to produce biogas on the farm, allowing farmers to become self-sufficient.
- ✚ Reduces Greenhouse Effect: Biogas is produced by using gases produced by landfills and thus the greenhouse effect is reduced. It is used as a form of energy. It uses simple technology and recycles the majority of biodegradable or organic wastes, so biogas has become an important resource [79].

2.11.2.5 Disadvantages of biogas

- ✚ Little Technological Advancement: Because very few technological advancements have been made or introduced to streamline and make the process cost-effective systems that are currently in use are inefficient. Most of the investors are not ready to put their capital investment in biogas production, although the investments could be a potential solution to the problems being faced.
- ✚ It consists of impurities: Despite going through numerous refining processes, biogas contains several impurities. If this impurity-laden biogas is used as a fuel after being compressed, the metals in an engine may begin to corrode.
- ✚ Biogas is not appealing on a large scale: Biogas is not economically viable on a large scale. Improving the efficiency of biogas systems is also very challenging[79].

2.11.3 Hydrogen

Hydrogen is the simplest and most abundant element on earth. Hydrogen easily combines with other chemical elements, and is always present as part of another substance, like hydrocarbon, water, or alcohol. Hydrogen can also be found in natural biomass, which includes animals and plants. As a result, it is regarded as an energy carrier rather than an energy source [80]. Hydrogen has many appealing characteristics as a clean energy carrier for electricity and heat, including a large storage capacity,

renewable production, high energy conversion, cleanliness and environmental friendliness, zero emissions, vast specific energy, a wide range of sources, reliability, and ease of storage and regeneration [81,82]. As a result, it is regarded as the cleanest and most promising energy source of the twenty-first century. Because hydrogen does not exist as a molecule in nature, it is created through the conversion of certain hydrogen-containing sources of materials such as carbohydrates or water. Hydrogen must be produced using other primary energy sources. Approximately, half (50%) of the hydrogen (H₂) produced worldwide, comes from natural gas (NG), mainly from steam methane (CH₄) reforming; the rest comes from oil (30%), the majority of which is used in hydro-processing applications in petroleum refineries; coal (19%), primarily for the manufacture of ammonia (NH₃); and the remaining (4%) comes from water electrolysis. Unfortunately, the majority of traditional technologies for producing hydrogen from fossil fuels are associated with significant environmental pollution and high-energy consumption. As a result, greater emphasis has been placed on the application of new technologies to produce hydrogen from nuclear and renewable sources, with increasingly stringent and relevant environmental protection regulations in place around the world. These techniques include electrolysis of water, biomass gasification, thermonuclear, and chemical methods.

2.11.4 Fuel variability in the IC Engines and Gas Turbines

Biogas, hydrogen, and biogas+hydrogen blends utilization in IC engines and gas turbines is cutting-edge and dependable technology. The important factor to consider in the usage of fuels in the engines is the Wobbe index, which is the most important criterion for gas exchangeability. Similar Wobbe indices imply that fuel may be exchanged for a given pressure and valve settings with similar power supplies. Wobbe index (WI) is a standard indicator of the fuel characteristics and interchangeability in the engines, counting both power facilities and original equipment manufacturers (OEMs). It was developed to describe the natural gas (NG) with different compositions [83].

$$WI = \frac{HHV_{fuel,Vol}}{\sqrt{\frac{\rho_{fuel}}{\rho_{air}}}} \quad MWI = \frac{LHV_{fuel,Vol}}{\sqrt{T_{gas} \frac{\rho_{fuel}}{\rho_{air}}}} \quad (2-8)$$

WI is presented as the fuel higher heating value (HHV) divided by the ratio of fuel density to air density. The Modified Wobbe Index (MWI) contains the lower heating

value (LHV) and the fuel temperature. There are several kinds of Wobbe index (WI) that are well described in the literature [83]. Table 2-6 presents Wobbe index values for biogas-H₂ mixture and other pure fuels, such as the pure hydrogen and syngas CO and CH₄ [84]. It can be seen that hydrogen has a similar Wobbe index as methane. In this case, the low density of hydrogen compensates for the lower volumetric heating value to maintain a similar WI.

Table 2-6 Wobbe index ranges at normal condition

<i>Fuel Category</i>	<i>Wobbe Index Range (MJ/Nm³)</i>
<i>Biogas-H₂ mixture</i>	24.67-25.79
<i>Biogas (90%CH₄-10%CO₂)</i>	44.41
<i>Biogas (60%CH₄-40%CO₂)</i>	24.64
<i>Syngas Type</i>	24-29
<i>Natural gas Type</i>	48-53
<i>LPG Type</i>	72-87
<i>Methane</i>	47-53
<i>Hydrogen</i>	40-48

2.11.5 Application of biogas in IC engines and GT Engines

For the biogas, in its purer form (containing more than 95 percent methane), has calorific values comparable to natural gas and it is suitable for use in all existing natural gas applications [85]. The performances of enriched biogas and natural gas at constant velocity IC engines have been compared. In terms of thermal efficiency, fuel economy, specific gas volume, brake power output, and emissions, the experiments reported comparable engine performance [70,86]. The biogas, as indicated in Tables (2-7), (2-8), and (2-9), is a high-octane fuel readily available in the SI, CI, and GTs engines


 *In the spark ignition engines:*

Table 2-7 presents some examples of the use of biogas in spark ignition (SI) internal combustion engines.

Table 2-7 Use of biogas on internal combustion engines for the spark ignition (SI)

<i>Authors</i>	<i>Fuel</i>	<i>Application</i>	<i>Findings</i>
<i>Whiston et al.</i> [87]	Biogas	spark- ignition engine	It is shown that the rate of turbulent combustion is lowered when concentrations of CO ₂ are increased.
<i>Anand et al.</i> [88]			They discovered that increased biogas CO ₂ concentration reduces NO _x emissions greatly, and the large proportion of CO ₂ volume can assist prevent engine knock.
<i>Papagiannakis et al.</i> [89]			They discovered that adjusting the compression ratio and ignition timing can boost efficiency. On the other side, increasing the compression ratio will increase NO emissions, especially under conditions of lean-burning.
<i>Chen et al.</i> [90]	They discovered that increasing the hydrogen concentration improves flame speed propagation and increases the heat release rate.		
<i>Park et al.</i> [91–93]	Biogas+hydrogen		The addition of H ₂ to the mixture can enhance combustion stability. The low-temperature range can also be expanded by hydrogen and HC emissions are lower and NO _x emissions increased. Furthermore, as hydrogen increased, the heat transfer loss increased, lowering thermal efficiency. - Hydrogen has been shown to enhance the stability of biogas combustion, although the high adiabatic flame temperature can produce more NO _x emissions.

✚ In the compression ignition engines:

Biogas is a high octane fuel that is hard to burn with a homogeneous engine. The combustion model is considered clean and effective for homogeneous charge compression ignition.

Table 2-8 Biogas applications in compression ignition engines

<i>Authors</i>	<i>Fuel</i>	<i>Application</i>	<i>Findings</i>
<i>Sudheesh et al.</i> [94]	Diethyl ether-Biogas	Homogeneous charge compression ignition (HCCI)	By adding diethyl ether, they could create stable HCCI combustion. The HCCI model powered by diethyl ether-biogas emits less smoke, NO, and HC, but produces higher CO.
<i>Nathan et al.</i> [95]	Biogas-diesel		They discovered that NO emissions are lowered in biogas/diesel HCCI mode while smoke emissions remain extremely low. The inert gas (CO ₂) in biogas reduces the burn rate of HCCI in HCCI combustion mode, thereby allowing the inhibition of knock.
<i>Mustafi et al.</i> [96]	Biogas-diesel	Dual fuel compression ignition combustion	The biogas/diesel dual fuel option dramatically reduced emissions of NO _x . This could be due to the high CO ₂ level of the biogas.
<i>Lounici et al.</i> [97]			They discovered that in dual fuel combustion mode, particle emissions are considerably decreased at high loads (biogas comprising 70% methane).

✚ In the gas turbine engines:

At comparable scales, turbines or micro-turbines are predicted to be marginally more efficient than IC engines. A range of fuels, including natural gas, methane, kerosene, propane, diesel, and biogas, can operate in micro-turbines.

Table 2-9 Application of biogas in gas turbines

<i>Authors</i>	<i>Fuel</i>	<i>Application</i>	<i>Findings</i>
<i>M.G.Rasul et al. [98]</i>	Biogas	Micro Gas Turbine	They discovered that in distant rural areas, small-scale micro turbine generation utilizing biogas can substitute diesel generators.
<i>Chia-Chi Chang et al. [99]</i>			This study reveals encouraging results with the use of biogas in a micro-gas generator, as well as a considerable reduction in greenhouse gas emissions, demonstrating the circular economy and environmental preservation ideas.
<i>Prasad Kaparaju et al. [100]</i>	Biogas	Gas Turbine and fuel cell	They discovered that the micro gas turbine and fuel cell offer significantly reduced NO _x and CO emissions, as well as decreased maintenance costs.

2.11.6 Earlier studies on combustion instability in gas turbine

Production of biogas can be operated on micro or industrial scales. Research studies have presented several important criteria that influence combustion instability characteristics in gas turbines, for example, the swirl number [101], equivalence ratio, combustion design, and fuel compositions. Jalalatian et al. [102] performed experiments on the effect of the Swirl Number, equivalence ratio, and Reynolds numbers on diffusion flame structure and emissions. They demonstrated that when the overall equivalence ratio (the global equivalence ratio) increases, there is an enhances in the flame length, an increase in swirl number leads to a slight decrease in temperature, CO concentrations, and NO thermal concentrations. Kotb and Saad [103] have predicted the effect of equivalence ratio on the flame stability and CO concentration. As a result, the swirl burner displays a lower CO concentration than the co-flow burner. Yılmaz [104] Conducted research on the Swirl Number effect on natural gas diffusion flames combustion properties and has been validated and compared with a simulation using a standard k-epsilon model. He proved that the swirl number has a strong effect on combustion characteristics like the flame temperature, the gas CH₄, CO₂, O₂, and H₂O concentrations.

2.12 Motivation

The following summary can be derived from the above-mentioned literature review. Biogas consists of CH_4 , and CO_2 with lower concentrations of nitrogen, oxygen, and volatile organic compounds. Biogas is a low-calorie fuel. Because of the high concentration of diluted carbon dioxide, which varies between 20% and 60% depending on the source of the biogas [92,105,106], its main composition varies according to the origin or the conditions of the digestive process [107]. Although carbon dioxide present in biogas can reduce emissions of pollutants, these studies have confirmed its negative effects on fuel characteristics [108–111]. Because carbon dioxide has limited flame stability, lower burning velocity, and lower flame temperature, the biogas combustion properties are inferior to natural gas (NG) [112–114]. This is because carbon dioxide is a diluent in the combustion chamber, which absorbs energy from the combustion, lowers gas temperatures, and affects the flame speed of the biogas + air mixture. The second major problem with biogas applied in industrial burners is its poor stability. Several researchers have mentioned the deleterious effect of dilute CO_2 on flame stability [114–116]. Many efforts are devoted to understanding the stability behavior of biogas [117,118]. The lower heating value, combined with the chemical and thermal properties of carbon dioxide, can restrict the use of biogas in practical combustion facilities. The problem of potential instability and low flame temperature, therefore, limits the application of pure biogas to industrial burners, because the biogas has a narrow scaling range and lower combustion velocity in nature [119].

In the table below 2-10, the main features of biogas are compared to other typical gaseous combustible fuels [120]. The table findings show that biogas, with its high amount of carbon dioxide, have an extremely low energy density based on volumes, a very low flame speed, and not very broad inflammability limitations.

Biogas burning velocity is only 25cm/s, compared to 275cm/s for hydrogen. In addition, when compared to other hydrocarbons (HC) fuels, biogas also demands a relatively low quantity of air for burning by unit mass of fuel, compared to other hydrocarbons (HC) fuels. Biogas has a high temperature of self-ignition and resists auto-ignition. Because of the presence of CO_2 , the combustion of the fuel is poor, the correct air-to-fuel ratio and the spark timing are crucial to maintaining. The relatively poor features of its fuel can be strengthened by mixing it with other high-quality fuels like hydrogen to improve the use of biogas. Research efforts were devoted to flame stabilization by adding

hydrogen. Table 2-10 illustrates some of the most recent research findings, which include higher reaction rates, higher flame temperature, and lower carbon monoxide emissions for biogas and hydrogen mixtures compared to raw biogas.

Table 2-10 Comparison biogas with other common gaseous fuels characteristics

<i>Characteristics</i>	<i>LPG</i>	<i>Natural Gas</i>	<i>Hydrogen</i>	<i>Biogas</i>	<i>Producer gas</i>
Fuel composition by volume (%)	30 C ₃ H ₈ 70C ₄ H ₁₀	85 CH ₄ 07 C ₂ H ₆ 02 C ₃ H ₈ 05 CO ₂ 01 N ₂	100 H ₂	60 CH ₄ 30 CO ₂ 0.18CO 0.18 H ₂	2.2 CH ₄ 9.3 CO ₂ 22.6 H ₂ 24.3 CO 41.2 N ₂
LHV (MJ/kg) at P= 1 atm, and T= 15 °C	45.7	50.1	120	17	3500–6000 KJ/m ³
The density at the same conditions	2.26	0.79	0.08	1.2	1.05
Borning velocity (cm/s)	38.25	34	275	25	20–30 (Should be a single number)
<i>Fuel/air stoichiometric (kg of air/ kg of fuel)</i>	15.5	17.3	34.2	11.6 Nm ³ air/ Nm ³ gas	1.2 0.95–1.3 Nm ³ air/ Nm ³ gas
<i>The flammability limits (rate of volume in the air)</i>					
The leaner mixture	2.15	5	4	7.5	7
The richer mixture	9.6	15	75	14	21.6
<i>The octane numbers</i>					
The autoignition temperature (°C)	405–450	540	585	650	625

The next chapter involves the numerical investigation of the combustion characteristics of biogas fuel blended with hydrogen at various compositions.

2.13 Conclusion

This chapter summarizes the experimental and numerical literature review that examined the effects of the addition of hydrogen to several premixed fuels, non-premixed, and partially-premixed flame modes under engine relevant conditions. Several gaps in the literature have been identified based on the brief literature presented. The motivation for the present study is to address the few identified gaps in the literature, according to the objectives that have been defined

CHAPTER 3

3 NUMERICAL MODELLING

3.1 Introduction

Computational simulations are widely utilized by several researchers for examining combustion characteristics in detail. The numerical model is described in detail in this chapter. The first part of this work, which includes the computational domain, the boundary conditions, the chemical kinetics, the radiation model, and the grid generation, inside the Can-type gas turbine combustor. In the second part of the work, containing also the computational domain, and the laminar flame velocity correlations, is used in the present study. The simulations are performed using the commercially available codes ANSYS-FLUENT, 0-D SENKIN, and 1-D PREMIX. A chemical kinetics mechanism GRI mech 3.0 having 53 species and 325 elementary reactions. Details of the grid and the numerical model procedure are presented.

3.2 Governing equations

The governing equations for a steady turbulent non-premixed combustion (continuity, momentum, energy, and additional equations for the standard k- ϵ turbulence model, radiation, and combustion) solved for the current study are shown below [31,121–124].

3.2.1 Continuity equation

$$\frac{\partial \bar{\rho} \tilde{u}_i}{\partial x_i} = 0 \quad (3-1)$$

3.2.2 Momentum equation

$$\frac{\partial \bar{\rho} \tilde{u}_i \tilde{u}_j}{\partial x_i} = -\frac{\partial \bar{p}}{\partial x_j} + \frac{\partial}{\partial x_i} (\bar{\tau}_{ij} - \bar{\rho} \widetilde{u''_i u''_j}) \quad (3-2)$$

The Reynolds stresses $\bar{\rho}(\widetilde{u''_i u''_j})$ are determined using Boussinesq expression

$$\bar{\rho} \widetilde{u''_i u''_j} = -\mu_t \left(\frac{\partial \tilde{u}_i}{\partial x_j} + \frac{\partial \tilde{u}_j}{\partial x_i} - \frac{2}{3} \delta_{ij} \frac{\partial \tilde{u}_k}{\partial x_k} \right) + \frac{2}{3} \bar{\rho} k \quad (3-3)$$

Where μ_t is a turbulent dynamic viscosity calculated using Eqn. (3-7), with τ_{ij} is the viscous tensor.

$$\tau_{ij} = \mu \left(\frac{\partial \tilde{u}_i}{\partial x_j} + \frac{\partial \tilde{u}_j}{\partial x_i} \right) - \frac{2}{3} \delta_{ij} \frac{\partial \tilde{u}_k}{\partial x_k} \quad (3-4)$$

It was added last term in Eqn. (3-3) to restore the correct expression of the turbulent kinetic energy k :

$$k = \frac{1}{2} \sum_{k=1}^3 \overline{u''_k u''_k} \quad (3-5)$$

The following transport equations for the standard k - ϵ model used to obtain:

3.2.3 Turbulent kinetic energy (k)

$$\frac{\partial(\bar{\rho} \tilde{u}_i k)}{\partial x_i} = \frac{\partial[(\mu + \mu_t/\sigma_k)(\partial k/\partial x_i)]}{\partial x_i} + P_k - \bar{\rho} \epsilon \quad (3-6)$$

$$\mu_t = \bar{\rho} C_\mu \frac{k^2}{\epsilon} \quad (3-7)$$

Where $C_\mu = 0.09$ is constant, σ_k is the turbulent Prandtl numbers for k . Also $\sigma_k = 1$ and P_k is the production of the turbulence kinetic energy, due to the mean velocity gradients, it defined as:

$$P_k = -\bar{\rho} \overline{u''_i u''_j} \frac{\partial \tilde{u}_i}{\partial x_j} \quad (3-8)$$

3.2.4 Dissipation of kinetic energy (ϵ)

$$\frac{\partial(\bar{\rho} \tilde{u}_i \epsilon)}{\partial x_i} = \frac{\partial[(\mu + \mu_t/\sigma_\epsilon)(\partial \epsilon/\partial x_i)]}{\partial x_i} + C_{\epsilon 1} \frac{\epsilon}{k} P_k - C_{\epsilon 2} \bar{\rho} \frac{\epsilon^2}{k} \quad (3-9)$$

Where: $C_{\epsilon 1} = 1.44$, $C_{\epsilon 2} = 1.92$ and $\sigma_\epsilon = 1.3$ where σ_ϵ is the turbulent Prandtl numbers for ϵ .

3.2.5 The energy equation

$$\frac{\partial}{\partial x_i} \left(\tilde{u}_i (\rho \tilde{E} + \bar{p}) \right) = \frac{\partial}{\partial x_j} \left(\left(k + \frac{c_p \mu_t}{Pr_t} \right) \right) \frac{\partial \tilde{T}}{\partial x_j} + \tilde{u}_i (\bar{\tau}_{ij})_{eff} + S_h \quad (3-10)$$

Where k presents thermal conductivity, Pr_t is the turbulent Prandtl number, S_h is the term source that includes the heat of chemical reaction, radiation, and any other volumetric heat sources. \tilde{E} is the total energy [121,125–127].

where $(\tau_{ij})_{eff}$ is the deviator stress tensor (the viscous heating) which is can be given as follows:

$$(\tau_{ij})_{eff} = \mu_{eff} \left(\left(\frac{\partial \tilde{u}_i}{\partial x_j} + \frac{\partial \tilde{u}_j}{\partial x_i} \right) - \frac{2}{3} \delta_{ij} \frac{\partial \tilde{u}_i}{\partial x_i} \right) \quad (3-11)$$

3.2.6 The radiation flux equation (q_r)

$$q_r = -\frac{1}{3(\tilde{\alpha} + \sigma_s) - C_{\sigma_s}} \nabla G \quad (3-12)$$

where $\tilde{\alpha}$, σ_s , and C are the absorption, the scattering coefficients, and the linear-anisotropic phase function coefficient respectively, the G is the incident radiation[121,128,129].

Where

$$\Gamma = -\frac{1}{3(\tilde{\alpha} + \sigma_s) - C_{\sigma_s}} \quad (3-13)$$

The transport equation for G is presented as

$$\nabla \cdot (\Gamma \nabla G) - \tilde{\alpha} G + 4 \tilde{\alpha} \eta^2 \theta T^4 = S_G \quad (3-14)$$

Where η is the medium refractive index, θ is the constant Stefan-Boltzmann, and S_G is a user-defined radiation source. When the P-1 model is active, this transport equation is used to determine the local incident radiation.

3.2.7 Mixture fraction f

$$\frac{\partial}{\partial x_i} (\bar{\rho} \tilde{u}_i \tilde{f}) = \frac{\partial}{\partial x_i} \left(\bar{\rho} \bar{D} \frac{\partial \tilde{f}}{\partial x_i} - \bar{\rho} \tilde{u}_i \tilde{f}'' \right) \quad (3-15)$$

Where

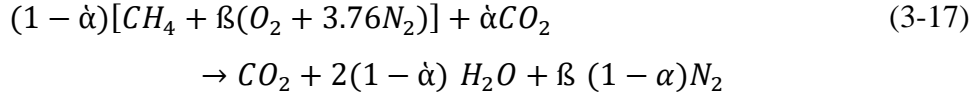
$$f = \frac{Z_i - Z_{i,ox}}{Z_{i,fuel} + Z_{i,ox}} \quad (3-16)$$

Where \bar{D} is a “mean” species molecular diffusion coefficient, Z is the elemental mass fraction for element i . the indices ox, fuel present the oxidizer/fuel stream inlets values.

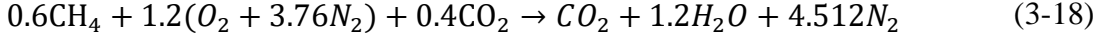
3.3 Chemical Reaction

The chemical composition is calculated using the air/fuel stoichiometric and the mass flow of air/fuel, the adiabatic temperature, the burner power for the biogas, and biogas-enhanced.

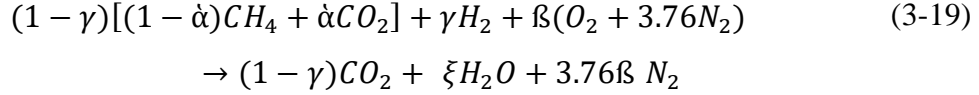
- Stoichiometric chemical reaction of biogas:



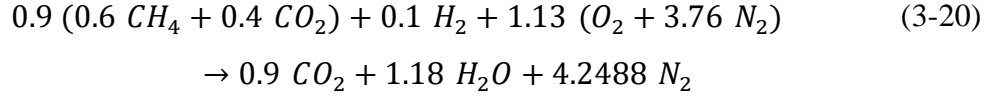
α : the molar fraction of carbon dioxide, β : the various minimum oxygen requirements of the fuel species, for a global equivalence ratio $\phi=1$, $\alpha=0.4$:



The chemical reaction of biogas/hydrogen blends (at the stoichiometric) is given by:



Where γ : the mole fraction of the hydrogen, ξ : the hydrogen mole fraction of products. Let's take the following example, the stoichiometric combustion equation, for fuel consisting in a volume of 54% methane, 10% hydrogen, and 36% carbon dioxide:



One of the properties that is very important in combustion is the equivalence ratio [130], which is the normalizing of the actual fuel-air ratio by the stoichiometric fuel-air ratio:

$$\phi = \frac{\text{Actual } F/A \text{ ratio}}{\text{Stoichiometric } F/A \text{ ratio}} \quad (3-21)$$

There are three types of flames (mixture), $\phi > 1$ is a rich mixture, $\phi=1$ is a stoichiometric mixture, and $\phi < 1$ is a lean mixture, in our case $0.2 \leq \phi \leq 0.5$ (excess of air), which is the standard practice for combustion in gas turbines.

The calculations are made by volume (%) since the biogas composition is commonly measured by Gas Chromatography[131] (GC) in vol.%, and most of the references in literature use volume unit. The stoichiometric fuel to oxidizer is calculated by the oxygen required for the mixture.

$$\text{stoichiometric } A/F = \frac{((2 \times CH_4\%) + (0.5 \times H_2\%))}{0.21} \quad (3-22)$$

In this work, the equivalence ratio is kept constant for the biogas and biogas-H₂. In this case, the actual fuel to oxidizer is the only variable; the equation of flame power (MW) is used to infer the volume flows (Q in (m³/s)):

$$P(MW) = LHV_{biogas} \times Q_{biogas} + LHV_{H_2} \times Q_{H_2} \quad (3-23)$$

The flame power is chosen constant and equal to 0.06MW or 60 kW. The lower heating value of the fuel (biogas doped by H₂ %) is calculated by:

$$LHV(Fuel) = (CH_4\% * LHV_{CH_4}) + (H_2\% * LHV_{H_2}) \quad (3-24)$$

With the LHV_{CH₄} = 35.87 (MJ/m³), and LHV_{H₂} = 10.75 (MJ/m³) in the index web.

To obtain the fuel and air mass flows, it has to multiply the volume of the stream by their densities, the equation that illustrates this is as follows:

$$m = \rho \times Q \quad (3-25)$$

Since ρ is the mixture of air or fuel density related to their 300k and atmospheric pressure compositions. The swirl number (SN) is defined as a dimensionless parameter; the ratio of the tangential momentum flux over the axial momentum flux is used to study the effect of the airflow swirling inlet on the flame combustion characteristics [62]:

$$SN = \frac{\frac{G_{tg}}{RG_{ax}} = \int_0^R \rho u w r^2 dr}{R \int_0^R \rho u^2} r dr \quad (3-26)$$

3.4 Can-Type Combustor Computational Domain

A three-dimensional computational domain of the can-type combustion chamber inspired by the Siemens SGT-750 dry-low emission (DLE) combustor considering identical dimensions and computationally solved using 3-D with double precision ANSYS-FLUENT solver is presented in Figure 3-1. The dimensions of the combustor chamber are (Z~0.59 m, Y~0.25 m, X~0.23 m). The primary air is directed through the vanes to supply the air with a swirling velocity. The diameter of the primary air is 0.10 m, and 45° was supposed for the angle, the swirl numbers greater than 0.7 for a typical can-type combustor, and this allows creating a vortex breakdown reverse flow, the swirl (SN) and Reynolds (Re) numbers are presented in table (3-1).

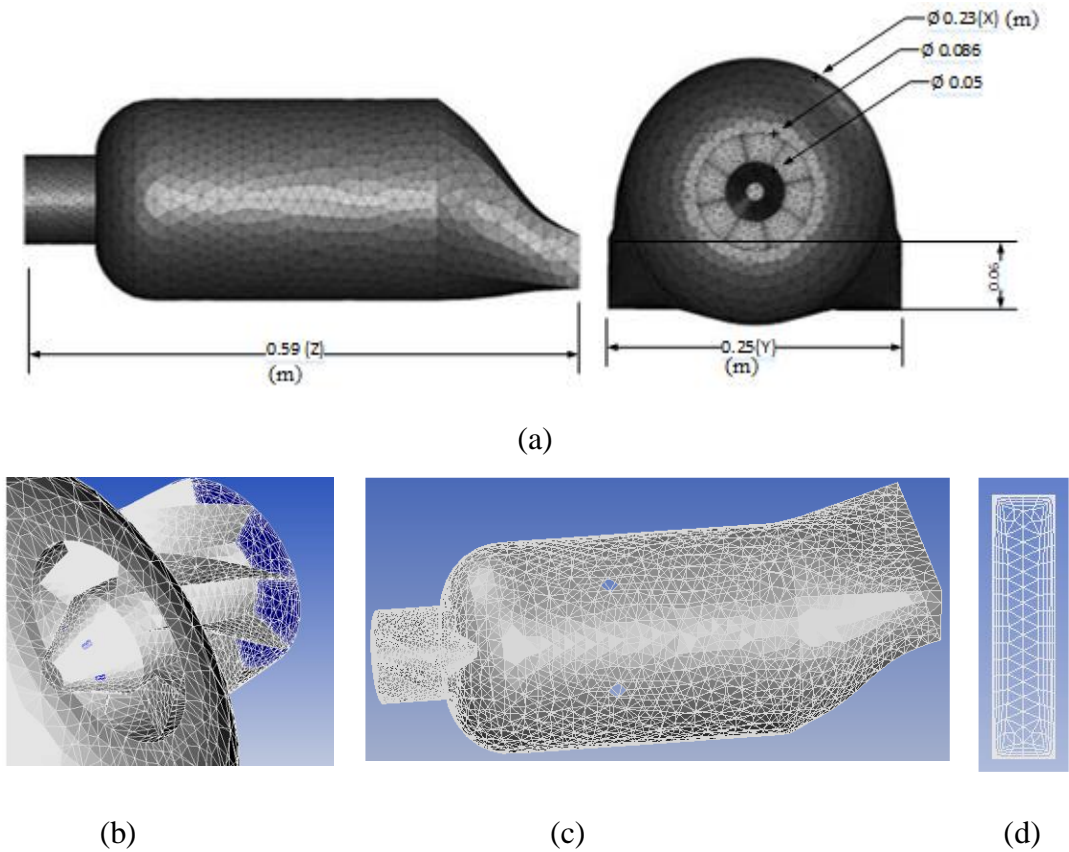


Figure 3-1 Three-dimensional can-type computational domain of combustion chamber with the mesh, (a) Combustion chamber details with dimensions, (b) air-fuel inlet, (c) combustor chamber, (d) combustor chamber outlet

The fuel and the secondary air are injected via the six holes; the diameter of the fuel and the secondary air of holes is 0.0042 m and 0.0016 m, respectively; each one of these six nozzles has a surface of $3.35 \times 10^{-5} \text{ m}^2$. Fuel and air are injected separately, but the flame base is lifted and is non-premixed. The secondary air is injected at 0.1 m from the fuel injector. The outlet has a surface area rectangular form of 0.015 m^2 . The idea behind the use of a three-dimensional model is that the curvature of the wall of combustion will greatly affect the numerical results. This is because the walls of combustion act as a catalyst to enhance combustion instability which can lead to massive interactions between the rate of heat release and pressure fluctuations. Thus, considering the geometrical impact on combustion instabilities necessitates the use of 3-D geometry.

3.5 Boundary Conditions and Meshing for Non-Premixed Model

The turbulence model used is standard k-epsilon. Several studies have used the Reynolds-averaged Navier Stokes (RANS) approach with the standard k-epsilon model for swirling flow. Marzouk and Huckaby [132] performed several numerical

simulations of swirling airflow using three versions of the k-epsilon ($k-\epsilon$) turbulence model (standard, realizable, and renormalisation group RNG), their results were compared with experimental mean velocity profiles. Their results showed that the standard model (SKE) achieved the best overall performance. Whereas, the realizable model was unable to predict the radial velocity satisfactorily. It is also the most expensive model, unlike the (SKE) model. Norwazan and Mohd Jaafar [133] have focused on the effects of flow axial and tangential velocities to obtain the center recirculation zone. In this study, the Reynolds-averaged Navier Stokes (RANS) of various models approached with standard k-epsilon, realizable k-epsilon, and RNG k-epsilon turbulence was applied. As a result, based on the global performance of the RANS models, it appears that the standard k-epsilon turbulence model gives more favorable results due to the center recirculation zone being well presented and reasonably priced, it is broader and shorter than others.

3.5.1 Studies on Can-Type Combustion with the same modelling Approach

Various studies used the Reynolds-averaged Navier Stokes (RANS) approach with the standard k-epsilon model, for swirling flow in the same geometry (can-type combustor). Naitik et al.[134] have performed modeling and CFD analysis of swirl can type combustion chamber using the standard k-epsilon model. Pathan et al.[135] have numerically studied the Combustion of Methane Air Mixture in Gas Turbine Can-Type Combustion Chamber. They have also used the standard k-epsilon turbulence model for turbulence modeling, PDF Flamelet Model, and Eddy Dissipation Combustion Model for non-premixed gas combustion. Ghenai [136] has studied the Combustion of Syngas Fuel in Gas Turbine Can-type Combustor chamber.

3.5.2 Studies using the same modelling approach other than Can-type combustors

Several studies have used the Reynolds-averaged Navier Stokes (RANS) approach with the standard k-epsilon model, for swirling flow with different geometries mentions [11,104,137,138]. Osama et al. [132] studied the Swirling Gas-Particle Flow Using Different k-epsilon Models and Particle-Parcel Relationships. They have performed several numerical simulations of swirling airflow a co-axial particle-laden in a vertical circular pipe using three versions of the k-epsilon turbulence model (standard, realizable, and renormalization group RNG), this result is compared with experimental

mean velocity profiles. Their results showed that the standard model (SKE) achieved the best overall performance. Whereas, the realizable model was unable to satisfactorily predict the radial velocity. It is also the most expensive model, unlike the (SKE) model.

Norwazan and Jaafar [133] have studied isothermal swirling flows with different RANS models in unconfined burners. They have focused on the effects of flow axial and tangential velocities that mainly obtain the center recirculation zone. In this study, the Reynolds-averaged Navier Stokes (RANS) of various models approached with standard k-epsilon, realizable k-epsilon, and RNG k-epsilon turbulence was applied. As a result, based on the global performance of the RANS models, it appears that the standard k-epsilon turbulence model gives more favorable results due to the center recirculation zone being well presented and reasonably priced, it is broader and shorter than others. This model is more economical and time-saving.

3.5.3 About the model limitations

Wen et al. [139] studied various turbulence models to improve reverse combustion performance. The results showed, when comparing the results with experimental, they found that the unsteady k-epsilon model performance is best with accuracy and arithmetic cost. Shamami and Birouk [140] concluded that the Reynolds-Averaged Navier Stokes (RANS) models can predict the center recirculation zone for the strongly swirling flow. Zhuowei et.al [141] performed the isothermal flow of low and high SN using the LES and RANS model. The results illustrate that the LES model displays improvement results over the RANS model. However, the RANS models are still significant to use in swirling flow studies.

This k-epsilon model is more economical and time-saving. The present study is applied to model combustion with the steady laminar flamelet model (SLF). The flamelet model uses dissipation to account for deviations from equilibrium. In the turbulent CFD simulation, the turbulent non-premixed flame is thus modeled as an ensemble group of overlaying laminar flamelets.

3.6 Boundary conditions, solver details

The operating conditions of the fuel and airflow inlets are summarized in Table (3-1), and as follows: the temperature 300 K, the atmospheric pressure, at the turbulence intensity is 10%. The fuel mass flow varies by LHV due to the change in fuel compositions, and the air mass flow is varied with a global equivalence ratio range (0.5

to 0.2). The power generation is equal to 60 KW. They are reserved constant for all case simulations, and they are presented in table (3-1). The hydrogen mixing (10% to 50%) to the pure biogas (60% CH₄ and 40% CO₂) is volumetric. The secondary air has the following operating conditions: the injection of the mass flow rate is 0.002 kg/s, with the temperature equal 300 K at the turbulence intensity is 10%. The scalar dissipation rate at the stoichiometric equals 0.01 (1/s), and the maximum number of grid points in the flamelet equals 64. Convergence is subordinated by the residuals whose convergence criteria are 10⁻³ for all the equations except the energy and radiation equations, which we consider this criterion is 10⁻⁶.

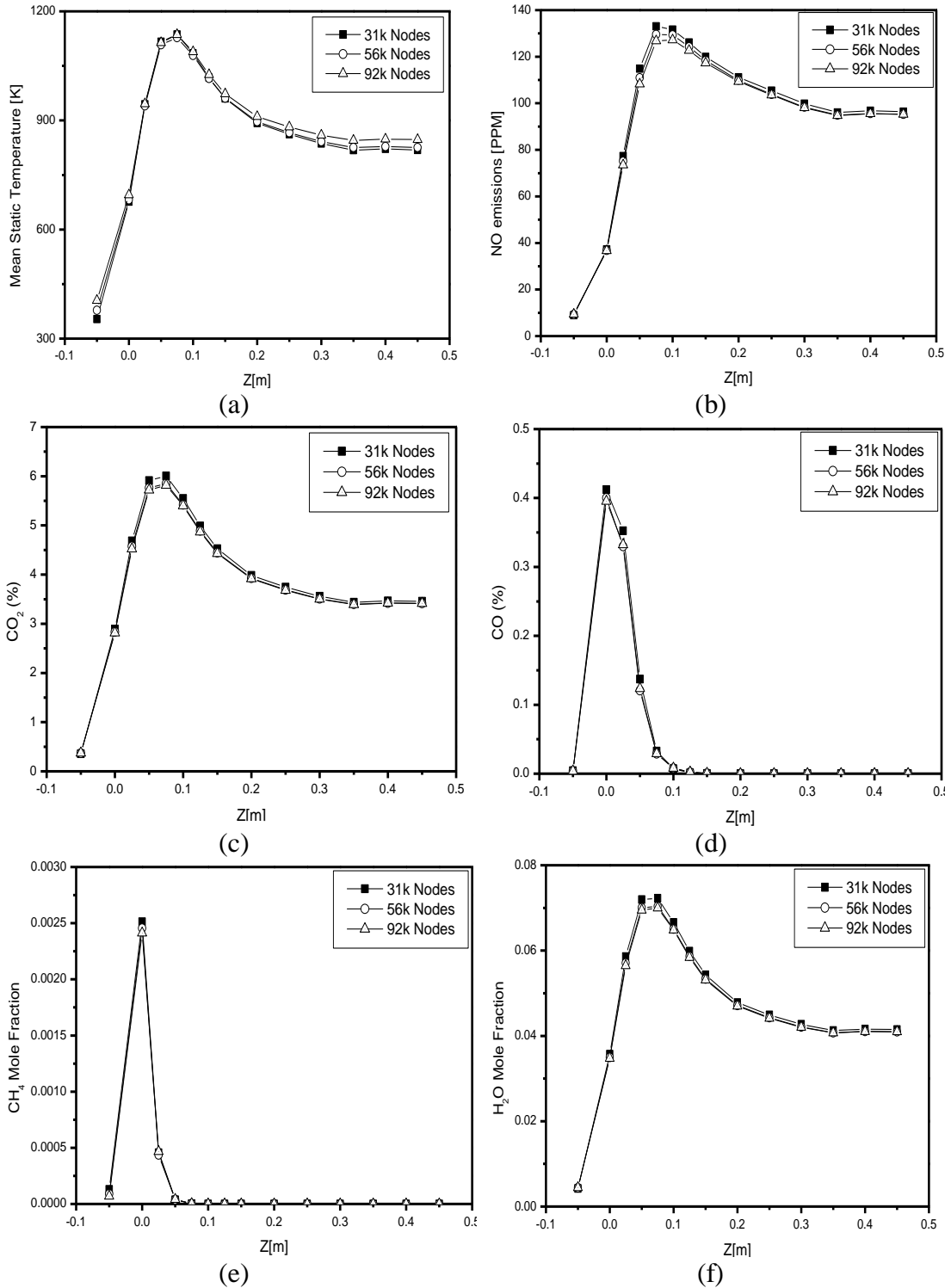
Table 3-1 Can-type gas turbine operational conditions with fuels compositions at 300K atmospheric pressure

ϕ	Swirl number (SN)		Reynolds Number (Re)		P (KW)	Fuel Mass flow (kg / s)	Air Mass flow (kg / s)		
0.5	0.77-0.73		25810- 24354		60	3.4 ^{E-3} -2.4 ^{E-3}	4.1 ^{E-2} -3.88 ^{E-2}		
0.4	0.89-0.84		32626- 30774				5.13 ^{E-2} -4.85 ^{E-2}		
0.3	1.03-0.98		43943- 41429				6.84 ^{E-2} -6.46 ^{E-2}		
0.2	1.22-1.18		66842- 62805				1.03 ^{E-1} -9.69 ^{E-2}		
Fuel compositions (vol.%)			Air compositions (vol.%)		Fuel Density g·m ⁻³	Fuel HHV MJ·m ⁻³	Fuel LHV MJ·m ⁻³	Fuel Specific Gravity	Wobbe Index MJ·m ⁻³
CH ₄	CO ₂	H ₂	O ₂	N ₂					
60	40	0	21	79	1219.564	23.933	21.568	0.943	24.641
54	36	10			1105.772	22.802	20.478	0.855	24.655
48	32	20			992.244	21.675	19.392	0.768	24.740
42	28	30			878.951	20.551	18.309	0.680	24.923
36	24	40			765.862	19.430	17.228	0.592	25.244
30	20	50			652.947	18.312	16.150	0.505	25.766

In this work, the PDF model (Probability Density Function) was investigated as a combustion model. The mixture fraction is considered an essential part of the diffusion model; the steady diffusion flamelet was used the GRI mech 3.0 for modeling the combustion with 53 species and 325 elementary reactions [142]. The Radiation Model (P-1) was adopted in this simulation.

3.7 Grid independence study

A grid independence study was conducted for the three-dimensional computations using three different meshes of sizes, 31500, 56250, and 91900 nodes, respectively. Figures 3-2(a-g) show the comparison of mean static temperature, NO, CO₂, and CO emissions, CH₄, H₂O, and H₂ mole fractions, respectively. The results demonstrate that there is no significant difference between the three meshes.



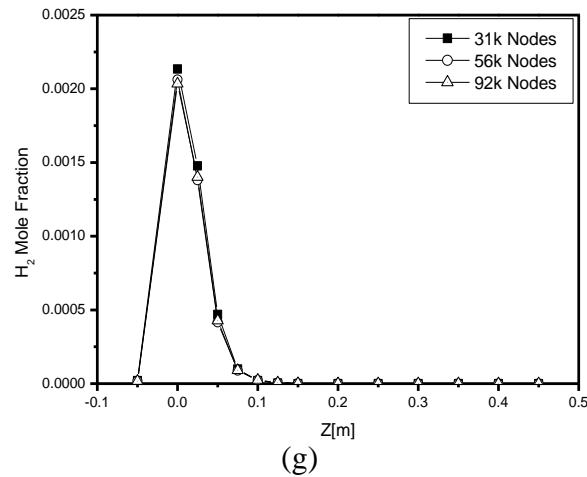


Figure 3-2 Grid independence study for three different mesh sizes along axial direction; (a) mean temperature profile, (b) mean NO emissions, (c) mean CO₂ mole fraction profile, (d) mean CO mole fraction profile, (e) mean CH₄ mole fraction profile, (f) mean H₂ mole fraction profile, and (g) mean H₂O mole fraction profile.

The difference is the peak values for mean static temperature, NO, CO₂, and CO emissions, CH₄, H₂O, and H₂ mole fractions is 10 k, 3.49 ppm, 0.18 %, 0.012 %, 5.8×10^{-3} %, 2.276×10^{-1} %, 7.07×10^{-3} %, respectively. Thus, the mesh with 31k nodes was chosen in this work to save computing power and time. Table (3-2) shows the details of the selected 31k nodes mesh. For this mesh maximum cell squish is 0.94, maximum cell skewness is 0.99, and a maximum aspect ratio is 83.17, respectively.

Table 3-2 Mesh statistics

Cell count (Number of Elements):	106651
1- Number of Nodes	31433
2- Tetrahedral	74189
3- Wedges	30473
4- Pyramids	1989
Face count	234368
Number of Nodes	31433

Ghenai [136] also generated a similar mesh with similar number of nodes and the current results are validated against his published results in the subsequent section.

3.8 Computational method Biogas+hydrogen combustion characteristics

The main objective of the computations is to investigate the effect of hydrogen mixing on the combustion characteristics of biogas for a variety of fuel oxidizer mixtures and initial conditions [143]. To understand the high and low-temperature combustion

characteristics of the biogas+hydrogen blends, two types of computations were performed: laminar flame speed (1D) and ignition delay (0D). In general, the laminar flame speed (LFS) is defined as a high-temperature combustion characteristic, while the ignition delay is a low-temperature characteristic.

- The laminar flame speed (LFS) represents the overall fuel consumption rate which mostly occurs at high temperatures and represents high-temperature combustion characteristics.
- The ignition delay time (ID) is simulated as the combustion process begins before the stable flame front is formed, and is thus expressed as a low-temperature combustion characteristic.

First, simulations of the one-dimensional (1 D) freely propagating flame code *PREMIX* were performed to determine laminar flame speed [144–146]. Second, the ignition delay was calculated using the zero-dimensional (0-D) homogeneous reactor model *SENKIN* [144–146]. The reaction zone is discretized and the mesh is refined with gradients and curves to solve the combustion characteristics of the fuel. Each GRID line contains the coordinate of a mesh point. The adaptive mesh parameters GRAD and CURV control the number of grid points inserted in high gradient and high curvature regions, respectively. The grid-independent laminar flame velocity were obtained for GRAD = 0.05 and CURV = 0.1. It was discovered that the mesh has no effect on the precise refinement. The thermodynamic databases, species kinetic data, and transport databases for the reaction mechanism are incorporated using Kee et al. [146] code. All these databases are studied using TRANFIT values contained in Kee et al [145], Kee et al. [144] code. The compositions of biogas+hydrogen/air mole fractions inputs for various equivalence ratios were studied with different temperature and pressure conditions.

3.9 Laminar flame velocity correlations

The laminar flame speed is affected by the equivalence ratio of the mixture, the unburned temperature, unburned pressure, and dilution concentrations. The most common correlation for describing the effect of unburned temperature and pressure on flame speed or burning velocity at the same time is explained by Liao et al. [147], Sharma et al. [148], Iijima and Takeno [149], and Gu et al. [150]

$$S_u = S_u^o(\phi, R_H) \left(\frac{T}{T_u} \right)^\alpha \left(\frac{P}{P_u} \right)^\beta \quad (3-27)$$

Where α and β are the temperature, and pressure exponents respectively. Yu et al. [151] also have studied and obtained the linear relationship (Equation. 3-28) for laminar flame velocity (S_u) as a function of equivalence ratio (ϕ), and hydrogen mole fraction (R_H) addition in the fuel [143].

$$S_u^o(\phi, R_H) = S_u^o(\phi, 0) + k(\phi)R_H \quad (3-28)$$

In the above (Equation. 3-28), $S_u^o(\phi, 0)$ and $S_u^o(\phi, R_H)$ represents laminar flame velocity for pure biogas-air mixtures ($R_H=0$), and biogas containing the fraction of hydrogen (v/v) in the fuel ($R_H=0.1$ to 0.5). In the Equation. (3-28), $k(\phi)$ represents the coefficient of flame velocity related to hydrogen mixing.

$$S_u^o(\phi, 0) = a_0 + a_1\phi + a_2\phi^2 + a_3\phi^3 + a_4\phi^4 \quad (3-29)$$

$$k(\phi) = k_0 + k_1\phi + k_2\phi^2 + k_3\phi^3 + k_4\phi^4 \quad (3-30)$$

The initial boundary conditions for temperature and pressure are $T=300$ K and $P=0.1$ MPa, respectively. The mole fraction of hydrogen in the biogas fuel blends (R_H) is given by:

$$R_H = \frac{n_{H_2}}{n_{CH_4} + n_{CO_2} + n_{H_2}} \quad (3-31)$$

Where n_{CH_4} , n_{CO_2} and n_{H_2} are the mole fractions of methane, carbon dioxide, and hydrogen, respectively. The volume fraction of hydrogen is varied from (0% to 50%), thus, the R_H value is between (0-0.5). The composition of air is (21 vol.% O_2 and 79 vol.% N_2).

Using the thermal theory, the laminar flame velocity is correlated with the initial values of the physical properties (Eqns. 3-32, 3-33, and 3-34).

$$S_u \sim (P_u^{n-2})^{1/2} \quad (3-32)$$

$$S_u = S_u^o \left(\frac{P}{P_u} \right)^\beta \quad (3-33)$$

$$\beta(\phi) = \beta_0 + \beta_1\phi + \beta_2\phi^2 \quad (3-34)$$

Where n is the order of the global chemical reaction. The overall order of the reaction is

- ✓ Less than 2 for flames with ($S_u < 0.5$ m/s)
- ✓ Equal to 2 for those with ($0.5 < S_u < 1.0$ m/s)
- ✓ Greater than 2 for those with ($S_u > 1.0$ m/s)

Lewis' pressure dependence implies that when ($S_u > 100$ m/s), ($0.5 < S_u < 1.0$ m/s), and $S_u < 0.5$ m/s, the pressure exponent is typically positive, zero, and negative, respectively. For several hydrocarbon fuels, the undergo second-order reactions, the flame speed is independent of pressure [38].

Although the theoretical dependence of flame speed on unburned temperature and pressure is simple, straight forward, estimating it in experiments is much more difficult. When results from different experimental methods are compared on the same scale, there is substantial scatter.

Similarly, Eqn. 3-35 shows the laminar flame velocity as a function of unburned temperature (refer to Akram and Kumar[152,153], Akram et al. [154] for details):

$$S_u = S_u^o \left(\frac{T}{T_u} \right)^\alpha \quad (3-35)$$

$$\alpha(\phi) = \alpha_0 + \alpha_1\phi + \alpha_2\phi^2 \quad (3-36)$$

Where, S_u^o is the laminar flame velocity at reference conditions ($T_u = 300$ K, $P_u = 1$ atm).

The temperature and pressure exponent α and β varies as a function of the equivalence ratio. The polynomial of the second order is useful to represent the non-linear dependence of temperature and pressure exponent α and β on the fuel equivalence ratio as suggested by [153–155].

Considering the correlation that combines the effect of pressure, temperature, and equivalence ratio on the laminar flame velocity (S_u) for various fuel-air mixtures one can express the correlation for S_u by (Eqn.3-37)

$$S_u = S_u^o(\phi, R_H) \left(\frac{T}{T_u} \right)^{\alpha(\phi)} \left(\frac{P}{P_u} \right)^{\beta(\phi, R_H)} \quad (3-37)$$

In the above Eqn. 3-37, $\alpha(\phi)$ and $\beta(\phi, R_H)$ are the temperature and pressure exponents given by Eqns. 3-36 and 3-38.

$$\beta(\phi, R_H) = \beta(\phi, 0) + k_\beta(\phi)R_H \quad (3-38)$$

Where,

$$\beta(\phi, 0) = \beta_0 + \beta_1\phi + \beta_2\phi^2 \quad (3-39)$$

$$k_\beta = k_{\beta 0} + k_{\beta 1}\phi + k_{\beta 2}\phi^2 \quad (3-40)$$

The laminar flame velocity data generated for the range of equivalence ratios ($\phi = 0.7-1.4$), hydrogen fraction in fuel ($R_H = 0.0 - 0.5$), unburned temperature ($T = 300 - 600$ K) and unburned pressure ($P = 0.1-7$ MPa) are used develop analytical correlations for laminar flame velocity, that is presented in the Eqn.3-37. The correlation data to interpolate the flame velocity at initial mixture (R_H, ϕ), unburned temperature T, and unburned pressure P under specified limits are summarized in Table (3-3).

Table 3-3 Summary of the correlations and their coefficients for biogas+hydrogen blends.

Parameter Range	Correlations with coefficients		R^2
$R_H = 0.0-0.5$ $\phi = 0.7-1.4$ $T = 300-600$ K $P=0.1-7.0$ MPa	$S_u^o(\phi, R_H) = S_u^o(\phi, 0) + k(\phi)R_H$	$S_u^o(\phi, 0) = 222.05 - 1065.7\phi$ $+1850.6\phi^2 - 1296.5\phi^3 +$ $314.64\phi^4$	0.9992
		$k(\phi) = -137.81 + 551.4\phi$ $-839.58\phi^2 + 719.93\phi^3 -$ $239.3\phi^4$	0.9973
	$S_u = S_u^o(\phi, R_H) \left(\frac{T}{T_u}\right)^\alpha$	$\alpha(\phi) = 5.7748 - 7.4312\phi + 3.5201\phi^2$	0.9979
	$S_u = S_u^o(\phi, R_H) \left(\frac{T}{T_u}\right)^{\alpha(\phi)} \left(\frac{P}{P_u}\right)^{\beta(\phi, R_H)}$	$\beta(\phi, 0) = -1.8749 + 2.6829\phi - 1.3163\phi^2$	0.9961
	$\beta(\phi, R_H) = \beta(\phi, 0) + k_\beta(\phi)R_H$	$k_\beta = 1.1637 - 2.2179\phi +$ $1.1026\phi^2$	0.9713

3.10 Conclusion

The numerical model is displayed in detail in this chapter. The governing equations, boundary conditions, solution methodology, domain and grid independence studies, the laminar flame velocity correlations, and ignition delay have also been studied and discussed in detail.

CHAPTER 4

4 RESULTS AND DISCUSSION

4.1 Introduction

This chapter describes the numerical investigation of the flame temperature contours, effects of H₂ enrichment, and equivalence ratio on temperature, emissions, species, ignition delay, laminar flame velocity at ambient conditions, high unburned pressure/temperature, at high pressures and combined between temperature and pressure, and the flame structure of biogas+hydrogen air mixtures at high unburned temperatures. In this chapter, the computation validations are presented.

4.2 Gas Turbine Computation Validation

This can-type combustor has been utilized for many experimental fundamental and numerical investigations using conventional fuel and air mixtures [135,156–160]. Rashwan [101] has examined and validated the k-epsilon model in the Can-type combustion chamber. The results are validated with an experimental work done by Alkabile et al. [161], using an identical combustor geometry of Siemens SGT-750. They found an excellent agreement with the experimental results in terms of the wall temperature values. Mats Andersson et al. [162] tested the total of lower heating value range (LHV) of natural gas with the Wobbe index (WI) range of 25-55 MJ/Nm³ of Siemens gas turbine SGT-600 and SGT-700. The results illustrate that it is not necessary to make any special adjustment to the gas turbine; it allows us to take full advantage of alternative fuels and provide energy with low fuel costs. This facilitates the use of biogas-H₂ mixture fuel because it has the Wobbe index of 25 MJ/Nm³ similar to the natural gas. Additionally and according to the literature, it was chosen the standard k-ε model for the Can-type combustor geometry to validate with available data in research by Ghenai et al. [136,163,164], where the natural gas (NG) is a reference fuel. The specific boundary conditions used to validate our model can be found in table 4-1 below:

Table 4-1 The detail conditions (fuel, boundary, and operating conditions)

<i>Fuel (compositions)</i>	<i>Natural Gas (95 % CH₄- 0% CO₂- 2% N₂- 3% C₂H₆)</i>
LHV (MJ/kg)	50
Fuel mass flow rate (kg/s)	1.0×10^{-3}
The primary air (m/s)	10
The secondary air (m/s)	6
Inlet temperature (fuel/ primary, secondary air) (K)	300
Pressure	atmospheric pressure
the turbulence intensity	10%
Power (kW)	50

Figure 4-1 displays the static temperature distribution of the natural gas composition with the same operating conditions by Ghenai et al. [163]. It can be observed that the maximum temperature for natural gas equals 2110 K. It can also be seen from the results of NG, two different peaks, the first peak in the zone of the injector with the temperature equal 1810 K and the other peak in the secondary zone with the maximum temperature equal 2110 K. Also, a decrease in the temperature after primary zone $Z = 0.1$ m, because of the dilution of air. When this result is compared with the work done by Ghenai et al. [163], it can be seen that the present data result is an excellent agreement with their results. The average error percentage (%) is 2.79% [124].

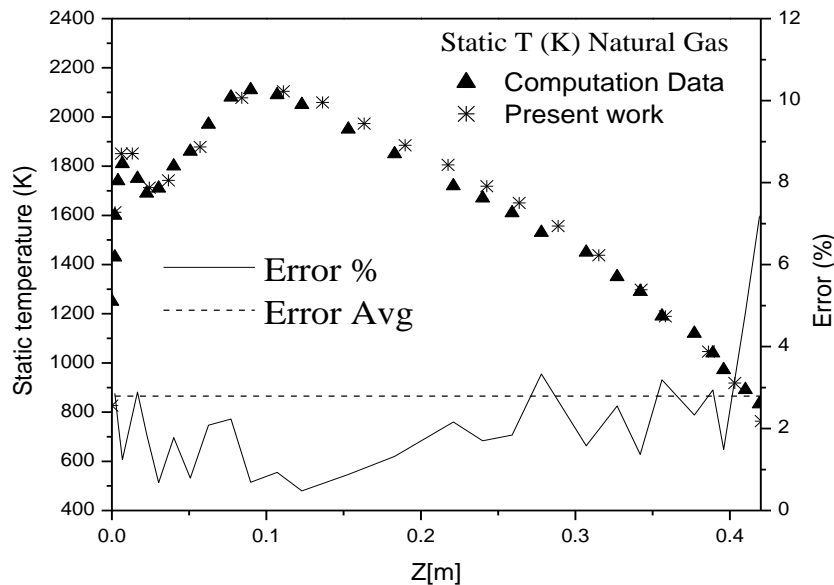


Figure 4-1 Validation of the static temperature profiles of Natural gas as compared to the work done by Ghenai et al. [136]

Figure 4.2 displays a validation of the static temperature contours of methane in the gas turbine can combustors as compared to the work done by Ghenai et al. [136] with the

operating conditions shown in the table (4-2). It can be observed that the maximum temperature for methane equals 2200 K. In order to validate the combustion model (SKE), flame temperature predicted for methane (100% CH₄) combustion is compared to the adiabatic flame temperature (AFT). For initial atmospheric conditions of methane, theoretical flame temperature molded through the flame with combustion reaction is 2233 K. Consequently, the expected maximum temperature is well compared with the theoretical adiabatic flame temperature. It can be seen that the data result (Ghenai data) [136] is in good agreement with our result[124].

Table 4-2 the operating conditions of Ghenai

<i>Constituents</i>	<i>Methane (CH₄)</i>
CH ₄	100
Volumetric heating value (KJ/m ³)	33570
Lower heating value (MJ/Kg)	50.1
Fuel mass flow rate (Kg/s)	0.001
With inlet temperature (K)	300
And turbulence intensity (%)	10
The velocity of primary air(m/s)	10
With inlet temperature (K)	300
And turbulence intensity (%)	10
Velocity of secondary air(m/s)	6
With inlet temperature (K)	300
And turbulence intensity (%)	10
Power (KW)	50.1

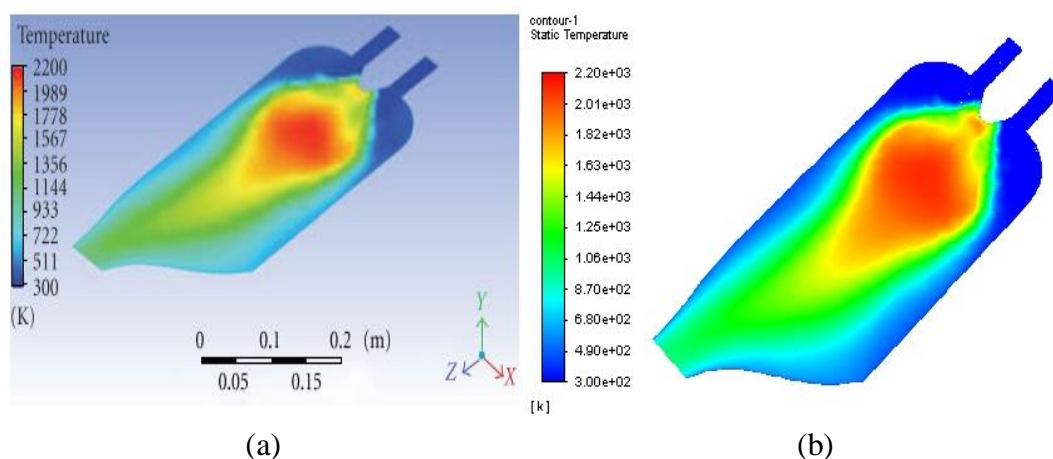


Figure 4-2 Validation of the static temperature contours of methane as compared to the work done by Ghenai: (a) Present work, (b) Ghenai Data

4.3 Flame temperature contours

Figure 4-3 presents the contours of the flame temperature distribution and NO emissions, with the H₂ (%) content and for a constant equivalence ratio ($\phi=0.5$). From these figures, it is observed that hydrogen helps maintain stable flame operation and that the flame spread along with the combustor chamber without touching the chamber wall due to the second air dilution effect. The combustion's hot zone is found to be moving towards the central axis and expanding downstream, as shown in Figure 4-3 for (biogas doped with 50% H₂). This indicates improved reactivity and intensifies the combustion process due to the addition of hydrogen. This is due to the combination of flow velocity, flow swirl, and enhanced flame speed due to hydrogen mixing and due to the fact that hydrogen is 6 to 7 times more reactive than methane, thus intensifying combustion leading temperature. This can be explained by the increase in the radical pool that accompanies the H₂ addition, such as H and OH radicals, which improves mixture reactivity and then flame speed. In other words, increasing flame speed and the effect of flow swirl will create a robust flame stable enough to resist flame extinction. The combined effect of these two is that the flame can stabilize at a much higher strain rate without getting extinguished. Besides, it will enhance premixing between the combustible gases and incoming mixtures, which helps maintain recirculation zones that promote flame stability, thus enhancing the combustion rate. It can also be seen that there is no significant change in flame temperature distribution is almost the same for a constant ϕ and burner power. Still, the NO emissions are increasing with the increase in the hydrogen rate[124].

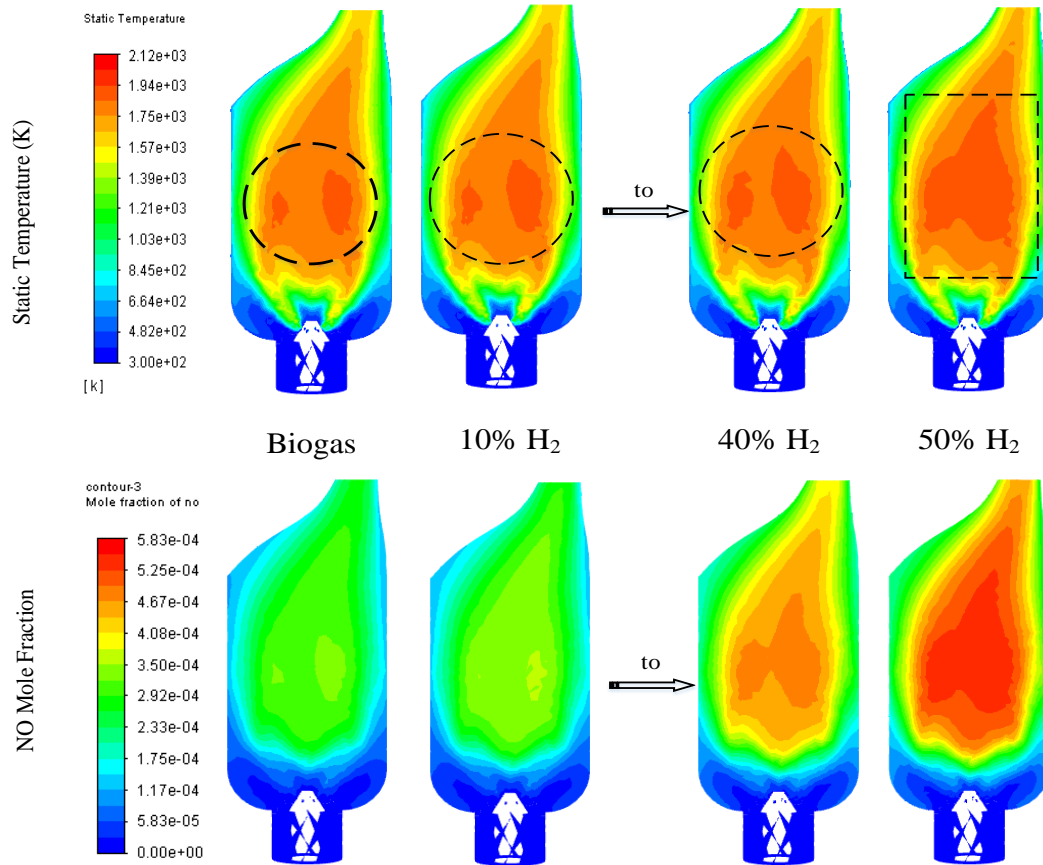


Figure 4-3 A sequence of images describing the biogas flame temperature distributions [K] (above) and NO emissions (below), with different rates of hydrogen concentration by Vol%

Figure 4-4 presents the contours of the flame temperature distribution and NO emission, for the biogas doped with 40% H₂ for different equivalence ratios (ϕ). From this figure, it is observed that the length and thickness of flame decreased gradually with decreasing in equivalence ratio and increases in swirl number. This is due to increasing air mass flow and the short time of reaction between the oxygen and nitrogen in the hot zone (reaction region); ultimately, it produces fewer nitrogen oxides. For that reason, the NO_x exhaust decreases. It worked on cooling the flame and dropped in the fuel mass flow when the equivalence ratio decreases for a burner power constant[143].

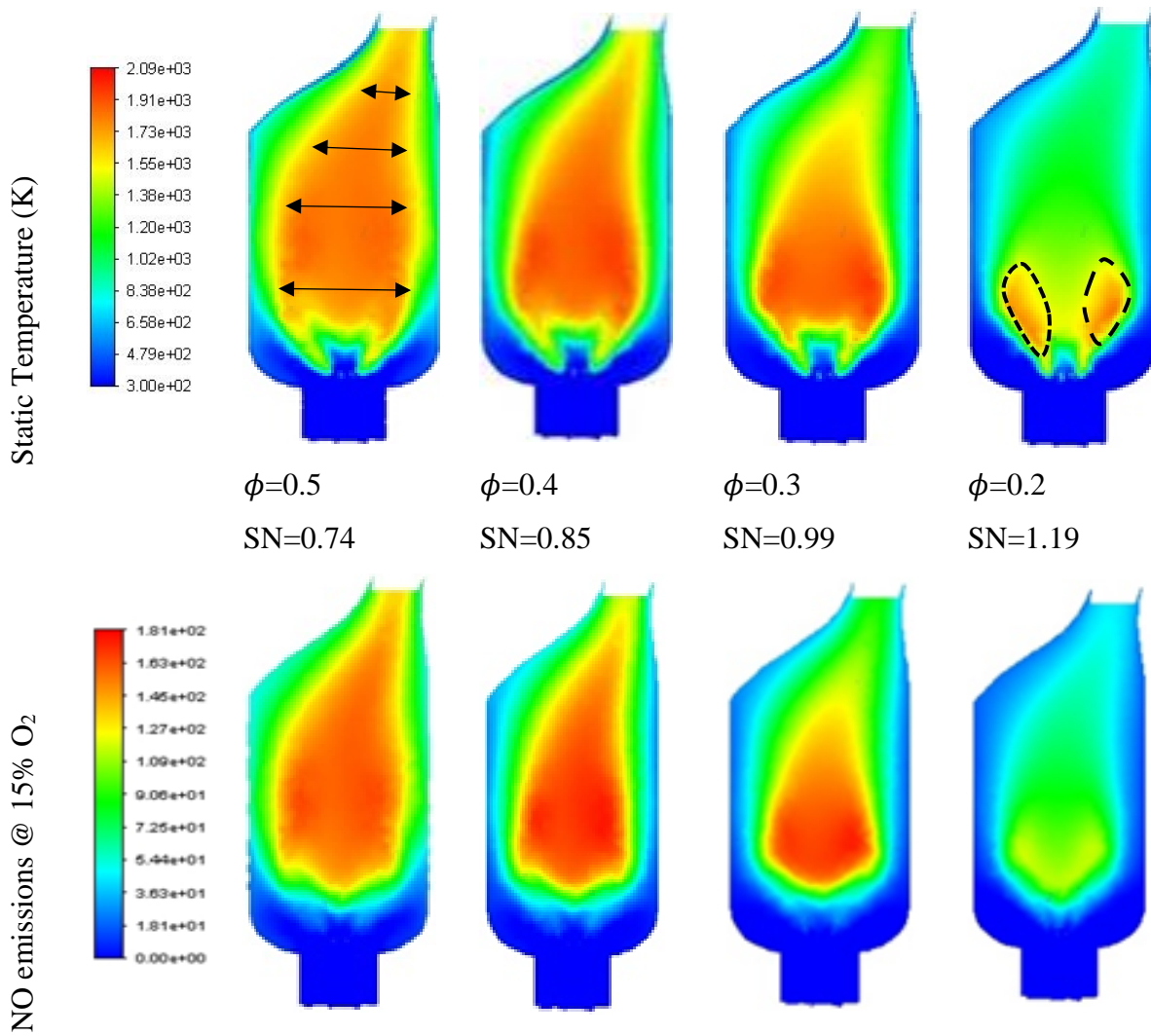


Figure 4-4 Comparison of flames temperature distributions and NO emissions, with different values of equivalence ratio: $\phi=0.3-0.5$ (CF: conical flame shape), $\phi=0.2$ (VF: "V" shaped flame)

Despite the large proportion of air for the equivalence ratio of 0.2, the flame is not extinguished when choosing these new boundary conditions. The length and thickness of NO emissions decreased; this is because of the decrease of the temperature and the equivalent between the air primary/secondary and fuel mass flow by keeping the burner power constant, it can be observed that the effect of the secondary air increases with decrease in equivalence ratio. It can be found that the flame takes different shapes, for example, it takes a conical shape for $\phi = 0.3-0.5$, it can be observed that the flame diameter reduces and the "V" shaped flame for $\phi = 0.2$, due to the flame stabilization on the central chamber combustion and the external burner lips, and it takes the (V) shape, the flame shapes are defined by Candel [165]. Figure 4-5 represents the cross-sections of flame temperature distribution for the biogas added with 50% H_2 , at the

equivalence ratio equal 0.2. This figure explains the cross-sections used to derive the results (by using surface integrals "Area-Weighted Average"), and it starts from the fuel inlet section at $Z = -0.05\text{m}$ to the outlet section of the combustion chamber at $Z = 0.45\text{m}$ and the secondary air inlets are identified at $Z = 0.1\text{m}$ [124].

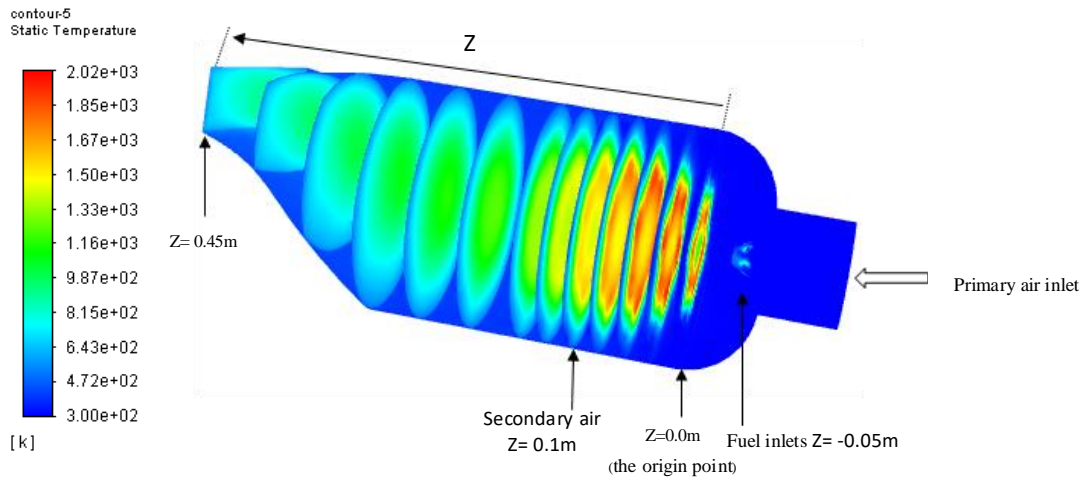


Figure 4-5 Flame temperature distributions cross-sections, for 50% H_2 hydrogen rate.

Figure 4-6 shows the effect of increasing the swirl number (for different equivalence ratios (ϕ)) on the velocity, for the biogas doped with 40% H_2 . The recirculation zones are formed closer to the inlet section and in the middle of the combustion chamber; these zones enhance the stability of flames by recycling and mixing the hot gases again with cold reactants, which produce durable flame. The increase in the swirl number (SN) leads to growing up the vortex in the middle of the combustion chamber and decreases the vortex in the corners of the chamber, especially for $\text{SN} = 1.19$. Further, an increase in the central recirculation zone indicates proper mixing of fuel and air, that increase may be because of two reasons, first because of the enhance and the increase in swirl velocity, especially the tangential flow velocity component (1.88 to 4.90), for ($\phi = 0.5$ to 0.2), respectively. Second because of the deflection of the flow from the central axis of the chamber, creates a low pressure in this zone, which increases the size of the vortex in the center of the combustor. Consequently, the (SN) has a significant effect on the flame size (thickness/length flames). The impact of secondary air was also considered. The secondary air has a mass flow rate of 0.002 kg / s , with a temperature equal to 300 K at the turbulence intensity is 10%. However, the secondary air effect is used to cool the wall and thus protect the combustion chamber and increase its efficiency[124].

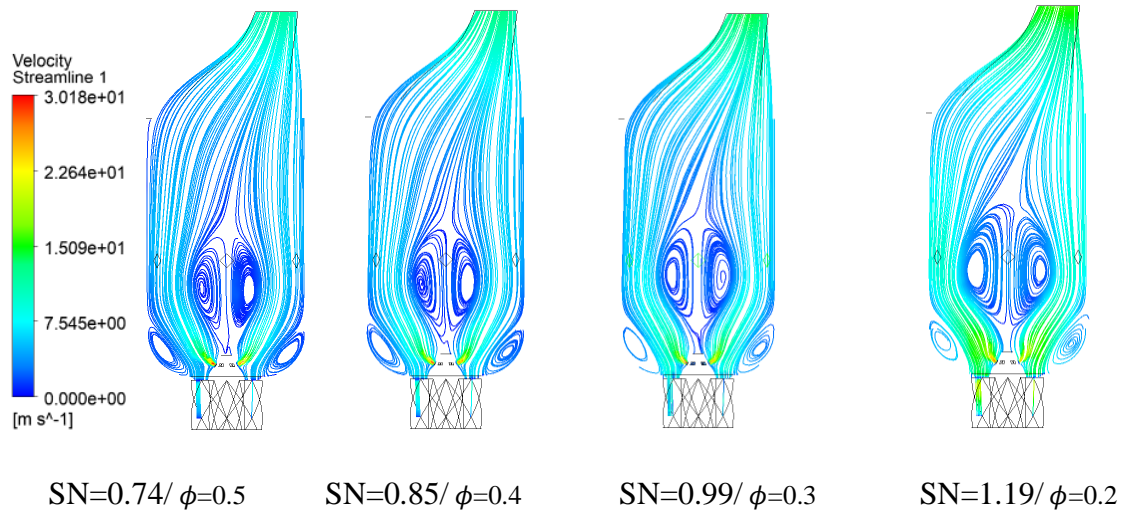
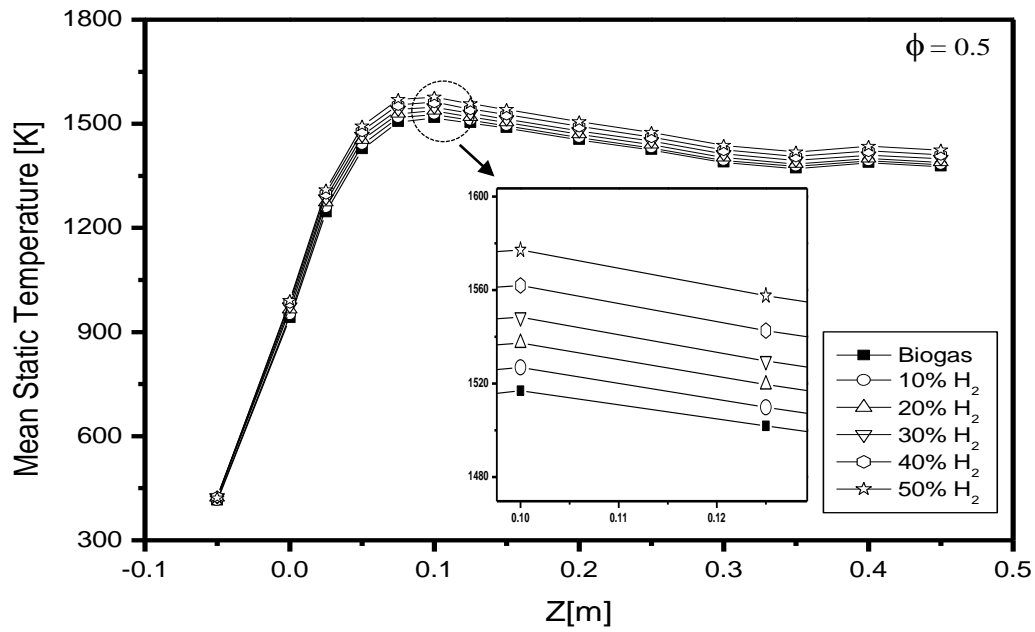


Figure 4-6 Velocity streamlines for 40% H₂ hydrogen rate, with different values of equivalence ratio: $\phi=0.5-0.2$ and different values of swirl number: 0.74-1.19

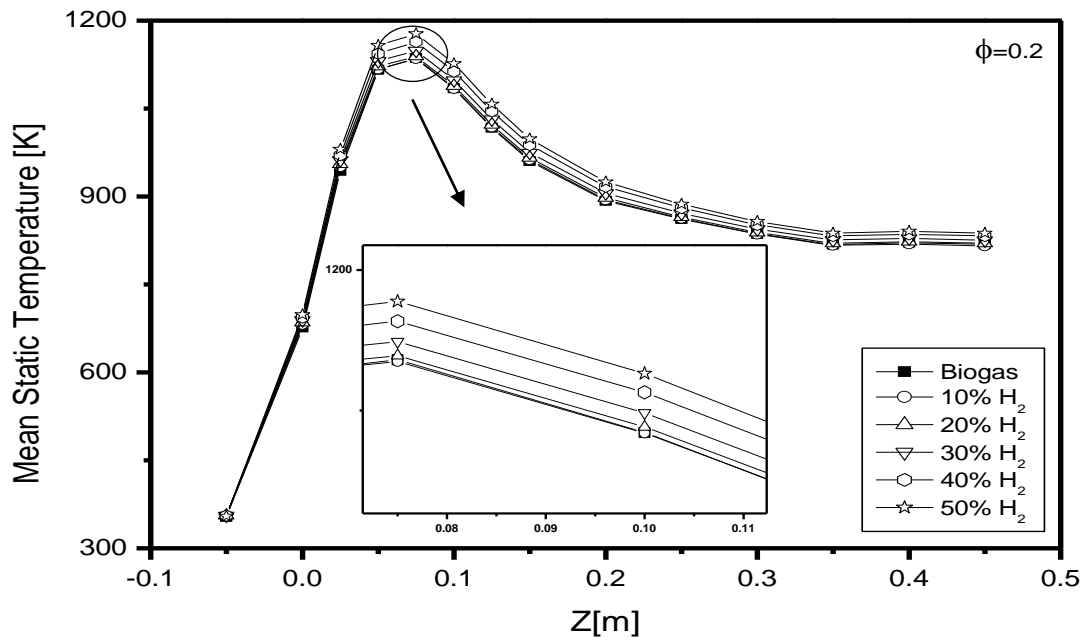
4.4 Effects of H₂ enrichment, and equivalence ratio on temperature

The average static temperature profiles along the central axis of the combustion chamber for the biogas and biogas doped with H₂ is shown in figure 4-7. Biogas (CH₄ = 60%, CO₂ = 40%), is utilized as the reference fuel. For figure 4-7 (a, b), when the hydrogen is added, the temperature reaches the maximum temperature (1557-1164 K) at a height of 0.1-0.75 m for 50% H₂ at ($\phi = 0.5$ and 0.2), respectively. Additionally, the temperature in the absence of hydrogen reaches the maximum (1517-1143 K) at 0.1-0.75 m for the ($\phi = 0.5$ and 0.2), respectively. Here the peak temperatures increased by (40-21 K) from the biogas pure to biogas with 40% H₂ additions at ($\phi= 0.5$ and 0.2), respectively. As well, there is a significant impact after $Z = 0.1$ m in the secondary zone of dilution air. Therefore, the temperature of the fuel decreases due to the secondary airflow, and this influence gets more significant when the ϕ reduces. The result reveals that the temperature increases with hydrogen increase, which means the hydrogen accelerates the reaction of combustion. Figure 4-7 (c) shows an increase in the temperature of the biogas reference, and the biogas blended with 40% H₂ when the (ϕ) increases. It can be seen that, almost the flame temperature at ϕ equal 0.2 with a high rate of hydrogen (40% H₂) close to the results of the pure biogas (0 % H₂) whereas for an ϕ superior of 0.2 the temperature of hydrogen added to the biogas increases, that due to the secondary air a significant impact at an $\phi = 0.2$, with low flame temperature. It can be observed that a decrease in the temperature with increases in the swirl number (0.74-1.19) and decreases in the equivalence ratio (0.5-0.2); because of the

improvements in (SN) leads the fuel-air mixture streams increases and that makes the fuel consumed as it presents in figure 4-7(d)[124].



(a)



(b)

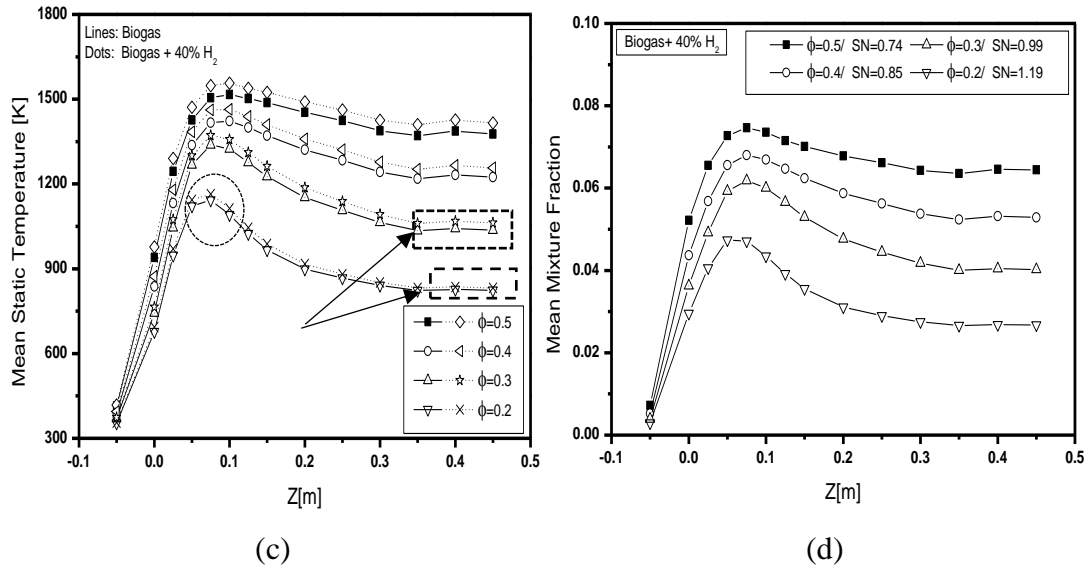


Figure 4-7 Axial temperature profiles for different hydrogen concentrations (a) $\phi=0.5$, (b) $\phi=0.2$, and (c) at different ϕ s for biogas and 40% H₂-Biogas (d) mixture fraction for 40% H₂ at different ϕ s/ SN

Figure 4-7(d) shows the axial mixture fraction for the biogas doped with 40% H₂. It can be seen, the mixture fraction decreases when the (SN) increases, and the (ϕ) decreases, which indicates mixing development; fuel consumption due to combustion. The mixture fraction can be described as the ratio between the mass flows of fuel and oxidizer. In this regard, the mixture fraction will be very similar to the equivalence ratio. From equation (3-16), it can be seen, when the air mass flow increases while keeping the mass flow of fuel constant, the mixture fraction will decrease, and vice versa and this is in agreement with Figure 4-7 (d)[124].

Figures 4-8 (a-b) studied the maximum temperature for different values of H₂ added to the biogas and different equivalence ratios. The maximum temperatures increase with the increase in the H₂ addition, and an increase in the ϕ . It can be noticed that the difference in the temperature when H₂ added decreases as the equivalence rate decreases. It can be observed that the highest gradient of the maximum static temperature is between $\phi = 0.3$ and $\phi=0.2$; this is due to the increased reaction rate, due to the increase of OH radicals, as shown in the figure.13 (c) between primary and secondary air, and this is in agreement with the decrease in length and thickness of the flame, when the ϕ is decreased; this is showed in Figure.4-4[124].

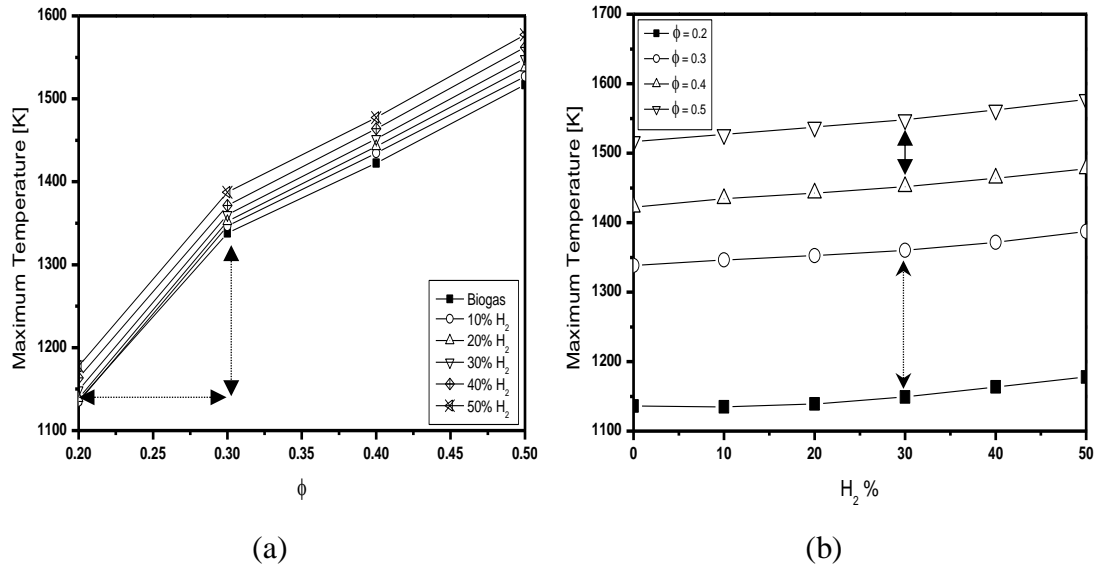
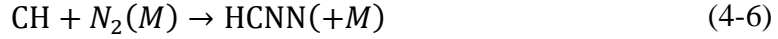


Figure 4-8 Maximum static temperature profiles (a) at different ϕ s (b) at different hydrogen concentrations (H₂%)

4.5 Effects of H₂ addition, and equivalence ratio on NO emissions

The impact of the biogas-H₂ blend on the distribution of NO emissions is shown in Figure 4-9. The addition of hydrogen leads to an increase in the flame temperature and will promote the formation of NO substantially in the injection zone. Thus, it can be seen at $\phi=0.2$; the NO is formed, peaked, and slightly reduced along the axis, while at $\phi = 0.5$, it maintained constant. It may be due to the increase in the equivalence ratio and the weak effect of the secondary air extended into the flame inside the chamber. It is an essential factor in the formation of NO-thermal and NO-prompt, or the formation of HCN, C₂H₂. It can also be observed that the creation of NO is better for ϕ equal to 0.2. Peak NO varies as the amount of H₂ in biogas increases from 10 to 50% by volume. This could explain that the addition of H₂ decreases the NO-prompt because the CH concentration is reduced, and because of the effect of the triple-bond contained in the formation of NO-prompt mechanism





The different routes for NO_x formation are determined by the broken down of the triple-bond of N₂ molecule, whereas the NO-thermal increases due to the higher temperature in this flames as is shown in figure 4-11(a)[124].

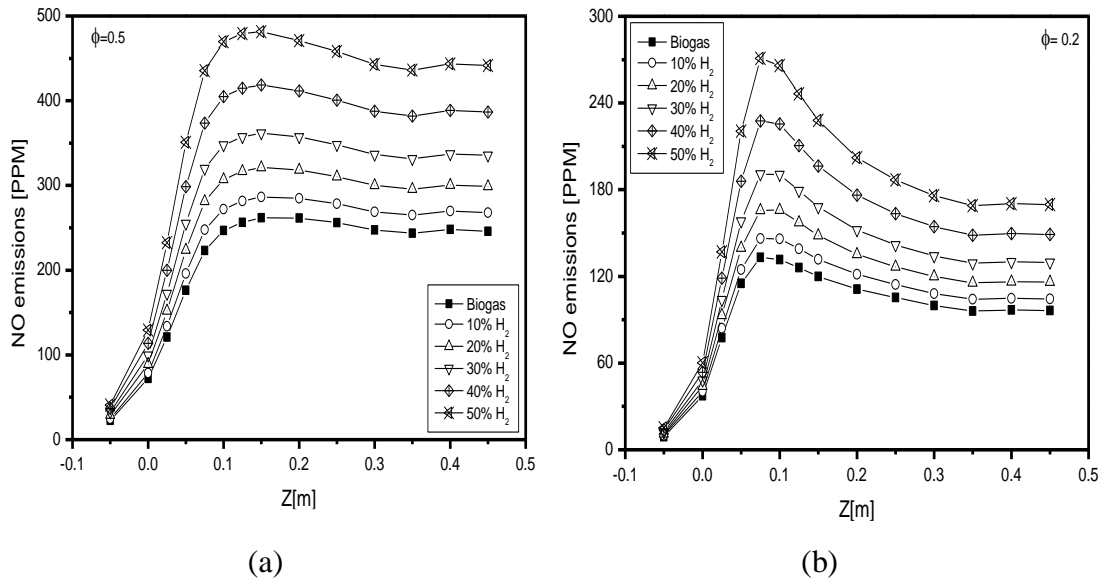


Figure 4-9 Axial NO emissions profiles at different hydrogen concentrations (a) $\phi=0.5$, (b) $\phi=0.2$.

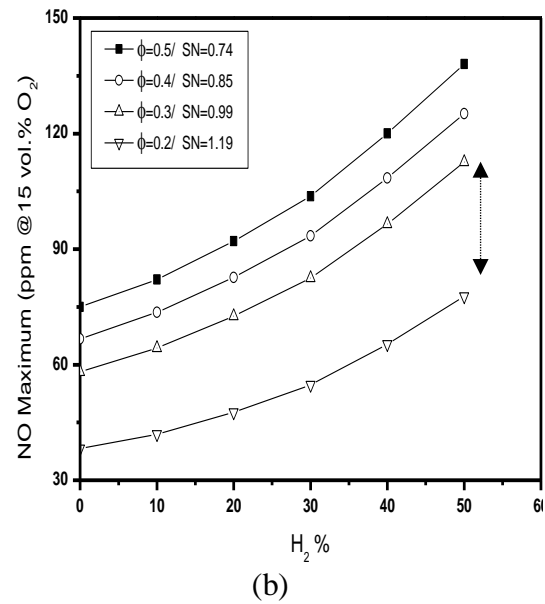
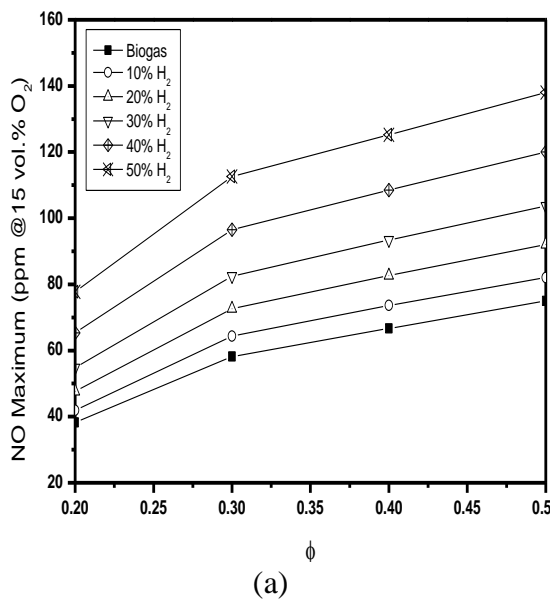
Figure.4-10 (a, b) displays the distribution of the maximum NO emissions for different values of H₂ added to the biogas and different equivalence ratios. It can be seen that the maximum magnitude of NO (ppm @ 15 vol. % O₂) increases with the increase in the hydrogen concentration in the biogas and with the increase in the equivalence ratio from 0.2 to 0.5. A critical observation is that NO emission is lower at a low H₂ enrichment % and low ϕ . According to the literature, NO decreases with increasing the swirl number [166–168], and due to the perfect premixing of the fuel-air. Then, the NO_x is going to be reduced, as displayed in Figures 4-10.

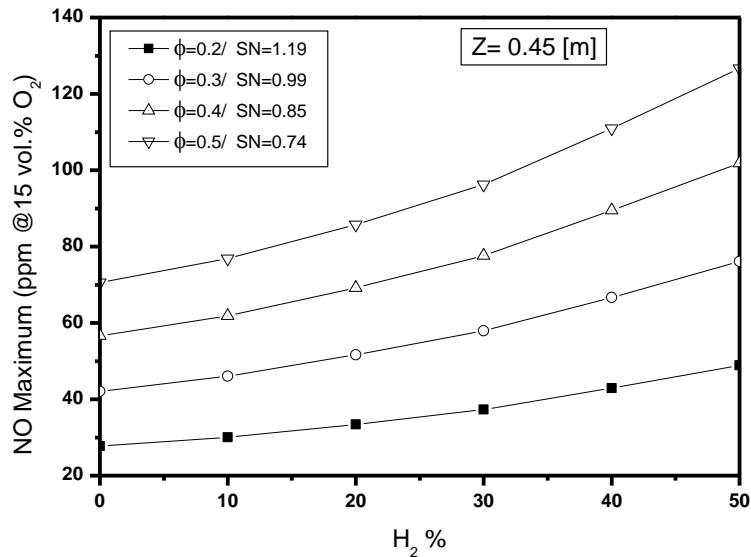
Figure 4-10 (c) shows the maximum NO emissions in the outlet chamber (ppm @15 vol.% O₂), The optimum of the equivalence ratio and the hydrogen enrichment are identified from this figure. It can be observed that the lower NO emissions values are recorded for the pure biogas combustion (0.0% H₂). In comparison, NO increases from

(28 to 70 ppm) at ($\phi=0.2$ to 0.5), with an average value of 49.38 ppm @15 Vol.% O_2 . This value is close to the case of 50% H_2 /biogas at $\phi=0.2$ with its temperature equal 1175K. Therefore, this mixture can be considered the optimal fuel for the can-type combustor. At $\phi \leq 0.4$, and below 30% H_2 (less than 77.8238 ppm @15 Vol.% O_2), which is also acceptable with temperature less than 1450 K, that because the NO_x level ≤ 75 ppm at @15 Vol.% O_2 is correspond to the New Source Performance Standards (NSPS) of the united states required for any gas turbine engine utility [169]. Therefore, the optimal mixtures will help flame stabilization, consistent power output, and low NO emissions, similar to what is usually achieved by the gas turbine engine fuels. Also, these temperatures can produce a reasonable output power as well as it will reduce the turbine blade cooling requirement.

Table 4-3 NO maximum emissions in the outlet chamber (ppm @15 vol.% O_2)

	Biogas	10% H_2	20% H_2	30% H_2	40% H_2	50% H_2
$\phi=0.2$	28.0829	30.5699	33.9896	38.0311	43.3161	49.2228
$\phi=0.3$	42.3834	46.4249	52.0207	58.2383	66.943	76.5803
$\phi=0.4$	56.6839	61.9689	69.7409	77.8238	89.9482	102.383
$\phi=0.5$	70.3627	76.8912	85.9067	96.4767	110.777	126.943
Average	49.3782	53.9637	60.4144	67.6424	77.7460	88.7822





(c)

Figure 4-10 Maximum NO emissions profiles at different hydrogen concentrations (a) at different ϕ s (b) at different hydrogen concentrations (H_2 %) and (c) different (H_2 %) at $Z=0.45m$

The thermal and prompt NO emissions profiles are displayed in Figure 4-11. The NO thermal used the reaction ($O + N_2 \rightarrow N + NO$) (4-8), and the NOx formation is determined by how N_2 is broken down, and the hard part of NO formation is not the intermediate species forming NO or NO_2 . The hardest part of NOx formation is to break the triple bond of the N_2 molecule. In this case, to estimate the different NO mechanisms, each mechanism was isolated by disabling only those breaking down N_2 in each route. For example, for NO, there are three reactions as follows:



In order to determine the thermal NO, the reaction (4-8) should be disabled. Because the intermediate species through other NO routes will still be generated and follow these reactions [29,170,171]. And it has been confirmed in Figure 4-11(c); where it can observe that match the result of the use of three reactions, and when using a single reaction (4-8). NO thermal increases as hydrogen in the biogas mixture increases from 0% to 50% by volume at $\phi=0.5$, due to the higher flame temperature displayed in figure 4-7 (a), whereas the NO prompt decreases after injection zone, and this because of the reduction in the CH concentration, as discussed in the context of Figure 4-9[124].

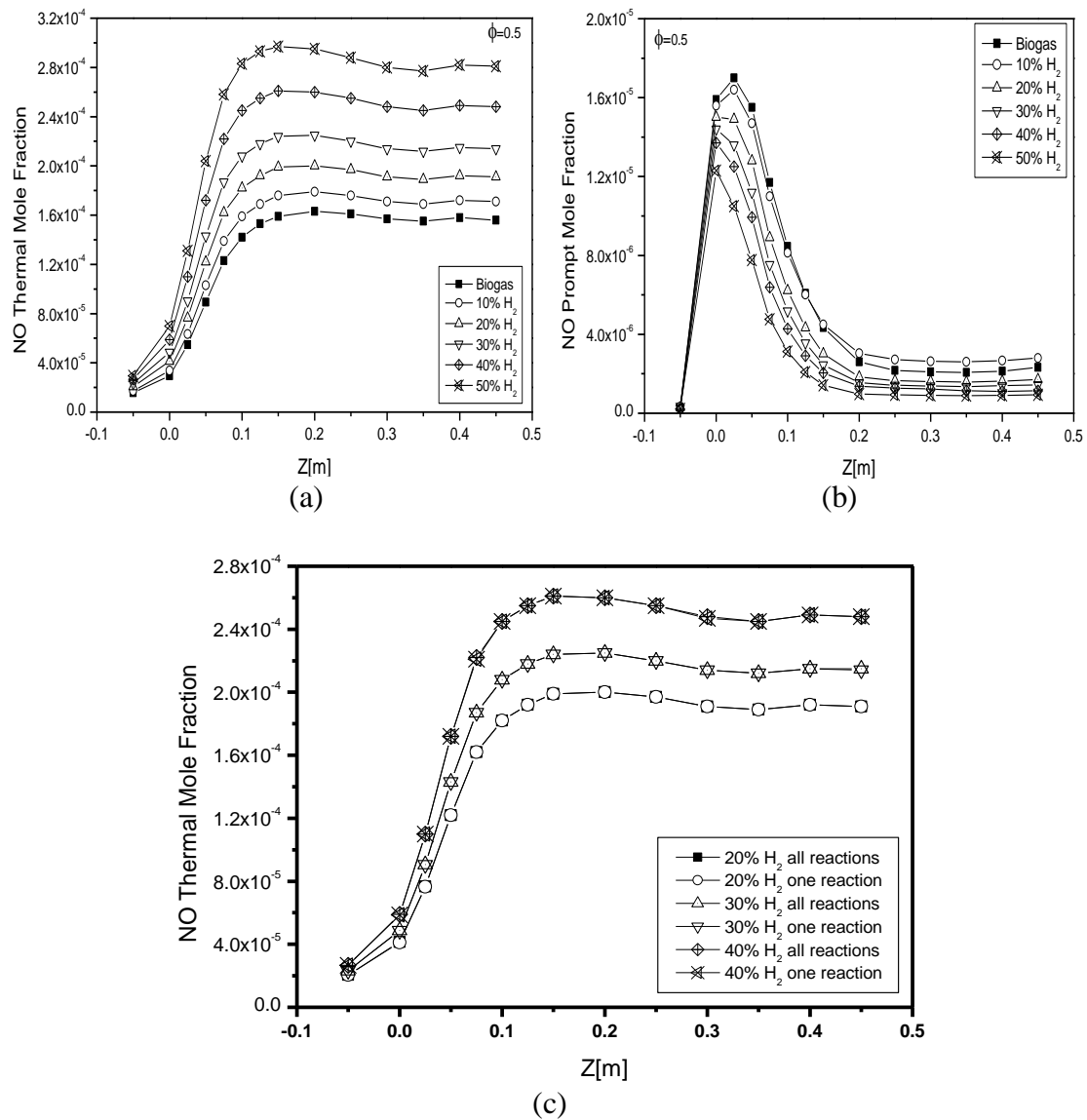


Figure 4-11 Axial NO mole fraction profiles (a) NO thermal and (b) NO prompt (c) comparison the reaction of NO thermal

4.6 Effects of H_2 addition on CO and CO_2 emissions

Figure 4-12 demonstrates the CO and CO_2 concentrations along the central axis of the combustor. It can be seen that the CO formation increases in the primary zone; this is due to incomplete combustion of fuel in the primary-zone; then, CO emissions are decreasing until the chamber outlet. The considerable reduction of CO emissions in the second reaction zone may be attributed to the increase in the OH radical, which favors the oxidation of CO to CO_2 . On the other hand, the cooling effect of the secondary air will reduce CO_2 emissions, which implies a reduction in CO emissions. Thus, decreasing CO_2 emission is due to the diminution of CO emission and due to the impact of cooling from the secondary air punctures. As also seen in this figure, CO_2 emission decreases with the hydrogen rate increases in the fuel mixture. The percentage of CO

reduces dramatically with the addition of hydrogen. This can mainly be due to two reasons, initially, because of the strain rate, the quantity of the carbon in the fuel mixture decreases with increasing hydrogen rate. Furthermore, the addition of hydrogen makes OH concentration increases in the flame, which is the dominant radical for CO mole fraction, and these results agree with figure 4-13 (c). It can also be seen that the % CO₂ decreases when the hydrogen increases because of reducing carbon composition in the fuel[124].

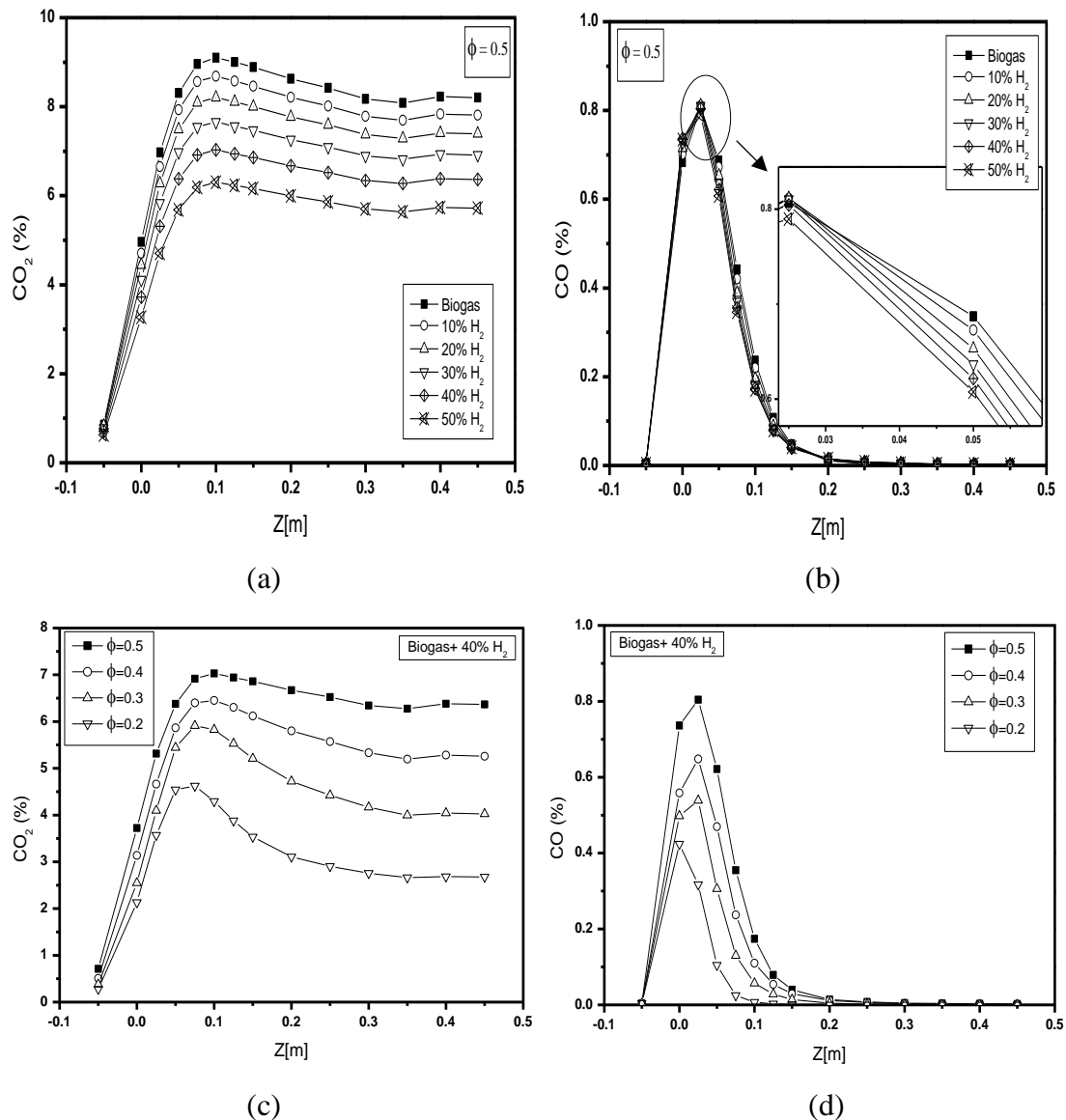
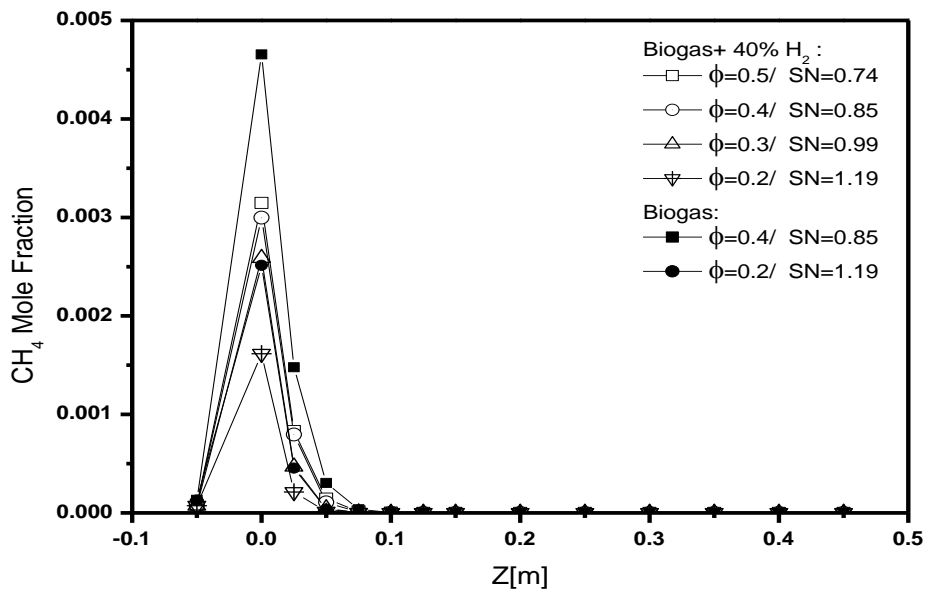


Figure 4-12 Axial concentration of CO₂ and CO profiles (a,b) at different H₂%, and $\phi=0.5$ (c,b) at 40 H₂ % and different ϕ s.

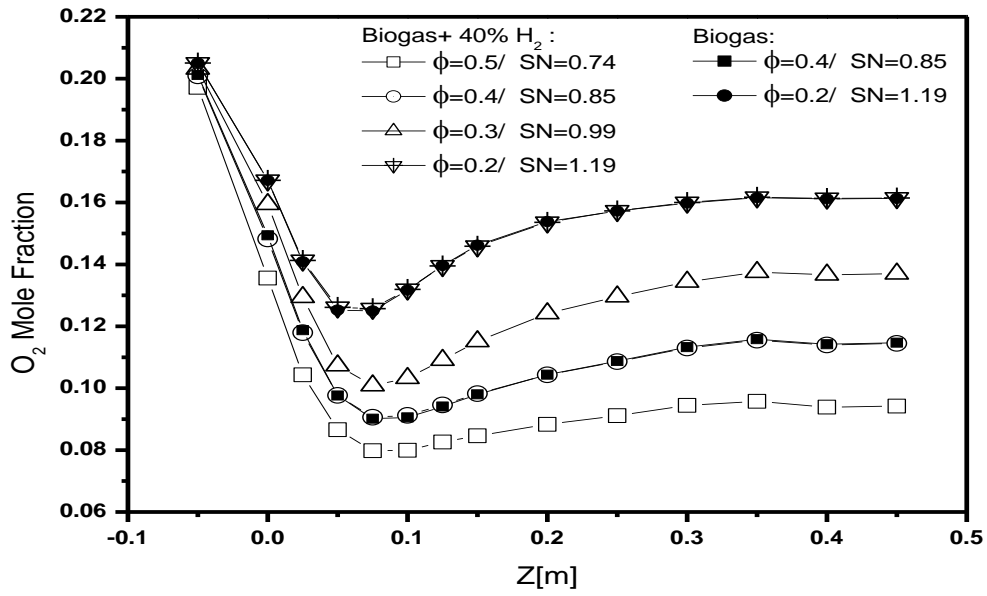
4.7 Effects of the equivalence ratio on CH₄, H₂, OH, and O₂

The profiles of CH₄, H₂, OH, and O₂ mole fractions of hydrogen-biogas mixture combustion are presented in Figures 4-13. In the case of biogas +40% H₂, the mole

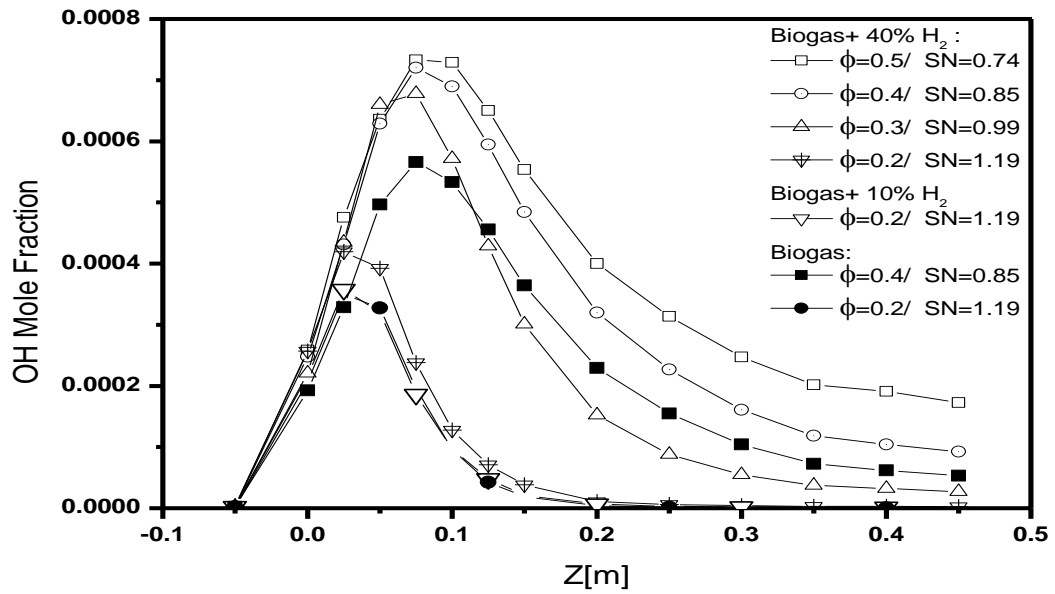
fraction of CH₄ and H₂ peaks near to the injector zone for ϕ equal to 0.5 and decreasing with the axial distance. Furthermore, the hydrogen enrichment leads to an essential increase in the radicals H and OH in the mix. Moreover, the effect of hydrogen mixing on the O₂ mole fraction is studied. In zone near to the secondary air, it is noted that the mole fraction of O₂ started to increase, whereas there is a reduction in CH₄; from that, we concluded that the hydrogen has an essential effect on the reaction zone and therefore is having an important impact on the flame thickness. A comparison is made between the pure biogas and biogas+40% H₂ mixture and is presented in Figures 4-13. In figure 4-13 (a), It can observe that the CH₄ mole fraction for pure biogas is more than the case of 40% H₂, and this makes sense because, pure biogas contains 60% CH₄, and only 36% CH₄ for the biogas doped by 40% H₂. The OH mole fraction represents the flame macrostructure, which peaks close to the inlet section at which the flame is stabilized, as in figure 4-13 (c). Whereas, it can be observed from figure 4-13 (d) that the H₂ mole fraction for pure biogas is less than 40% H₂ addition. This is because pure biogas does not contain hydrogen in its compositions. As for the ratio of hydrogen is caused by interactions between the compositions[124].



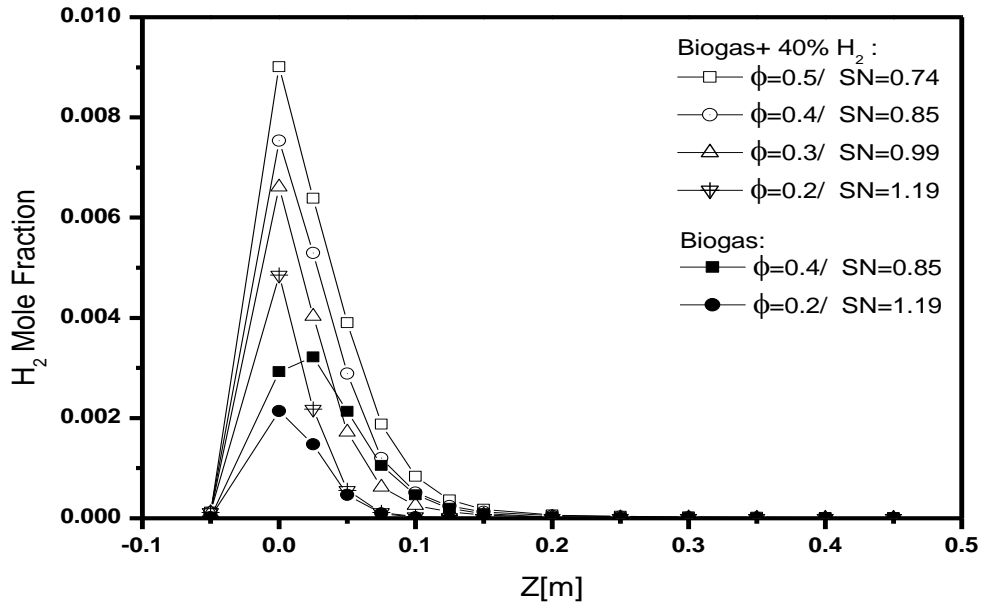
(a)



(b)



(c)



(d)

Figure 4-13 Axial mole fractions profiles at different ϕ s, and 40 H₂ % of (a) CH₄ mole fraction (b) O₂ mole fraction (c) OH mole fraction, and (d) H₂ mole fraction

4.8 Hydrogen Biogas Combustion Characteristics Computation Data Validation

4.8.1 Computation Validation of Ignition Delay

The low-temperature oxidation associated with the fuel initial fuel decomposition is characterized by the ignition delay time. This is an essential performance parameter that may lead to pre-ignition (cool flames and knocking in IC engines), proper ignition, and no ignition. For the purpose of validation, standard methane and air mixture is used with the dilution of different percentages of CO₂. The ignition delay obtained from the computational prediction is compared with the experimental data taken from the existing literature of Zeng et al. [172]. The shock tube was used to obtain the ignition delay for this mixture as reported by Zhang et al. [173,174]. The ignition delay (in microseconds on log-scale) is plotted against the 1000 times the unburned gas temperature (per K), which is the usual practice in combustion researchers, and is shown in Figure 4-14. The symbols represent experimental data of Zeng et al. [172] whereas lines represent computation predictions. Both experiments and predictions suggest that ignition delay shortens with an increase in temperature. However, for the same temperature, an increase in CO₂ leads to prolong delay in ignition. Present computational predictions obtained using GRI mech 3.0 are in remarkably well agreement with the experiments [143].

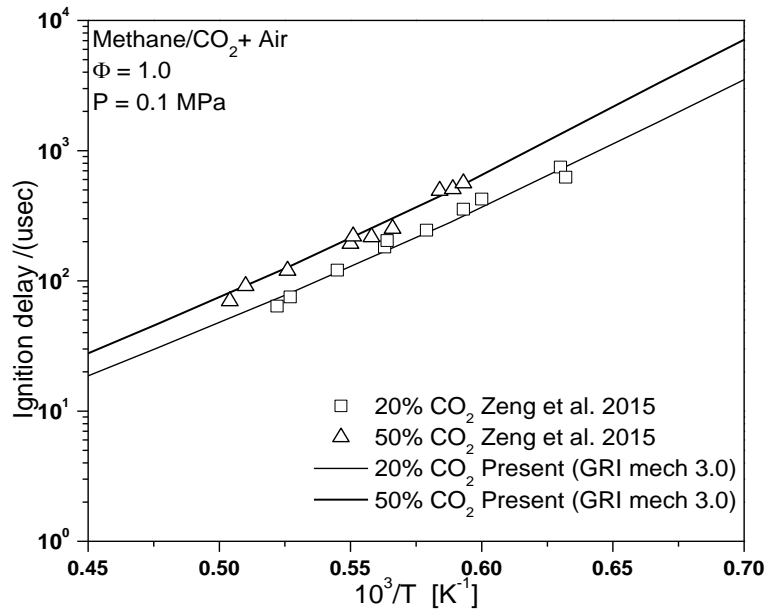


Figure 4-14 Comparison of ignition delay prediction with experiments for stoichiometric CH₄/CO₂-air mixture at unburned pressure of 0.1 MPa. Symbols: experiments; lines: computations

4.8.2 Laminar flame velocity at ambient conditions

As explained in the previous chapter, laminar flame speed LFS is a fundamental quantity depicting the burning intensity. The GRI mech 3.0 which was successfully validated for the ignition delay is tested for the LFS predictions using the experimental data of Yadav et al. [27]. They measured the LFS of biogas air mixtures blended with different hydrogen percentages at STP. The LFS is plotted against the mixture equivalence ratio as can be seen in Fig. 4-15. The open symbols represent present computational predictions of GRI mech 3.0 and other symbols represent experimental data of Yadav et al. [27]. A closer look into the graph concludes that flames near stoichiometry propagate fastest and slows down on both sides of stoichiometry. Pure biogas air mixture propagates with a maximum speed of around 20 cm/s. The addition of hydrogen makes the propagation faster. For example, the addition of 40% hydrogen to the stoichiometric biogas mixture enhances the speed from 20 cm/s to 44.8 cm/s. All these observation can also be witnessed with the prediction results. This confirms that present numerical simulation domains, models, and mechanisms are convincingly validated and can be utilized for further investigations [143].

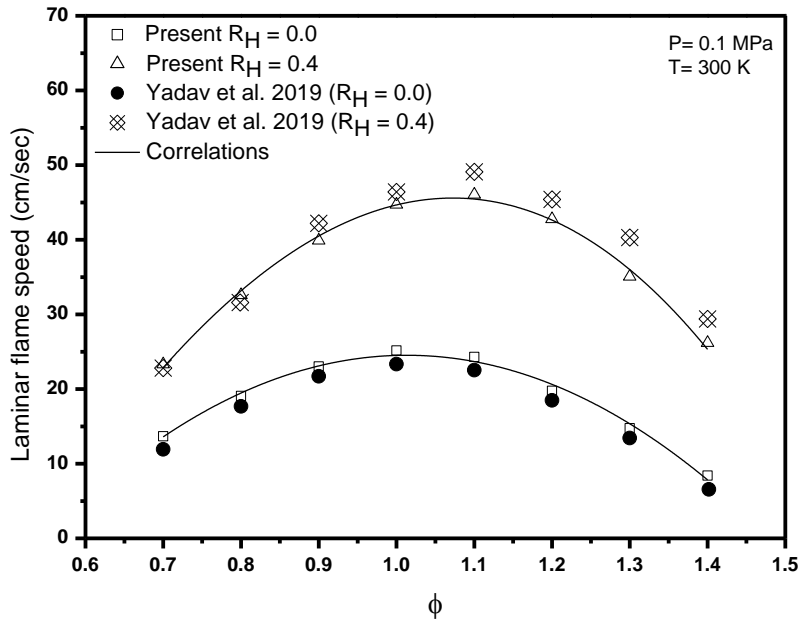
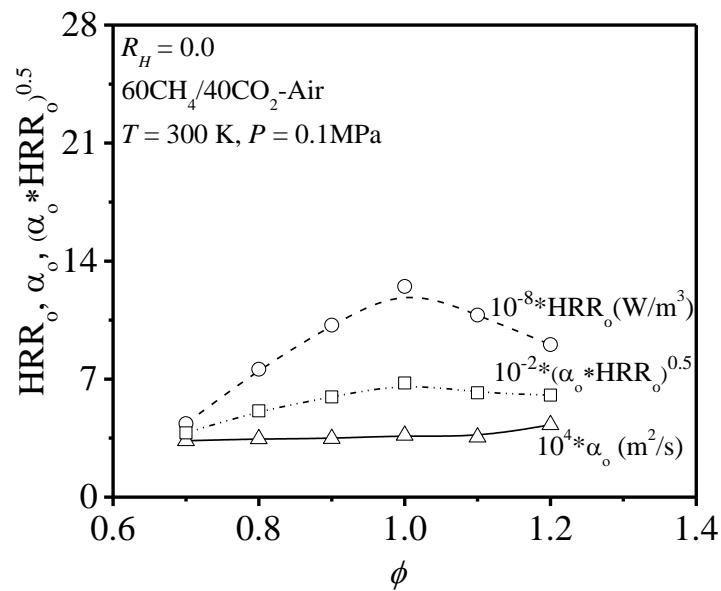


Figure 4-15 Laminar flame speed vs equivalence ratio for hydrogen added biogas air mixtures at STP

The enhancement in the LFS due to hydrogen addition can be associated to the high radical pool formation and significantly high heat release rates. The heat release rates (HRR_o), average thermal diffusivity (α_o), and $\sqrt{\alpha_o HRR_o}$ are plotted against the mixture equivalence in Figs 4-16 (a) and (b) for biogas air and 40% hydrogen added biogas air mixture respectively [143].



(a)

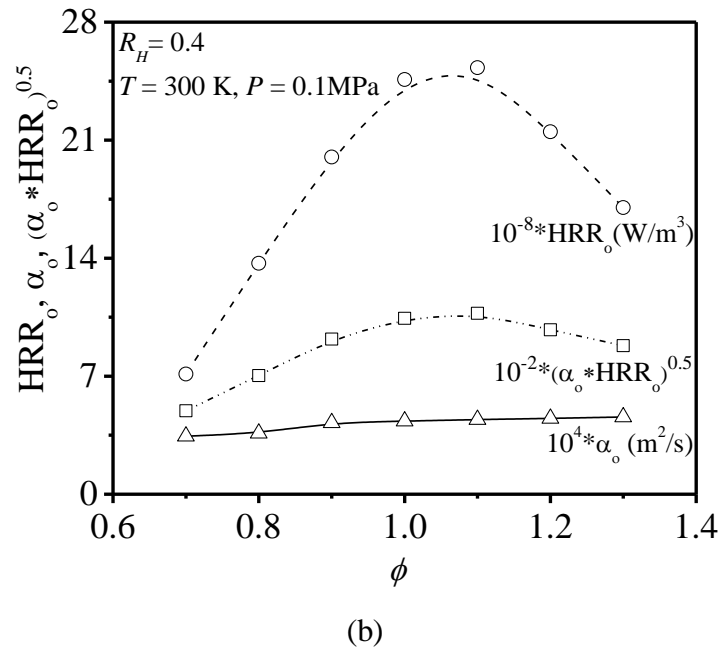
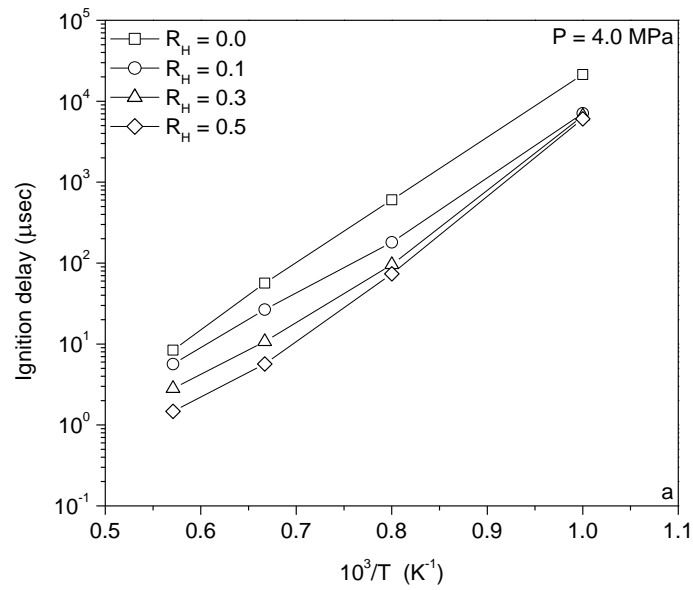


Figure 4-16 Variation of average thermal diffusivity (α_o), (HRR_o) and $\sqrt{\alpha_o HRR_o}$ vs equivalence ratio for (a) $R_H = 0$ (b) $R_H = 0.4$

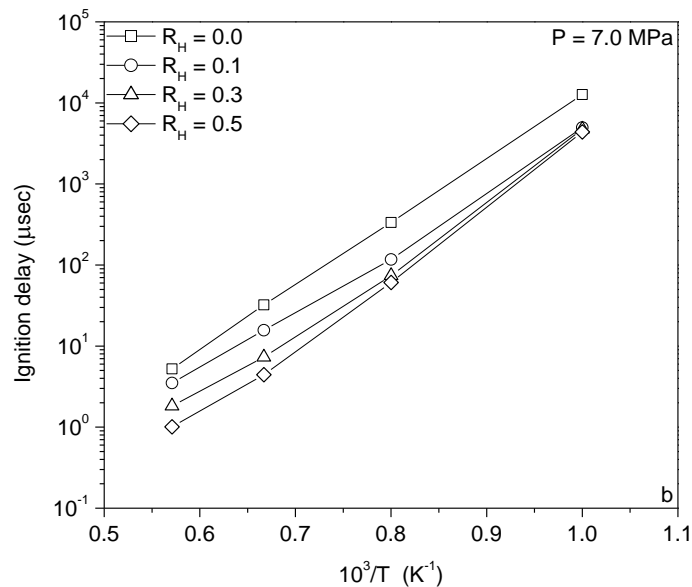
For biogas air rich mixtures, α_o and heat release rate varies in opposite ways. However, for $R_H = 0.4$ rich mixtures, α_o and HRR both varies in likewise manner. The product factor $\sqrt{\alpha_o HRR_o}$ found to dictate the increment and decrement of flame speed with equivalence ratio [143].

4.9 Ignition delay

The ignition delay time (in microsecond with log-scale) plotted against the 1000 times the unburned gas temperature reciprocal (A usual practice by combustion researchers) in Figs. 4-17 (a) 4 MPa and (b) 7 MPa respectively for different biogas+hydrogen air mixtures [143].



(a)



(b)

Figure 4-17 The biogas+hydrogen ignition delay time at (a) 4 MPa and (b) 7 MPa

The ignition delay shortens with the increase in unburned gas temperature for all mixtures. This shortening in delay time with initial temperature is higher for higher addition of hydrogen. For same unburned gas temperature and mixture composition, ignition delay is shortened for high initial pressure as can be seen. The H abstraction and formation of radical pool are the main corroborators in deciding the ignition delay as pointed by Hu et al. [175].

The H radical chain branching reactions (for instance $H + O_2 \leftrightarrow O + OH$) are predominantly responsible for ignition delay (refer to Hu et al. [175] for details), the change in concentration of H radical explains the variation in ignition delay (τ_i). Figure 4-18 shows the comparison of variation in mole fraction of H-radical (X_H) with normalized induction time (t/τ_i) with the increase in hydrogen percentage in biogas/hydrogen-air mixture at initial $P = 4$ MPa and $T = 1000$ K. The induction time is normalized using the corresponding ignition delay (τ_i) of a given fuel-oxidizer mixture [143].

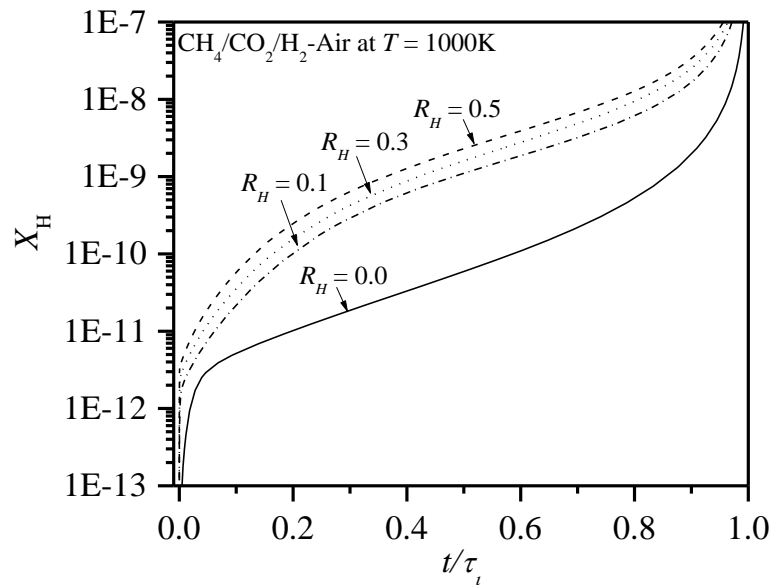


Figure 4-18 Comparison of variation in mole fraction of H-radical (X_H) with normalized induction time (t/τ_i) with increase in hydrogen percentage in biogas/hydrogen-air mixture at initial $P = 4$ MPa and $T = 1000$ K.

The data shows that the highest percentage increase in H radical mole fraction is observed with the initial 10 % hydrogen mixing ($R_H = 0.1$) in the biogas-air mixture. For instance, if we take one condition for normalized induction time (say $t/\tau_i = 0.5$) for comparison, X_H increase by 17.3 times ($6.23e^{-11}$ to $1.08e^{-09}$) with the initial 10 % hydrogen mixing ($R_H = 0.1$) in the biogas-air mixture. This leads to maximum reduction (~ 3.1 times of pure biogas-air mixture) in ignition delay time (τ_i) for only 10 % hydrogen mixing in the mixture. The next 20 and 40 % increase in hydrogen in the mixture ($R_H = 0.3$ and 0.5) leads to minimal change in X_H (~ 1.5 - 2 times increase at $t/\tau_i = 0.5$) in comparison to first 10 % hydrogen mixing (17.3 times increase at $t/\tau = 0.5$). Hence, no significant improvement in ignition delays (τ_i) were observed with for cases $R_H = 0.3$ and 0.5 in comparison to $R_H = 0.1$.

For high-temperature ignition conditions (1800 K), ignition delay shows a continuous improvement with an increase in hydrogen percentage in the mixture. Figure 4-19 shows the comparison of variation in mole fraction of H-radical (X_H).

Figure 4-19 shows the comparison of variation in mole fraction of H-radical (X_H) with normalized induction time (t/τ_i) with the increase in hydrogen percentage in biogas/hydrogen-air mixture at initial $P = 4$ MPa and $T = 1800$ K [143].

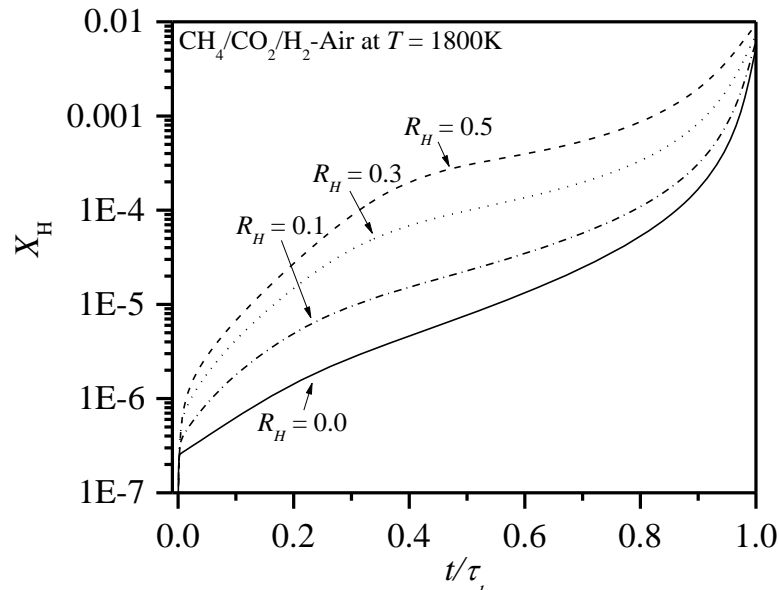
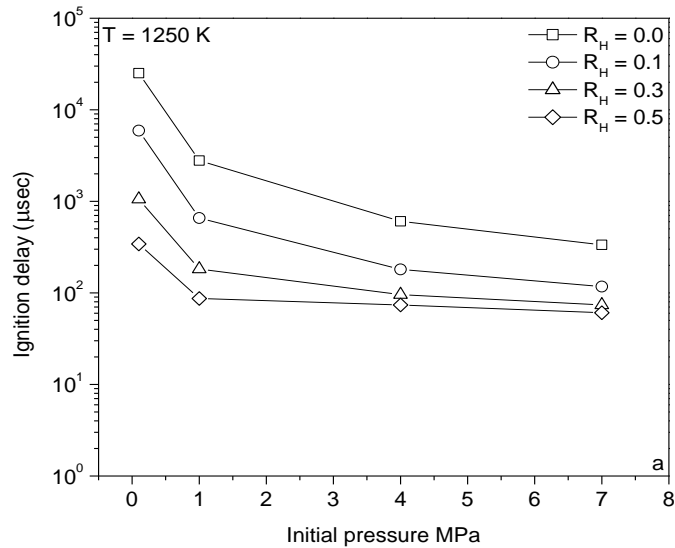
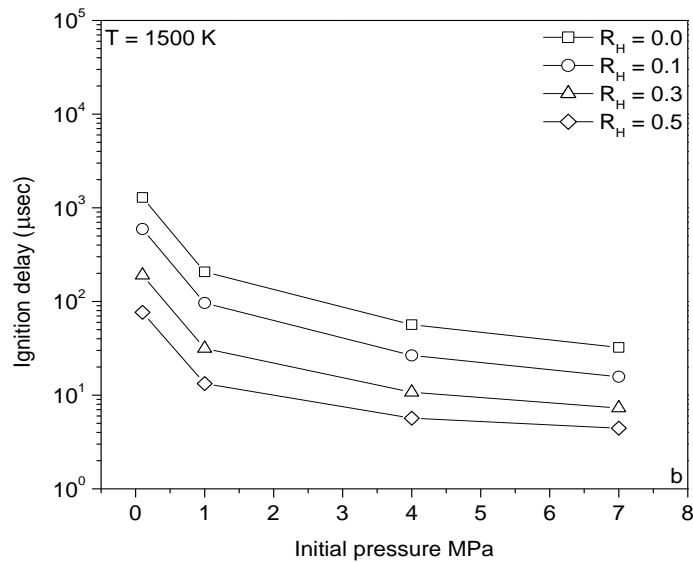


Figure 4-19 Comparison of variation in mole fraction of H-radical (X_H) with normalized induction time (t/τ) with increase in hydrogen percentage in biogas/hydrogen-air mixture at initial $P = 4.0$ MPa and $T = 1800$ K.

The data shows that the H radical mole fraction increases significantly with an increase in hydrogen mixing in the mixture reducing the ignition delay timing. Thus, ignition delay time shows significant improvement with hydrogen mixing at the unburned temperature of 1800 K. These observations on ignition delay are consistent with the earlier works of Aravind et al. [17] on the hydrogen mixing to hydrocarbon fuels. The next ignition delay comparison was performed for four stoichiometric biogas/hydrogen-air mixtures under two fixed temperature conditions ($T = 1250$ and 1500 K) [143].



(a)



(b)

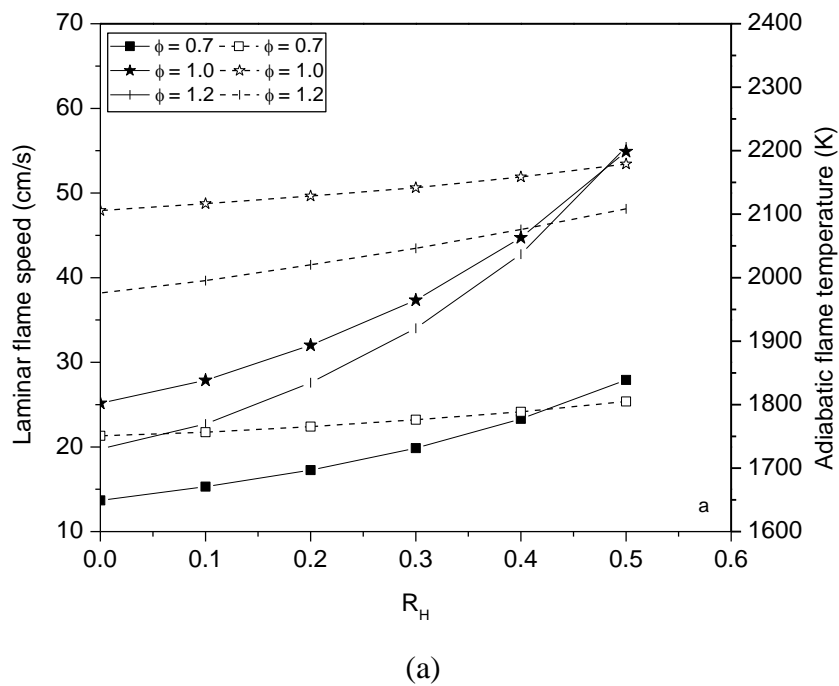
Figure 4-20 Variation of ignition delay with an increase in hydrogen fraction added to biogas-air mixture at stoichiometric conditions against the unburned pressure (a) $T = 1250$ K (b) $T = 1500$ K

Figures 4-20a and 4-20b show the ignition delay of biogas/hydrogen-air stoichiometric mixtures with increasing unburned pressure at two different unburned temperatures ($T = 1250$ and 1500 K). A substantial shortening of ignition delay is observed from 0.1 MPa to 1.0 MPa. The slope of ignition delay decreases with further enhancement of unburned pressure for all the mixtures showing a reduction in the improvement of ignition delay time. So, from these results is it inferred that for a particular biogas/hydrogen-air mixture under high-pressure conditions (≥ 7 MPa), ignition delays become weakly coupled with unburned pressure. The data shows that

the addition of 10–50 % of hydrogen mixing has improved the ignition delay timing by 3 to 30 times in comparison to pure biogas-air mixtures [143].

4.10 Laminar flame velocity at ambient condition

Figures 4-21a and 4-21b show the variation of laminar flame velocity (S_u), adiabatic flame temperatures (T_{ad}) and their corresponding normalized values for three different biogas/hydro-air mixtures ($\phi = 0.7, 1.0, \text{ and } 1.2$) at ambient conditions ($T = 300 \text{ K}$ and $P = 0.1 \text{ MPa}$). In the Figs. 4-21a and 4-21b dashed line with open symbols represent temperature and continuous line with close symbol represents laminar flame velocity [143].



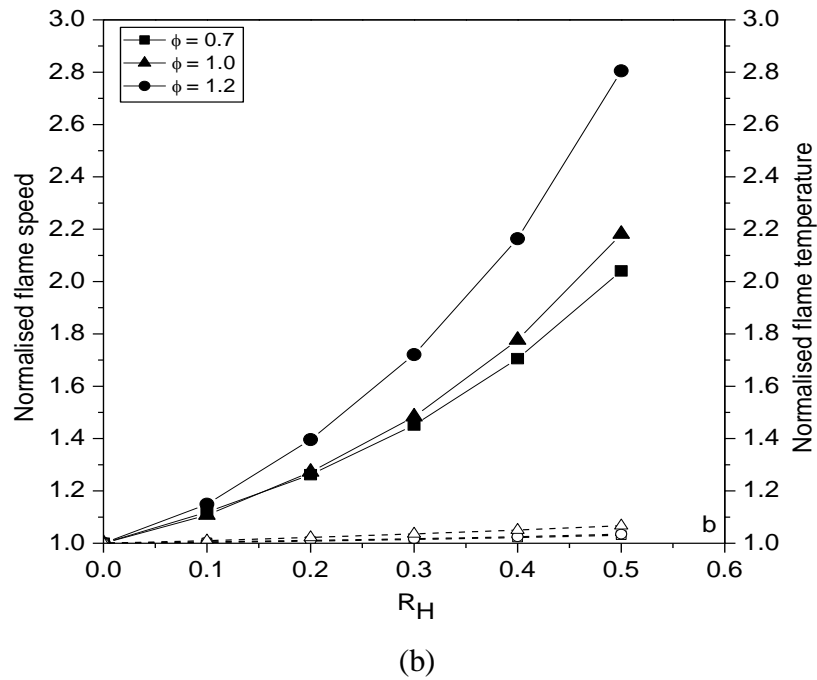
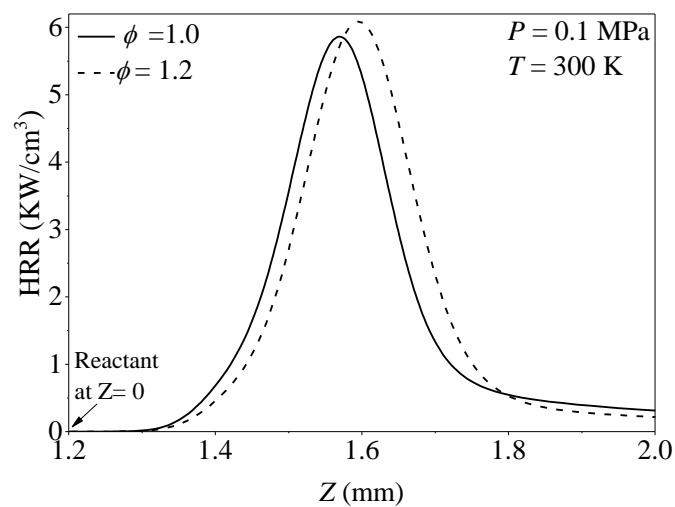
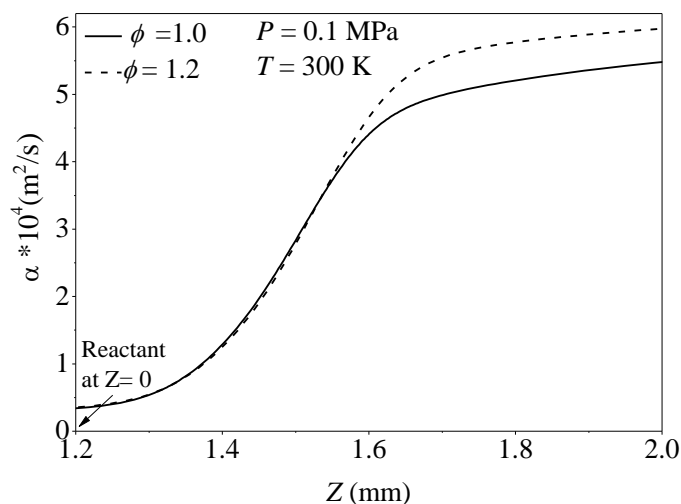


Figure 4-21 Variation of laminar flame velocity (S_u), normalized laminar flame velocity (left axis, filled symbols, and continuous lines), adiabatic flame temperature (T_{ad}) and the normalized flame temperatures (right axis, open symbols, and dash lines) of biogas-air mixtures

The data show that both the laminar flame velocity (S_u) and adiabatic flame temperature (T_{ad}) increases with increase in hydrogen fraction in biogas/hydrogen-air mixtures. The data shows that the S_u for the rich mixture ($\phi = 1.2$) and stoichiometric mixture ($\phi = 1.0$) increase with hydrogen mixing and intersect close to $R_H = 0.5$. Figures 4-22a and 4-22b show the variation of heat release rate profile (HRR) and thermal diffusivity (α) along the flame thickness for two equivalence ratios ($\phi = 1.0$ and 1.2) at $R_H = 0.5$ for ambient conditions ($P = 0.1$ MPa and $T = 300$ K) [143].



(a)



(b)

Figure 4-22 Variation of heat release rate profile (HRR) and thermal diffusivity (α) along with the flame thickness for two equivalence ratios ($\Phi = 1.0$ and 1.2) at $R_H = 0.5$ for ambient conditions ($P = 0.1$ MPa and $T = 300$ K)

The data shows that both release rate (HRR) and thermal diffusivity (α) increases for the rich case ($\phi = 1.2$) in comparison to the stoichiometric case at $R_H = 0.5$ for ambient conditions ($P = 0.1$ MPa and $T = 300$ K). The comparison of the average heat release rate (HRRo) for these two cases shows an increment of 10 % (3.2 to 3.52 kW/cm³) with an increase in equivalence ratio from 1 to 1.2. Also, the average thermal diffusivity (α) increases by 25 % (3.56 to 4.44 cm²/s) with the increase in equivalence ratio from 1 to 1.2. Since laminar flame velocity is proportional to the square root of product thermal diffusivity and heat release rate, the overall effect is that laminar flame speeds have a larger value for rich hydrogen mixtures ($\phi = 1.2$) at $R_H = 0.5$ (refer to Fig. 4-16b for more details) [143].

Adiabatic flame temperature (T_{ad}) exhibits a direct impact on the S_u of mixtures through Arrhenius rate parameters in the kinetics mechanism. It is observed that the addition of hydrogen increases flame temperature by 5–7%. The data shows an enhancement in the adiabatic flame temperature by 54 K, 73 K, and 133 K with an increase in R_H from 0 to 0.5 in mixtures for $\phi = 0.7$, 1.0, and 1.2, respectively. It is therefore inferred that the hydrogen mixing has a profound effect on adiabatic flame temperature (or heat release rate) and laminar flame velocity for the range of fuel-oxidizer mixtures studied. Figure 4-21b show that for the equivalence ratio of $\phi = 0.7$, the adiabatic flame temperature tends to a maximum of 1800 K at $R_H = 0.5$, which is the limit for starting of thermal NO_x production. It is observed from Fig. 4-21b that the normalized laminar flame

velocity increases for the equivalence ratio of 0.7, 1.0, and 1.2 by 20 %, 28 %, and 22 %, respectively [143].

4.11 Laminar flame velocity at elevated unburned pressure

Figures 4-23 a-d show the dependence of the laminar flame velocity on the mixture's unburned pressure. Figure 4-23a shows the data at ambient conditions ($P = 0.1$ MPa and $T = 300$ K) explained in detail in the previous section 4.11. Figures 4-23 b-d shows the laminar flame velocity (S_u) data at unburned temperature (T) of 300 K for three different pressures (1.0, 4.0, and 7.0 MPa) with different values of hydrogen mixings. The correlation developed matches closely with the experiments and computations for the range of conditions studied [143].

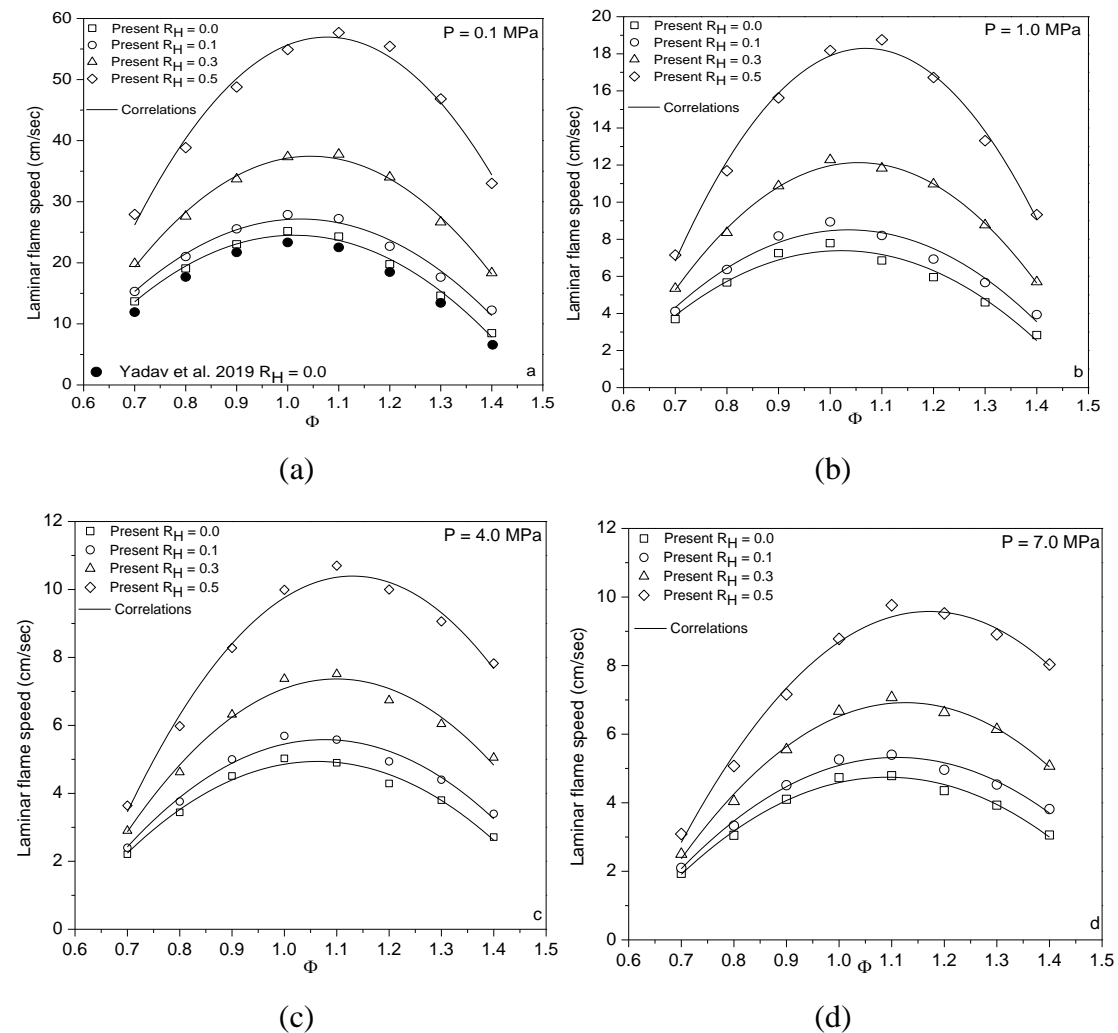


Figure 4-23 The laminar flame velocity with increase in hydrogen fraction added to biogas-air mixtures for various elevated pressures (a) $P = 0.1$ MPa (b) $P = 1.0$ MPa (c) $P = 4.0$ MPa (d) $P = 7.0$ MPa and $T = 300$ K. Symbols: computations; lines: correlations

The data shows that maximum laminar flame velocity increases by 2 to 3 times of the pure biogas-air mixture with 50 % addition of hydrogen at the four pressure conditions studied. But, the laminar flame velocity (S_u) drops by 4 to 6 times the ambient conditions values with the increase in unburned pressure from 0.1 to 7 MPa. For 50 % hydrogen mixing, maximum flame velocity decreases from 54.9 cm/s to less than 10 cm/s with increase in unburned pressure from 0.1 to 7 MPa. This decrease in (S_u) with an increase in pressure can lead to the extinction of the flame inside the engine or gas turbine combustors with heat lost to the walls. The problem of reduced laminar flame velocity at elevated pressure leading to flame extinction should be resolved by increasing the unburned temperature of the biogas/hydrogen-air mixture (refer to section 4.13 for more details). As the unburned pressure increases, the influence of hydrogen found to be diminishing slightly for all equivalence ratios and significantly for stoichiometric fuel-air mixtures. The next part presents these results in more detail.

The flame velocity for $R_H = 0.0$ and $R_H = 0.4$ at an unburned temperature of 300 K different elevated pressures is plotted against the equivalence ratios in Figs. 4-24a and 4-24b. It is observed that the maximum flame velocity shifts towards the richer mixtures as the unburned pressure is varied from 0.1 MPa to 7.0 MPa. The laminar flame velocity is observed to decrease non-linearly with the increase in unburned pressure for both of these mixtures [143].

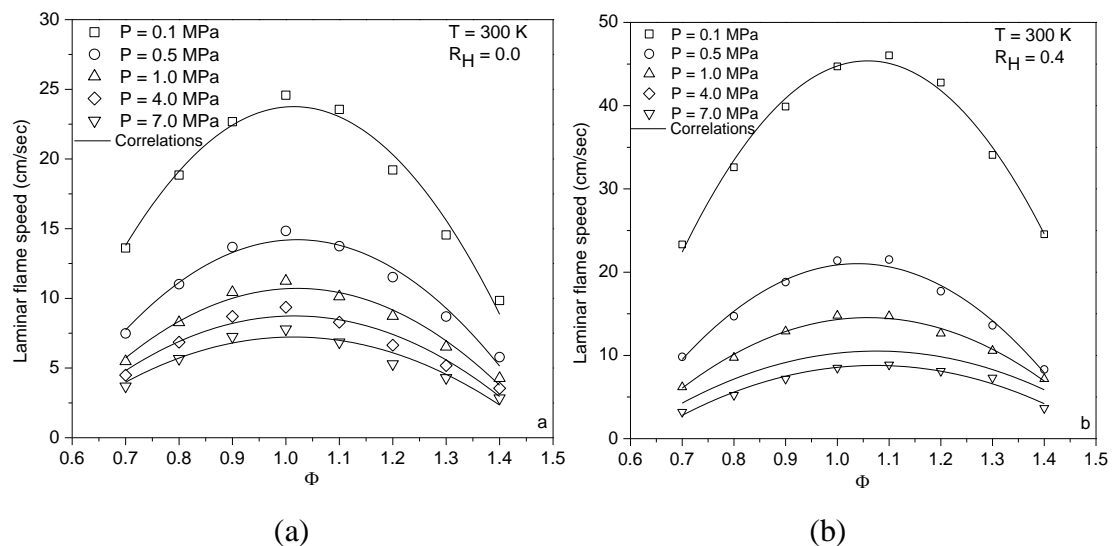


Figure 4-24 The laminar flame velocity of hydrogen added biogas air mixtures for various elevated pressures (a) $R_H = 0.0$ (b) $R_H = 0.4$ at 300 K. Symbols: present computation; lines: present correlation

The pressure exponent of the power-law equation is found to vary non-linearly with equivalence ratio for all the mixtures as shown in Fig. 4-25. The data suggest that mixtures near the stoichiometric conditions ($\beta \sim 0.48-0.52$) are least dependent on the pressure compared to highly lean ($\beta \sim 0.56-0.64$) and rich mixtures ($\beta \sim 0.6-0.7$). The curvature of the β curves reduces with the increase in hydrogen fraction. Thus reducing the difference between magnitudes of pressure exponent (β) at different equivalence ratios. Hence, the pressure dependency of flame velocity goes on decreasing with the addition of hydrogen into biogas-air mixtures. Similar conclusions with hydrogen mixing in the fuel-oxidizer mixture are also drawn from the recent studies of Konnov et al. [42], Goswami et al. [176]. To further explore the reason for this pressure dependence of S_u on unburned pressure, sensitivity analysis is performed in terms of elementary reaction rates [143].

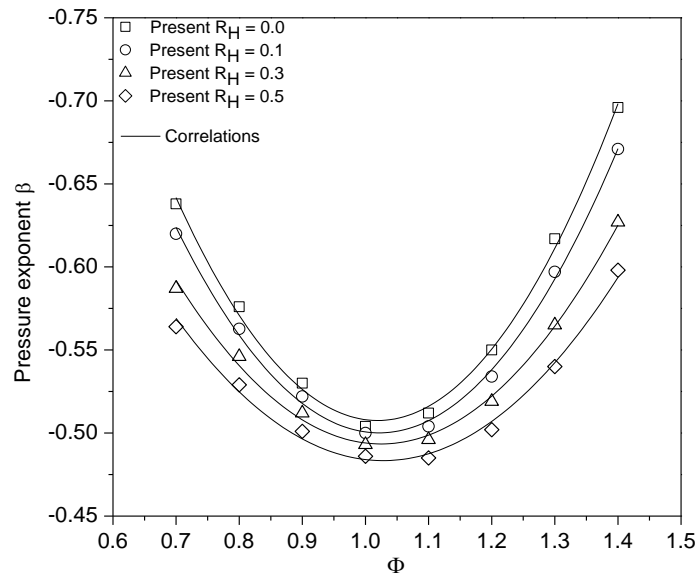


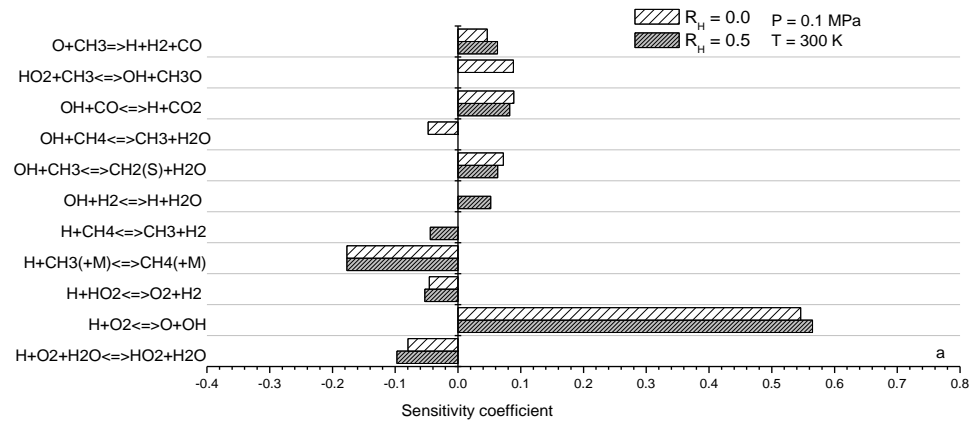
Figure 4-25 Variation of pressure exponent (β) against equivalence ratio for various biogas/hydrogen-air mixtures

The sensitivity coefficient (σ) used for the sensitivity analysis is given as follows.

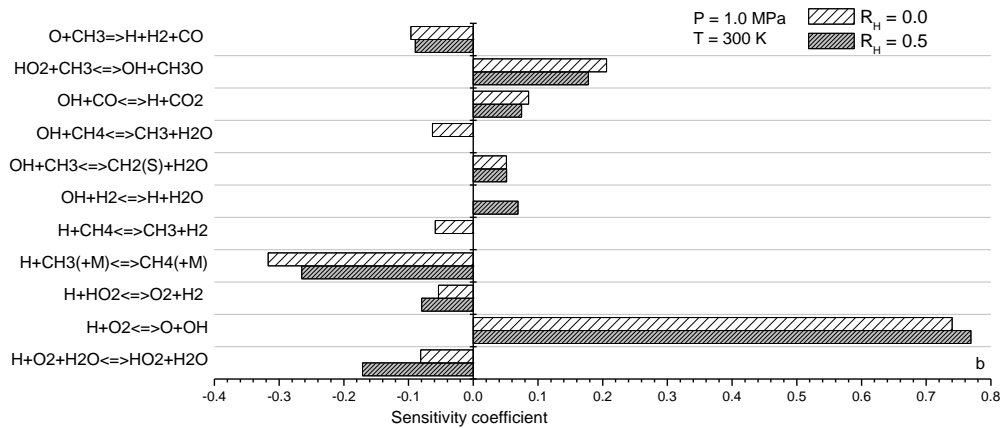
$$\sigma = \frac{d \ln S_u}{d \ln A_i} \quad (4-11)$$

In the above Eqn. 4-11, S_u is the laminar flame velocity, and (A_i) is the pre-exponential factor for the chemical reaction i . Figures 4-26a and 4-26b show the value of reaction rate sensitivity coefficient for eleven important elementary reactions for biogas/hydrogen-air mixture at two pressure conditions. These calculations were performed for pure biogas-air ($R_H = 0.0$) and biogas/hydrogen-air ($R_H = 0.5$)

stoichiometric mixtures at two different unburned pressure of 0.1 MPa and 1.0 MPa [143].



(a)



(b)

Figure 4-26 Comparison of sensitivity coefficient (σ) of important reaction pathways for hydrogen added to biogas-air stoichiometric mixtures at $T = 300$ K and (a) $P = 0.1$ MPa (b) $P = 1.0$ MPa, respectively

The H radical consumption reactions ($H + CH_3(+M) \leftrightarrow CH_4(+M)$, $H + O_2 \leftrightarrow O + OH$, and $H + O_2 + H_2O \leftrightarrow HO_2 + H_2O$) are slightly dominant with higher sensitivity coefficients for hydrogen mixing cases at all unburned pressures.

The reaction $OH+H_2 \leftrightarrow H+H_2O$ is observed to appear only for the hydrogen added biogas mixtures at these two pressures. Hence, the $OH+H_2 \leftrightarrow H+H_2O$ reaction is the main reaction for the increase in H-radical concentration with the addition of hydrogen in the biogas-air mixture for the two pressure conditions studied [143].

The chain branching reaction ($\text{H} + \text{O}_2 \leftrightarrow \text{O} + \text{OH}$) is accelerated by the reaction $\text{OH} + \text{H}_2 \leftrightarrow \text{H} + \text{H}_2\text{O}$. The chain branching reaction ($\text{H} + \text{O}_2 \leftrightarrow \text{O} + \text{OH}$) is also observed as the most sensitive reaction. This leads to the formation of highly reactive OH radical which enhances the flame velocity with the addition of hydrogen. The higher production of OH radical is also evident from the reaction $\text{HO}_2 + \text{CH}_3 \leftrightarrow \text{OH} + \text{CH}_3\text{O}$ having a significant contribution at high pressures. The data shows that this reaction is absent at ambient pressure but contributes significantly at high pressure for hydrogen added biogas-air mixtures. The other important observation made was 1.5 to 2 times increase in the negative sensitivity coefficient for the third body reaction $\text{H} + \text{CH}_3 \leftrightarrow \text{CH}_4(+\text{M})$. The negative sensitivity coefficient of the third body included reaction $\text{H} + \text{CH}_3(+\text{M}) \leftrightarrow \text{CH}_4(+\text{M})$ increases with pressure and will lead to the retardation of flame velocity at elevated pressures [143].

4.12 Laminar flame velocity at the elevated unburned temperature

Figures 4-27a and 4-27b show the variation of the laminar flame velocity of pure biogas and biogas+40% H_2 -air mixture for a range of equivalence ratios (0.7-1.4) and temperatures (300-600 K) at 0.1 MPa (symbols represent computations and lines represents the proposed correlations). The laminar flame velocity at 400 K for $R_H = 0.4$ is closed to 40–65 cm/s which is in between the S_u values for iso-octane and n-decane at 400 K[42]. The laminar flame velocity of biogas/hydrogen-air mixture at higher temperatures (300–600 K) is about 1.8 to 2 times of pure biogas-air mixtures[143].

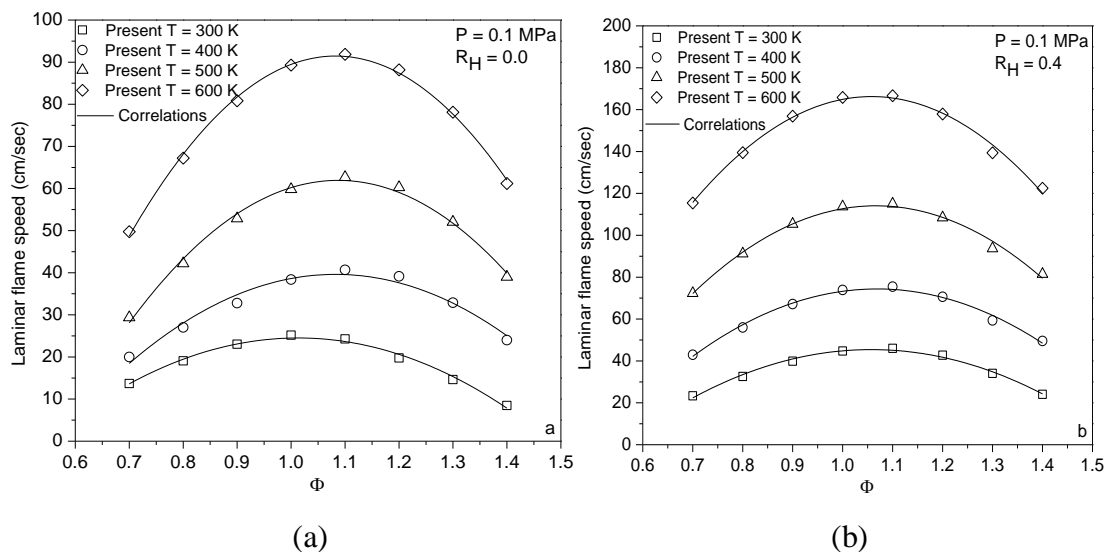


Figure 4-27 The laminar flame velocity of (biogas/hydrogen)air mixtures at elevated temperatures for (a) $R_H = 0.0$ (b) $R_H = 0.4$ at 0.1 MPa. Symbols: computations; lines: correlations

Temperature exponent (α) quantitatively represents the enhancement of the flame velocity with the increase in unburned temperature. Higher the value of α , higher is the contribution of unburned temperature in the enhancement of flame velocity. Figure 4-28 shows the temperature exponent (α) of different mixtures of biogas with addition of hydrogen. The temperature exponent (α) value is least near the stoichiometric mixtures and rises on both sides (rich and lean mixtures) [143]. This is conformal with the variation of temperature exponent (α) of other hydrocarbons[42,152,153].

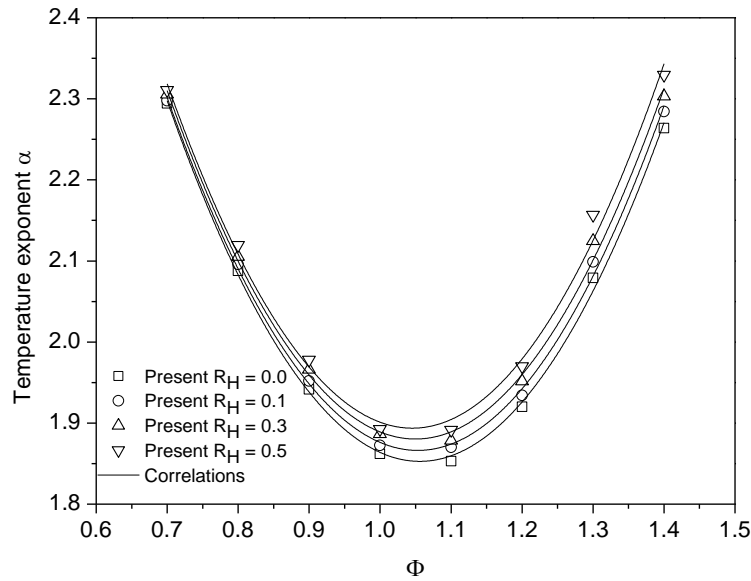


Figure 4-28 Variation of temperature exponent (α) against equivalence ratio for various biogas/hydrogen-air mixtures

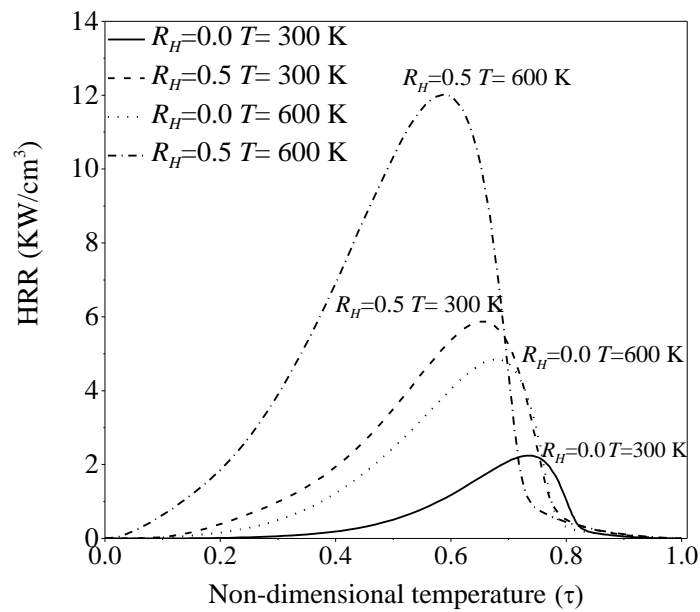
4.13 Flame structure of biogas/hydrogen-air mixtures at elevated unburned temperatures

The increase in the unburned temperature of the mixture affects the flame structure. This influence is understood using heat release rate (HRR) and important major/minor species variations with an increase in unburned temperature. A non-dimensional temperature is a useful parameter to understand the unburned temperature effect which is defined by Eqn. 4-12

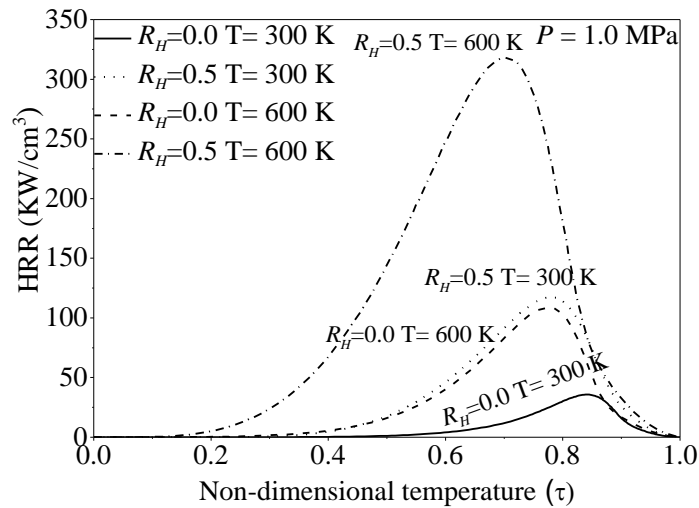
$$\tau = \frac{(T_i - T)}{(T_i - T_{ad})} \quad (4-12)$$

In the above Eqn. 4-12, T is the unburned temperature, T_i instantaneous temperature, and T_{ad} adiabatic flame temperature (for details on the analysis used refer to Mohammad and Juhany[177]). Figures 4-29a and 4-29b demonstrate the variation of the volumetric heat release rate for different stoichiometric mixtures against non-

dimensional temperature. These data were obtained for elevated pressure and temperature conditions for pure biogas-air and biogas/hydrogen-air mixtures. The biogas air stoichiometric mixture at 300 K releases the lowest amount of heat, whereas, $R_H = 0.5$ stoichiometric mixture at 600 K releases the highest amount of heat comparatively for both pressure conditions. The amount of heat release and the area under the curve escalate and shift towards the smaller non-dimensional temperature with hydrogen mixing and increase in unburned temperature. It can also be observed that the reaction zone (and flame thickness) becomes thinner with hydrogen mixing. The results show that the HRR increases with an increase in pressure for all four conditions. Hence, a reduction in laminar flame velocity with an increase in pressure should be due to a decrease in thermal conductivity and an increase in the density of the mixture under elevated pressure conditions[143].



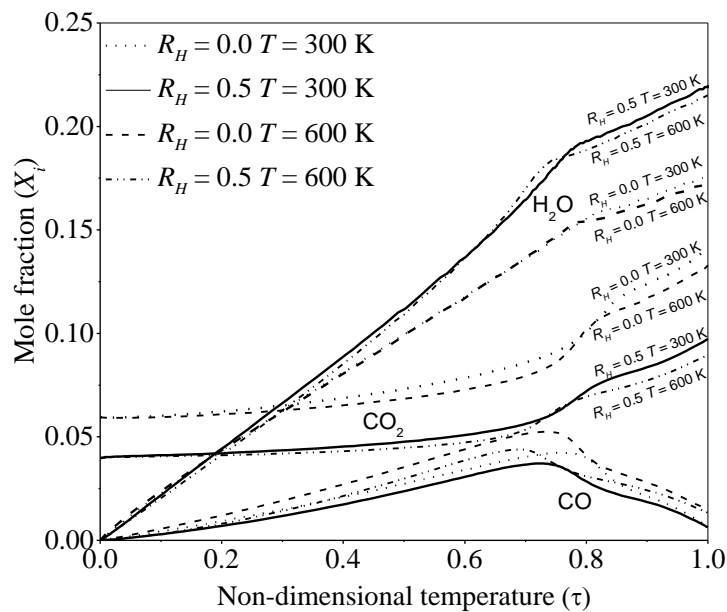
(a)



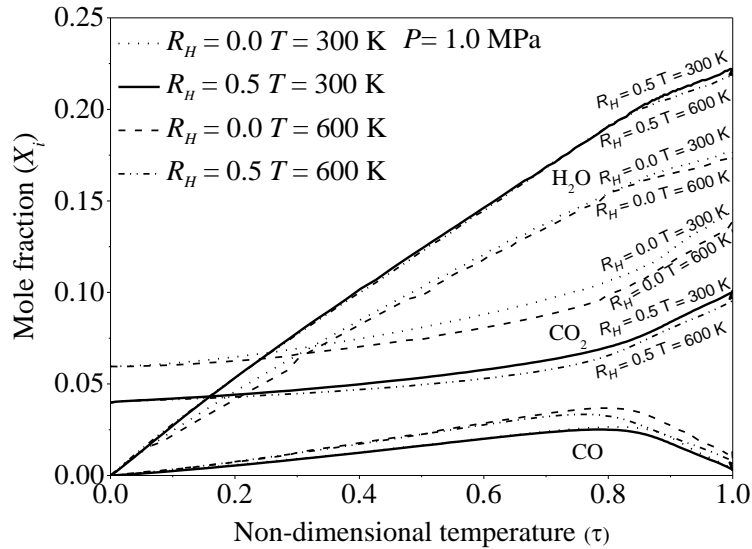
(b)

Figure 4-29 Heat release rates of biogas/hydrogen-air mixtures against the non-dimensional temperature

Figures 4-30a and 4-30b represent the variation of mole fractions of CO, CO₂, and H₂O against the non-dimensional temperature for $R_H = 0.0$ and $R_H = 0.5$ at the unburned temperature of 300 K and 600 K and unburned pressure of 0.1 MPa and 1 MPa. The data shows that the mole fractions of CO₂ decrease and that of H₂O increase with hydrogen mixing due to their participation in fuel components varies. The temperature and pressure elevation would significantly vary the amount of these species but not their mole fractions. The CO production has comparatively insignificant variations with both hydrogen mixing and unburned temperature elevation[143].



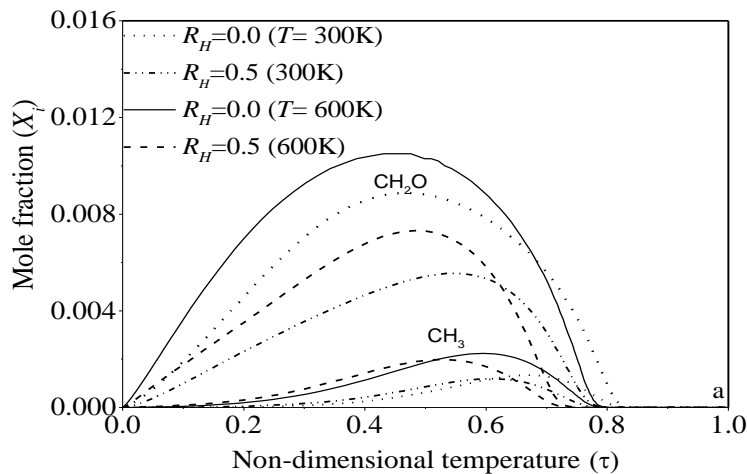
(a)



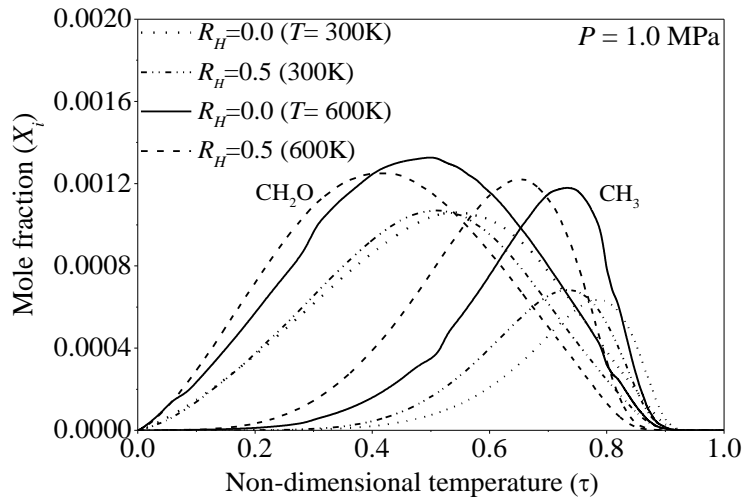
(b)

Figure 4-30 Mole fractions of major species against the non-dimensional temperature

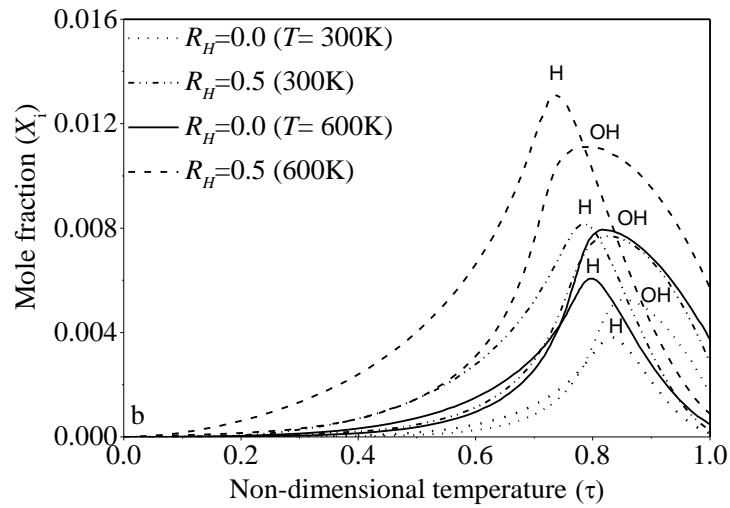
Figures 4-31(a-d) show the variation of minor species against the non-dimensional temperature for $R_H = 0.0$ and $R_H = 0.5$ at the unburned temperature of 300 and 600 K and unburned pressure of 0.1 MPa and 1 MPa respectively. The increase in hydrogen fraction and the unburned temperature has a significant influence on these species' production. This corroborates to the escalation in the flame velocity magnitudes (refer to Fig. 4-27 for details). H and OH's radical concentration increased in the flame with an increase of hydrogen fraction, leading to higher flame temperature and enhanced combustion. In contrast, the CH_2O and CH_3 mole fractions are decreased with the increase of hydrogen fraction; this indicates the possibility of reducing aldehyde emissions and reducing the formation of methyl from methane combustion when adding hydrogen[143].



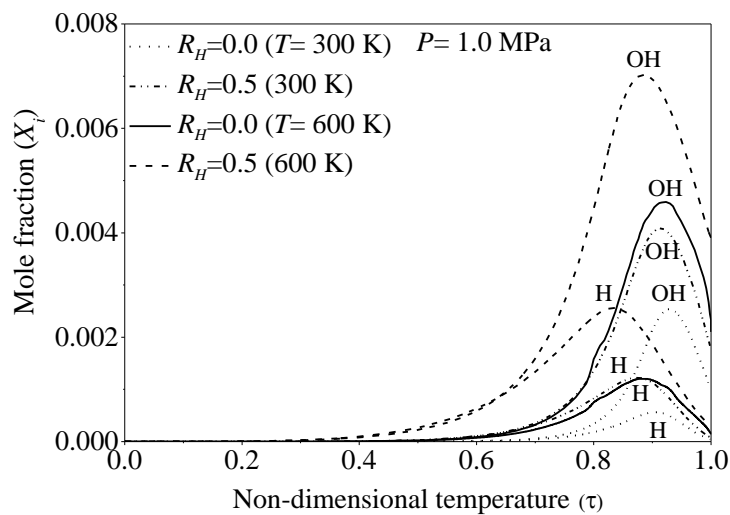
(a)



(b)



(c)



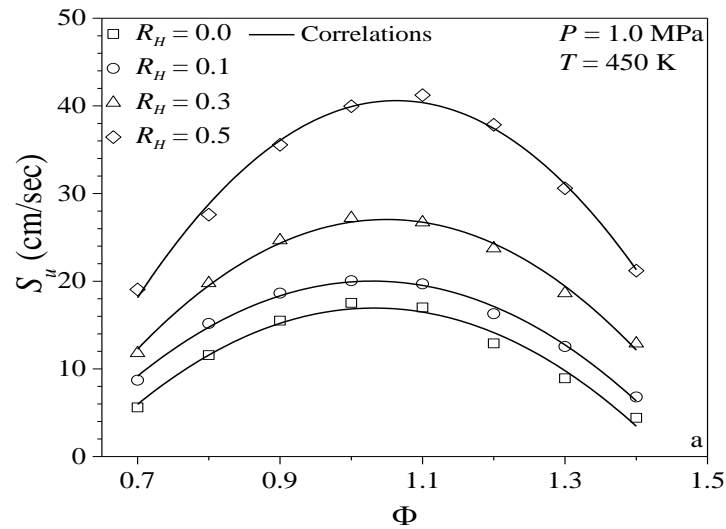
(d)

Figure 4-31 Minor species variation with the non-dimensional temperature

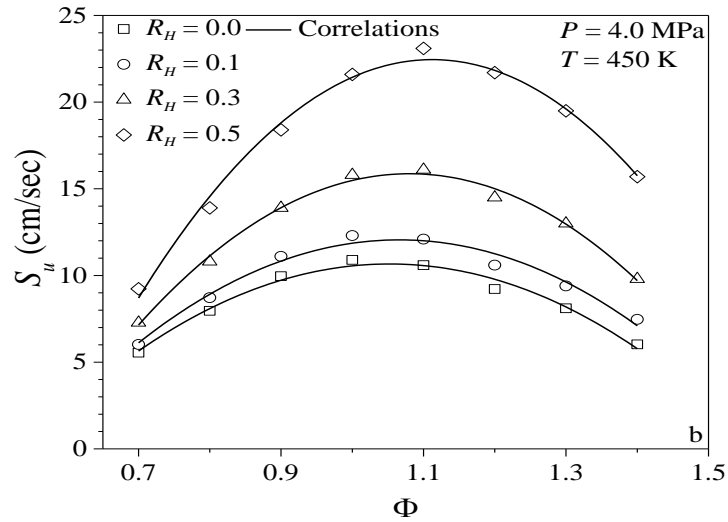
With the increase in unburned pressure (0.1 MPa to 1 MPa), a significant decrease in H radical peak (≈ 6 times) is observed for $R_H = 0.5$. This observation is in line with the sensitivity analysis study performed, which shows the importance of H radical production/consumption reactions. The last section 4.15 presents the accuracy of these correlations with the laminar flame velocity predictions at elevated temperature and pressure[143].

4.14 Laminar flame velocity at elevated pressures and temperatures combined

The results from the previous sections showed that flame velocity is significantly increased with an increase in unburned temperature and decreases with an increase in unburned pressures. Therefore it is important to address the flame speeds at combined high pressures and temperatures. This is important considering many practical combustion devices work under these elevated conditions. Figures 4-32a and 4-32b show the flame velocity at the unburned temperature of 450 K and two unburned pressures of 1.0 MPa and 4.0 MPa for biogas/hydrogen-air mixtures[143].



(a)



(b)

Figure 4-32 Variation of the laminar flame velocity of biogas/air mixtures at elevated pressure, 4.0 MPa, and fuel temperature, 450 K, for different hydrogen mixings. Symbols: computations; lines: correlations

The maximum flame velocity for $R_H = 0.0$ and $R_H = 0.5$ at 450 K are 16.2 cm/s and 42 cm/s at 1.0 MPa and 10.4 cm/s and 23.6 cm/s at 4.0 MPa, respectively. These magnitudes are much lower compared to the 24.4 cm/s and 54.9 cm/s for $R_H = 0.0$ and $R_H = 0.5$ at ambient conditions. However, the flame speeds for the mixtures between $R_H = 0.3$ – 0.5 are comparable to various liquid fuels such as n-heptane data form Konnov et al.[42].

4.15 Conclusion

The numerical investigations clear bring out the effect of hydrogen (H_2) content in the biogas mixture on the combustion characteristics. In the first part, the results indicate that hydrogen enrichment and the variation of the equivalence ratio and the swirl numbers significantly impacted the flame macrostructure. Indeed, hydrogen enrichment will increase the flame temperature, in comparison; the decrease in the equivalence ratio with high swirl numbers will decrease it. However, the NO maximum emissions in the outlet chamber have been dropped by 43 and 78 (ppm @15 vol.% O_2) for the biogas and biogas-50% H_2 , respectively, due to the reduction in the flame temperature. Almost the flame temperature and NO emissions at $\phi = 0.2$ with a high rate of hydrogen (50% H_2) are close to the results of pure biogas (0% H_2) at the same equivalence ratio. The results show that CO and CO_2 emissions decrease with increasing hydrogen concentration and decreasing the equivalence ratio; due to a

decrease in the amount of carbon, the cooling effect, and an increase in the OH concentration. In the second part, the results show that hydrogen mixing to the biogas improves both the flame speed and ignition delay. The boost in flame speed due to elevation of unburned temperature is found to be invariant hydrogen mixing. However, the extent of reduction in flame speed due to the elevation of unburned pressure is found to be a linear function of hydrogen concentration added to biogas. Furthermore, the sensitivity analysis was studied to assess the influence of hydrogen added to the biogas. The understanding of combustion characteristics of these mixtures at given initial conditions will lead to feasibility conformity, optimal blends of biogas+hydrogen, and design improvements.

CHAPTER 5

5 CONCLUSIONS

5.1 Summary

The combustion characteristics, such as temperature distributions, flame stabilization, emissions, species, laminar flame speed, ignition delay...etc of biogas-H₂ air mixture premixed and non-premixed, inside gas turbine and engine, respectively, are investigated in this thesis. In the first part of the thesis, we have presented an investigation of the effects of hydrogen blending to biogas mixture and equivalence ratio/swirl number on the stability of the flame, the temperature distribution, temperature contours, velocity streamlines contours, emissions of NO, and species concentrations. The burner power is kept constant at 60 kW, the equivalence ratio is fixed, and biogas blended with hydrogen at different concentrations (0% to 50%). The k- ϵ standard and steady laminar flamelet (SLF) models are used to study the non-premixed flame generated by the combustion of the biogas+hydrogen on the can-type combustor. The numerical model shows that the results are in good accord with available data in the literature. The most important conclusions of this study can be summarized as follows:

The addition of H₂ in biogas improves the stability of the flame as well as the emissions (which reinforces the reaction zone). The length and the thickness of the biogas flame are expanded when hydrogen is introduced to the fuel mixture, also with increasing ϕ .

The optimum proportion of hydrogen and equivalence ratio for the combustor chamber is 50% H₂ for $\phi=0.2$, with its temperature equal to 1175K. At these conditions, the flame temperature and the NO emissions are close to the results of pure biogas at the same equivalence ratio and much less for the equivalence ratio in the range of 0.3-0.5.

At $\phi \leq 0.4$ and below 30% H₂, the biogas/hydrogen mixture is acceptable and will help flame stabilization, reasonable power output, and low NO_x emissions, similar to what is usually achieved by the gas turbine engine fuels.

- ✓ The decrease in the equivalence ratio leads to an increase in the swirl number; this allows for the creation of the recirculation zone established, enhancing the flame stabilization.
- ✓ Reduces the maximum flame temperature when operating at extra-lean conditions ($\phi = 0.5$ to 0.2) with the presence of hydrogen will decrease the hot zone temperature, reducing the thermal NO_x.
- ✓ The increase in the swirl number and decrease of equivalence ratio causes a reduction in the flame macrostructure in terms of length and flame thickness. This allows the expansion of a surface area for the flame's heat exchange with the wall of the chamber, especially with the secondary air.
- ✓ Higher swirl numbers lead to improve premixing between air and fuel streams due to increasing the tangential flow velocity and the deflection of the flow from the chamber's central axis, which increases the size of the vortex in the center of the combustor.
- ✓ Zones of air dilution play an essential role in flame stabilization, which reduces NO_x and CO formation.

The second part of the thesis, was devoted to the laminar flame speed and the ignition delay of methane/biogas-air mixture blended by H₂, varying by volume from R_H (0 to 0.5), were simulated for different values of temperature, pressure, and equivalence ratio. For this purpose, the GRI mech 3.0 mechanism. The numerical validation displays that the results are in good accord with the available experimental data. The flame speed correlations of biogas+hydrogen and air mixtures for hydrogen mixing (R_H = 0.0-0.5) over a range of equivalence ratios ($\phi = 0.7$ -1.4), unburned temperatures (T = 300-600 K), and unburned pressures (P = 0.1-7.0 MPa) are reported in this paper[143]

Pure biogas is found to be the least reactive of all the mixtures studied. An enhancement of reactivity of the biogas is observed with an increase in hydrogen content. The flame speed rises with the increase in fuel amount till near the stoichiometric mixture and then falls for pure biogas mixtures. The peak drifts towards a rich mixture with an increase in hydrogen content. The boost in flame speed due to elevation of unburned temperature is found to be invariant hydrogen mixing. However, the extent of reduction in flame speed due to elevation of unburned pressure is found to be a linear function of hydrogen mixing to biogas.

Regarding crude biogas-air mixtures, flame speed is found to increase with the increase in unburned temperature and decrease in unburned pressure respectively. A nonlinear trend of flame speed variation with the mixture equivalence ratio is observed with a maximum magnitude for the slightly rich mixture. The ignition delay is also found to be dependent on the initial mixture conditions. The sensitivity analysis was studied to assess the influence of hydrogen added to the biogas. The reaction $\text{HO} + \text{H}_2 = \text{H} + \text{H}_2\text{O}$ is considered the principal reaction generating hydrogen pool, through this the hydrogen fraction increases, thus the chain branching reaction was enhanced.

The H and OH mole fractions are increased in the flame with the hydrogen fraction added; this leads to enhanced combustion, while the CH_2O and CH_3 mole fractions are decreased with the hydrogen mole fraction added, this indicates the possibility of reducing aldehydes emissions, and reducing the formation methylene from methane combustion when adding the hydrogen.

The increase in the normalized laminar flame velocity, the heat release rate, and the normalized adiabatic flame temperature with an increase in unburned temperature are due to the large production of the active roots that accelerate the combustion process.

It can be concluded that biogas with $\text{RH} > 0.3$ is comparable to various conventional fuels as their flame speed, flame structure, and ignition delay data match at various initial thermo-physical conditions.

5.2 Scope for Future Work

Using syngas as a renewable source of hydrogen and mixing it with biogas gives a good alternative for fossil fuels. This mixture can be investigated in the future, along with the thermoacoustic instabilities of gas turbine combustors.

REFERENCES

- [1] Keith DW, Holmes G, St. Angelo D, Heidel K. A Process for Capturing CO₂ from the Atmosphere. *Joule* 2018;2:1573–94.
- [2] Nemitallah MA, Rashwan SS, Mansir IB, Abdelhafez AA, Habib MA. Review of Novel Combustion Techniques for Clean Power Production in Gas Turbines. *Energy & Fuels* 2018;32:979–1004.
- [3] Lazaroiu G, Pop E, Negreanu G, Pisa I, Mihaescu L, Bondrea A, et al. Biomass combustion with hydrogen injection for energy applications. *Energy* 2017.
- [4] Diaz-Gonzalez C, Arrieta A-A, Suarez J-L. Comparison of combustion properties of simulated biogas and methane. *Ciencia, Tecnol y Futur* 2009;3.
- [5] Porpatham E, Ramesh A, Nagalingam B. Effect of compression ratio on the performance and combustion of a biogas fuelled spark ignition engine. *Fuel* 2012;95:247–56.
- [6] Rashwan SS, Nemitallah MA, Habib MA. Review on Premixed Combustion Technology: Stability, Emission Control, Applications, and Numerical Case Study. *Energy & Fuels* 2016;30:9981–10014.
- [7] Teng F. The Effect of Hydrogen Concentration on the Flame Stability and Laminar Burning Velocity of Hydrogen-Hydrocarbon-Carbon Dioxide Mixtures. University of Sheffield, 2014.
- [8] Sheffield JW. An outlook of hydrogen as an automotive fuel. *Int J Hydrogen Energy* 1989;14.
- [9] Karim GA, Wierzbka I, Al-Alousi Y. Methane-hydrogen mixtures as fuels. *Int J Hydrogen Energy* 1996;21:625–31.
- [10] El-Ghafour SAA, El-Dein AHE, Aref AAR. Combustion characteristics of natural gas–hydrogen hybrid fuel turbulent diffusion flame. *Int J Hydrogen Energy* 2010;35:2556–65.
- [11] Rohani B, Saqr KM. Effects of hydrogen addition on the structure and pollutant emissions of a turbulent unconfined swirling flame. *Int Commun Heat Mass Transf* 2012;39:681–8.

- [12] Wu L, Kobayashi N, Li Z, Huang H, Li J. Emission and heat transfer characteristics of methane–hydrogen hybrid fuel laminar diffusion flame. *Int J Hydrogen Energy* 2015;40:9579–89.
- [13] Sanusi YS, Mokheimer EMA, Shakeel MR, Abubakar Z, Habib MA. Oxy-combustion of hydrogen-enriched methane: experimental measurements and analysis. *Energy & Fuels* 2017;31:2007–16.
- [14] Hermanns RTE. Laminar burning velocities of methane-hydrogen-air mixtures. 2007.
- [15] Gersen S, evinsky LHB. Ignition properties of methane/hydrogen mixtures in a rapid compression machine. *Int J Hydrogen Energy* 2008;33.
- [16] Ji C, Wang D, Yang J, Wang S. A comprehensive study of light hydrocarbon mechanisms performance in predicting methane/hydrogen/air laminar burning velocities. *Int J Hydrogen Energy* 2017;42:17260–74.
- [17] Kishore VR, Mohammad A. Combustion characteristics of the effect of hydrogen addition on LPG-air mixtures. *Int J Hydrogen Energy* 2015;40.
- [18] Tang CL, Law CK. Determination, correlation, and mechanistic interpretation of effects of hydrogen addition on laminar flame speeds of hydrocarboneyair mixtures. *Proc Combust Inst* 2011;33.
- [19] Hui X, Zhang C, Xia M, Sung C-J. Effects of hydrogen addition on combustion characteristics of n-decane/air mixtures. *Combust Flame* 2014;161:2252–62.
- [20] Rakopoulos CD, Michos CN, Giakoumis EG. Studying the effects of hydrogen addition on the second-law balance of a biogas-fuelled spark ignition engine by use of a quasi-dimensional multi-zone combustion model. *Proc Inst Mech Eng Part D J Automob Eng* 2008;222:2249–68.
- [21] Juste GL. Hydrogen injection as additional fuel in gas turbine combustor. Evaluation of effects. *Int J Hydrogen Energy* 2006;31:2112–21.
- [22] Gupta KK, Rehman A, Sarviya RM. Bio-fuels for the gas turbine: A review. *Renew Sustain Energy Rev* 2010;14:2946–55.
- [23] Kobayashi N, Mano T, Arai N. Fuel-rich hydrogen-air combustion for a gas-

- turbine system without CO₂ emission. *Energy* 1997;22:189–97.
- [24] Hairuddin AA, Yusaf T, Wandel AP. A review of hydrogen and natural gas addition in diesel HCCI engines. *Renew Sustain Energy Rev* 2014;32:739–61.
- [25] Alrazen HA, Talib ARA, Adnan R, Ahmad KA. A review of the effect of hydrogen addition on the performance and emissions of the compression–Ignition engine. *Renew Sustain Energy Rev* 2016;54:785–96.
- [26] Zhen HS, Wei ZL, Chen ZB, Xiao MW, Fu LR, Huang ZH. An experimental comparative study of the stabilization mechanism of biogas-hydrogen diffusion flame. *Int J Hydrogen Energy* 2019;44:1988–97.
- [27] Kumar Yadav V, Ray A, Ravi MR. Experimental and computational investigation of the laminar burning velocity of hydrogen-enriched biogas. *Fuel* 2019;235:810–21.
- [28] Wei Z, Zhen H, Fu J, Leung C, Cheung C, Huang Z. Experimental and numerical study on the laminar burning velocity of hydrogen enriched biogas mixture. *Int J Hydrogen Energy* 2019.
- [29] Irvin G, Richard Y. *Combustion* 2008.
- [30] Law CK. *Combustion physics*. Cambridge university press; 2010.
- [31] Poinot T, Veynante D. *Theoretical and numerical combustion*. RT Edwards, Inc.; 2005.
- [32] Winterbone DE, Turan A. Chapter 15 - Combustion and Flames. In: Winterbone DE, Turan A, editors. *Adv. Thermodyn. Eng. (Second Ed. Second Edition, Boston: Butterworth-Heinemann; 2015, p. 323–44.*
- [33] Warneck P. Jürgen Warnatz, Ulrich Maas, Robert W. Dibble, *Combustion*, 3rd edn. *J Atmos Chem* 2002;41:315–7.
- [34] Poinot TJ, Veynante DP. *Combustion. Encycl Comput Mech Second Ed* 2018:1–30.
- [35] Peters N. Laminar diffusion flamelet models in non-premixed turbulent combustion. *Prog Energy Combust Sci* 1984;10:319–39.
- [36] Forman A. Williams. *Combustion Theory*. 2nd ed. Princeton, New Jersey: The

- Benjamin/Cummings Publishing Copmany; 1984.
- [37] Chung K. Law. Combustion Physics: Chung K. Law: 9780521154215: Amazon.com: Books n.d.
- [38] Kuo KK. Principles of Combustion. 2nd ed. Hoboken, New Jersey: John Wiley and Sons Inc.; 2005.
- [39] Wang H, Sheen DA. Combustion kinetic model uncertainty quantification, propagation and minimization. Prog Energy Combust Sci 2015;47:1–31.
- [40] Wu F, Liang W, Chen Z, Ju Y, Law CK. Uncertainty in stretch extrapolation of laminar flame speed from expanding spherical flames. Proc Combust Inst 2015;35:663–70.
- [41] Law CK, Wu F, Egolfopoulos FN, Gururajan V, Wang H. On the Rational Interpretation of Data on Laminar Flame Speeds and Ignition Delay Times. Combust Sci Technol 2014;187:27–36.
- [42] Konnov AA, Mohammad A, Kishore VR, Kim N II, Prathap C, Kumar S. A comprehensive review of measurements and data analysis of laminar burning velocities for various fuel+air mixtures. Prog Energy Combust Sci 2018;68:197–267.
- [43] Tanford C. Theory of burning velocity. I. temperature and free radical concentrations near the flame front, relative importance of heat conduction and diffusion. J Chem Phys 1947;15:433–9.
- [44] Fristrom RM, Westenberg AA. Fundamental processes and laminar flame structure. APL Tech Dig 1962;1:10.
- [45] Metghalchi M, Keck JC. Burning velocities of mixtures of air with methanol, isooctane, and indolene at high pressure and temperature. Combust Flame 1982;48:191–210.
- [46] McAllister S, Chen J-Y, Fernandez-Pello AC. Thermodynamics of combustion. Fundam. Combust. Process., Springer; 2011, p. 15–47.
- [47] Kumar S. Numerical studies on flame stabilization behavior of premixed methane-air mixtures in diverging mesoscale channels. Combust Sci Technol

- 2011;183:779–801.
- [48] Turns SR. An introduction to combustion. vol. 499. McGraw-hill New York; 1996.
- [49] Behrendt T, Lengyel T, Hassa C, Gerenda's M. Characterization of Advanced Combustor Cooling Concepts Under Realistic Operating Conditions. vol. Volume 4: Heat Transfer, Parts A and B, 2008, p. 1801–14.
- [50] Joos Hamburg (Germany). Inst. fuer Energietechnik] F [Univ. der B. Technical combustion. Technology, modelling, emissions; Technische Verbrennung. Verbrennungstechnik, Verbrennungsmodellierung, Emissionen. Germany: Springer, Berlin (Germany); 2006.
- [51] Lefebvre AH, Ballal DR. Gas turbine combustion: alternative fuels and emissions. CRC press; 2010.
- [52] Caron M, Goethals M, De Smedt G, Berghmans J, Vliegen S, Van't Oost E, et al. Pressure dependence of the auto-ignition temperature of methane/air mixtures. *J Hazard Mater* 1999;65:233–44.
- [53] Aldhaidhawi M, Chiriac R, Badescu V. Ignition delay, combustion and emission characteristics of Diesel engine fueled with rapeseed biodiesel – A literature review. *Renew Sustain Energy Rev* 2017;73:178–86.
- [54] Heywood JB. Internal combustion engine fundamentals. McGraw-Hill Education; 2018.
- [55] Hoang VN, Thi LD. Experimental study of the ignition delay of diesel/biodiesel blends using a shock tube. *Biosyst Eng* 2015;134:1–7.
- [56] Abdelhafez A, Nemitallah MA, Rashwan SS, Habib MA. Adiabatic Flame Temperature for Controlling the Macrostructures and Stabilization Modes of Premixed Methane Flames in a Model Gas-Turbine Combustor. *Energy and Fuels* 2018;32.
- [57] Ganesan V. Internal combustion engines. McGraw Hill Education (India) Pvt Ltd; 2012.
- [58] Wang Z, Liu H, Ma X, Wang J, Shuai S, Reitz RD. Homogeneous charge

- compression ignition (HCCI) combustion of polyoxymethylene dimethyl ethers (PODE). *Fuel* 2016;183:206–13.
- [59] Winterbone DE, Turan A. Chapter 17 - Gas Turbines. In: Winterbone DE, Turan A, editors. *Adv. Thermodyn. Eng. (Second Ed. Second Edition, Boston: Butterworth-Heinemann; 2015, p. 381–422.*
- [60] Sarkar DK. Chapter 7 - Gas Turbine and Heat Recovery Steam Generator. In: Sarkar DK, editor. *Therm. Power Plant, Elsevier; 2015, p. 239–83.*
- [61] Khandelwal B. Development of gas turbine combustor preliminary design methodologies and preliminary assessments of advanced low emission combustor concepts 2012.
- [62] Grech N, Koupper C, Zachos PK, Pachidis V, Singh R. Considerations on the numerical modeling and performance of axial swirlers under relight conditions. *J Eng Gas Turbines Power* 2012;134.
- [63] Noroozian R, Asgharian P. Chapter 4 - Microturbine Generation Power Systems. In: Gharehpetian GB, Mousavi Agah SM, editors. *Distrib. Gener. Syst., Butterworth-Heinemann; 2017, p. 149–219.*
- [64] Rapp V, Killingsworth N, Therkelsen P, Evans R. 4 - Lean-Burn Internal Combustion Engines. In: Dunn-Rankin D, Therkelsen P, editors. *Lean Combust. (Second Ed. Second Edition, Boston: Academic Press; 2016, p. 111–46.*
- [65] Viswanathan B. Chapter 3 - Natural Gas. In: Viswanathan B, editor. *Energy Sources, Amsterdam: Elsevier; 2017, p. 59–79.*
- [66] Awe OW, Zhao Y, Nzihou A, Minh DP, Lyczko N. A review of biogas utilisation, purification and upgrading technologies. *Waste and Biomass Valorization* 2017;8:267–83.
- [67] Bhatia SC. 17 - Biogas. In: Bhatia SC, editor. *Adv. Renew. Energy Syst., Woodhead Publishing India; 2014, p. 426–72.*
- [68] Swedish Gas Technology Centre: Basic data of biogas. *Phys Radiol* 2012;719–739.
- [69] Hosseini SE, Wahid MA. Development of biogas combustion in combined heat

- and power generation. *Renew Sustain Energy Rev* 2014;40:868–75.
- [70] Persson M, Jönsson O, Wellinger A. Biogas upgrading to vehicle fuel standards and grid injection. IEA Bioenergy task, vol. 37, 2006, p. 1–34.
- [71] Bauer F, Persson T, Hulteberg C, Tamm D. Biogas upgrading—technology overview, comparison and perspectives for the future. *Biofuels, Bioprod Biorefining* 2013;7:499–511.
- [72] Sun Q, Li H, Yan J, Liu L, Yu Z, Yu X. Selection of appropriate biogas upgrading technology—a review of biogas cleaning, upgrading and utilisation. *Renew Sustain Energy Rev* 2015;51:521–32.
- [73] Guo M, Song W, Buhain J. Bioenergy and biofuels: History, status, and perspective. *Renew Sustain Energy Rev* 2015;42:712–25.
- [74] Ryckebosch E, Drouillon M, Vervaeren H. Techniques for transformation of biogas to biomethane. *Biomass and Bioenergy* 2011;35:1633–45.
- [75] Huertas JI, Giraldo N, Izquierdo S. Removal of H₂S and CO₂ from Biogas by Amine Absorption. *Mass Transf Chem Eng Process* 2011;307.
- [76] Abatzoglou N, Boivin S. A review of biogas purification processes. *Biofuels, Bioprod Biorefining* 2009;3:42–71.
- [77] Yentekakis I V, Goula G. Biogas Management: Advanced Utilization for Production of Renewable Energy and Added-value Chemicals. *Front Environ*
- [78] Appels L, Baeyens J, Degrève J, Dewil R. Principles and potential of the anaerobic digestion of waste-activated sludge. *Prog Energy Combust Sci* 2008;34:755–81.
- [79] Bhardwaj S, Das P. A review: Advantages and disadvantages of biogas. *Int Res J Eng Technol* 2017;4:890–3.
- [80] Kalamaras CM, Efstathiou AM. Hydrogen production technologies: current state and future developments. *Conf. Pap. Sci.*, vol. 2013, Hindawi; 2013.
- [81] Sánchez JM, Barreiro MM, Maroño M. Bench-scale study of separation of hydrogen from gasification gases using a palladium-based membrane reactor. *Fuel* 2014;116:894–903.

- [82] Pereira CA, Coelho PM, Fernandes JF, Gomes MH. Study of an energy mix for the production of hydrogen. *Int J Hydrogen Energy* 2017;42:1375–82.
- [83] Taamallah S, Vogiatzaki K, Alzahrani FM, Mokheimer EMA, Habib MA, Ghoniem AF. Fuel flexibility, stability and emissions in premixed hydrogen-rich gas turbine combustion: Technology, fundamentals, and numerical simulations. *Appl Energy* 2015;154:1020–47.
- [84] Treloar RD. *Gas installation technology*. John Wiley & Sons; 2010.
- [85] Persson T, Baxter D. Task 37 country overview-Energy from biogas. IEA BIOENERGY 2014.
- [86] Gomez CDC. Biogas as an energy option: an overview. *Biogas Handb* 2013:1–16.
- [87] Whiston PJ, Abdel-Gayed RJ, Girgis NS, Goodwin MJ. Turbulent burning velocity of a simulated biogas combustion in a spark ignition engine. SAE Technical Paper; 1992.
- [88] Anand G, Gopinath S, Ravi MR, Kar IN, Subrahmanyam JP. Artificial neural networks for prediction of efficiency and NO_x emission of a spark ignition engine. SAE Technical Paper; 2006.
- [89] Papagiannakis RG, Zannis TC. Thermodynamic analysis of combustion and pollutants formation in a wood-gas spark-ignited heavy-duty engine. *Int J Hydrogen Energy* 2013;38:12446–64.
- [90] Chen L, Shiga S, Araki M. Combustion characteristics of an SI engine fueled with H₂–CO blended fuel and diluted by CO₂. *Int J Hydrogen Energy* 2012;37:14632–9.
- [91] Park C, Park S, Kim C, Lee S. Effects of EGR on performance of engines with spark gap projection and fueled by biogas–hydrogen blends. *Int J Hydrogen Energy* 2012;37:14640–8.
- [92] Park C, Park S, Lee Y, Kim C, Lee S, Moriyoshi Y. Performance and emission characteristics of a SI engine fueled by low calorific biogas blended with hydrogen. *Int J Hydrogen Energy* 2011;36:10080–8.

- [93] Park S, Park C, Kim C. Effect of exhaust gas recirculation on a spark ignition engine fueled with biogas-hydrogen blends. SAE Technical Paper; 2011.
- [94] Sudheesh K, Mallikarjuna JM. Diethyl ether as an ignition improver for biogas homogeneous charge compression ignition (HCCI) operation-An experimental investigation. *Energy* 2010;35:3614–22.
- [95] Swami Nathan S, Mallikarjuna JM, Ramesh A. Homogeneous charge compression ignition versus dual fuelling for utilizing biogas in compression ignition engines. *Proc Inst Mech Eng Part D J Automob Eng* 2009;223:413–22.
- [96] Mustafi NN, Raine RR. A study of the emissions of a dual fuel engine operating with alternative gaseous fuels. SAE Technical Paper; 2008.
- [97] Lounici MS, Loubar K, Tazerout M, Balistrrou M, Tarabet L. Experimental investigation on the performance and exhaust emission of biogas-diesel dual-fuel combustion in a CI engine. SAE Technical Paper; 2014.
- [98] Rasul MG, Ault C, Sajjad M. Bio-gas Mixed Fuel Micro Gas Turbine Co-Generation for Meeting Power Demand in Australian Remote Areas. *Energy Procedia* 2015;75:1065–71.
- [99] Chang C-C, Do M Van, Hsu W-L, Liu B-L, Chang C-Y, Chen Y-H, et al. A Case Study on the Electricity Generation Using a Micro Gas Turbine Fuelled by Biogas from a Sewage Treatment Plant. *Energies* 2019;12:2424.
- [100] Kaparaju P, Rintala J. 17 - Generation of heat and power from biogas for stationary applications: boilers, gas engines and turbines, combined heat and power (CHP) plants and fuel cells. In: Wellinger A, Murphy J, Baxter D, editors. *Biogas Handb.*, Woodhead Publishing; 2013, p. 404–27.
- [101] Rashwan SS. The Effect of Swirl Number and Oxidizer Composition on Combustion Characteristics of Non-Premixed Methane Flames. *Energy & Fuels* 2018;32:2517–26.
- [102] Jalalatian N, Tabejamaat S, Kashir B, EidiAttarZadeh M. An experimental study on the effect of swirl number on pollutant formation in propane bluff-body stabilized swirl diffusion flames. *Phys Fluids* 2019;31:55105.
- [103] Kotb A, Saad H. Case study for co and counter swirling domestic burners. Case

- Stud Therm Eng 2018;11:98–104.
- [104] Yılmaz I. Effect of swirl number on combustion characteristics in a natural gas diffusion flame. *J Energy Resour Technol* 2013;135.
- [105] Yang L, Ge X, Wan C, Yu F, Li Y. Progress and perspectives in converting biogas to transportation fuels. *Renew Sustain Energy Rev* 2014;40:1133–52.
- [106] Divya D, Gopinath LR, Christy PM. A review on current aspects and diverse prospects for enhancing biogas production in sustainable means. *Renew Sustain Energy Rev* 2015;42:690–9.
- [107] Combustion characteristic and heating performance of stoichiometric biogas–hydrogen–air flame. *Int J Heat Mass Transf* 2016;92:807–14.
- [108] Charest MRJ, Gülder ÖL, Groth CPT. Numerical and experimental study of soot formation in laminar diffusion flames burning simulated biogas fuels at elevated pressures. *Combust Flame* 2014;161:2678–91.
- [109] Hinton N, Stone R. Laminar burning velocity measurements of methane and carbon dioxide mixtures (biogas) over wide ranging temperatures and pressures. *Fuel* 2014;116:743–50.
- [110] Mordaunt CJ, Pierce WC. Design and preliminary results of an atmospheric-pressure model gas turbine combustor utilizing varying CO₂ doping concentration in CH₄ to emulate biogas combustion. *Fuel* 2014;124:258–68.
- [111] Fischer M, Jiang X. An investigation of the chemical kinetics of biogas combustion. *Fuel* 2015;150:711–20.
- [112] Ju Y, Masuya G, Ronney PD. Effects of radiative emission and absorption on the propagation and extinction of premixed gas flames. *Symp. Combust.*, vol. 27, Elsevier; 1998, p. 2619–26.
- [113] Lee C-E, Hwang C-H. An experimental study on the flame stability of LFG and LFG-mixed fuels. *Fuel* 2007;86:649–55.
- [114] Chao Y-C, Wu C-Y, Lee K-Y, Li Y-H, Chen R-H, Cheng T-S. Effects of dilution on blowout limits of turbulent jet flames. *Combust Sci Technol* 2004;176:1735–53.

- [115] Kalghatgi GT. Blow-Out Stability of Gaseous Jet Diffusion Flames. Part I: In Still Air. *Combust Sci Technol* 1981;26:233–9.
- [116] Karbassi M. Stability limits of non-premixed flames. Ph. D. thesis. University of Calgary, 1997.
- [117] Wilson DA, Lyons KM. Effects of dilution and co-flow on the stability of lifted non-premixed biogas-like flames. *Fuel* 2008;87:405–13.
- [118] Dai W, Qin C, Chen Z, Tong C, Liu P. Experimental studies of flame stability limits of biogas flame. *Energy Convers Manag* 2012;63:157–61.
- [119] Zhen HS, Leung CW, Cheung CS, Huang ZH. Characterization of biogas-hydrogen premixed flames using Bunsen burner. *Int J Hydrogen Energy* 2014;39:13292–9.
- [120] AVSR R. Experimental investigations on the performance of a lean burn spark ignited gas engine. Indian Institute of Technology, 2001.
- [121] Fluent A. 12.0 Theory Guide. Ansys Inc 2009;5:15.
- [122] Versteeg HK, Malalasekera W. An introduction to computational fluid dynamics: the finite volume method. Pearson education; 2007.
- [123] Peters N. Turbulent Combustion. *Meas Sci Technol* 2001;12:2022.
- [124] Benaissa S, Adouane B, Ali SM, Rashwan SS, Aouachria Z. Investigation on combustion characteristics and emissions of biogas/hydrogen blends in gas turbine combustors. *Therm Sci Eng Prog* 2022;27:101178.
- [125] Oumrani N, Aouissi M, Bounif A, Yssaad B, Tabet F, Gokalp I. A first-and second-order turbulence models in hydrogen non-premixed flame. *Int J Heat Technol* 2015;33:27–34.
- [126] Obieglo A. PDF modeling of H₂ and CH₄ chemistry in turbulent nonpremixed combustion. Eidgenössische Technische Hochschule Zürich, 2000.
- [127] Launder BE, Sandham ND. Closure strategies for turbulent and transitional flows. Cambridge University Press; 2002.
- [128] Wang L, Haworth DC, Turns SR, Modest MF. Interactions among soot, thermal radiation, and NO_x emissions in oxygen-enriched turbulent nonpremixed

- flames: a computational fluid dynamics modeling study. *Combust Flame* 2005;141:170–9.
- [129] Modest MF. Radiative heat transfer. Academic press; 2013.
- [130] Speight JG. Chapter 10 - Combustion of Hydrocarbons. In: Speight JG, editor. *Handb. Ind. Hydrocarb. Process.*, Boston: Gulf Professional Publishing; 2011, p. 355–93.
- [131] Abdel-Hadi MA. A simple apparatus for biogas quality determination. *Misr J Ag Eng* 2008;25:1055–66.
- [132] Marzouk OA, Huckaby ED. Simulation of a Swirling Gas-Particle Flow Using Different k-epsilon Models and Particle-Parcel Relationships. *Eng Lett* 2010;18.
- [133] Norwazan AR, Jaafar MNM. Studies of isothermal swirling flows with different RANS models in unconfined burner. *World Congr. Sustain. Technol., IEEE*; 2014, p. 48–53.
- [134] Gor NH, Pandya MJ. Modeling and CFD analysis of swirl can type combustion chamber. *Adv Eng Res Dev* 2015;2:204–10.
- [135] Pathan H, Partel K, Tadvi V. Numerical investigation of the combustion of methane air mixture in gas turbine can-type combustion chamber. *Int J Sci Eng Res* 2012;3:1–7.
- [136] Ghenai C. Combustion of Syngas Fuel in Gas Turbine Can Combustor. *Mech Eng* 2010;2010:13.
- [137] İlbaş M, Şahin M, Karyeyen S. 3D numerical modelling of turbulent biogas combustion in a newly generated 10 KW burner. *J Energy Inst* 2018;91:87–99.
- [138] Norwazan AR, Jaafar MNM. The Reynold's Number Effect in High Swirling Flow in Unconfined Burner. *J Teknol* 2015;72.
- [139] Wen X, Wang PC, Man SYC. Numerical study of performance of reverse flow combustor. 2016 IEEE Aerosp. Conf., IEEE; 2016, p. 1–13.
- [140] Shamami KK, Birouk M. Assessment of the performances of RANS models for simulating swirling flows in a can-combustor. *Open Aerosp Eng J* 2008;1.
- [141] Li Z, Kharoua N, Redjem H, Khezzar L. RANS and LES simulation of a swirling

- flow in a combustion chamber with different swirl intensities. Proc. CHT-12. ICHMT Int. Symp. Adv. Comput. Heat Transf., Begel House Inc.; 2012.
- [142] Smith GP, Golden DM, Frenklach M, N. W. Moriarty BE, Goldenberg M, Bowman CT, et al. GRI mech 3.0 2000.
- [143] Benaissa S, Adouane B, Ali SM, Mohammad A. Effect of hydrogen addition on the combustion characteristics of premixed biogas/hydrogen-air mixtures. Int J Hydrogen Energy 2021;46:18661–77.
- [144] Kee RJ, Rupley FM, Miller JA. Chemkin-II: A Fortran chemical kinetics package for the analysis of gas-phase chemical kinetics. Sandia National Labs., Livermore, CA (USA); 1989.
- [145] Kee RJ, Dixon-Lewis G, Warnatz J, Coltrin ME, Miller JA. A Fortran computer code package for the evaluation of gas-phase multicomponent transport properties. Sandia Natl Lab Rep SAND86-8246 1986;13:80401–1887.
- [146] Kee R, Grcar J, Smooke M, Miller J, Meeks E. PREMIX: A FORTRAN program for modeling steady laminar one-dimensional. SANDIA Natl Lab ... 1985:1–87.
- [147] Liao S, Jiang DM, Cheng Q. Determination of laminar burning velocities for natural gas. Fuel 2004;83:1247–50.
- [148] Sharma SP, Agrawal DD, Gupta CP. The pressure and temperature dependence of burning velocity in a spherical combustion bomb. Symp Combust 1981;18:493–501.
- [149] Iijima T, Takeno T. Effects of temperature and pressure on burning velocity. Combust Flame 1986;65:35–43.
- [150] Gu XJ, Haq MZ, Lawes M, Woolley R. Laminar burning velocity and Markstein lengths of methane–air mixtures. Combust Flame 2000;121:41–58.
- [151] Yu G, Law CK, Wu CK. Laminar flame speeds of hydrocarbon + air mixtures with hydrogen addition. Combust Flame 1986;Volume 63:339–47.
- [152] Akram M, Kumar S. Experimental studies on dynamics of methane-air premixed flame in meso-scale diverging channels. Combust Flame 2011;158:915–24.

- [153] Akram M, Kumar S. Measurement of laminar burning velocity of liquified petroleum gas air mixtures at elevated temperatures. *Energy and Fuels*, vol. 26, 2012, p. 3267–74.
- [154] Akram M, Saxena P, Kumar S. Laminar burning velocity of methane-air mixtures at elevated temperatures. *Energy and Fuels* 2013;27:3460–6.
- [155] Akram M, Kishore VR, Kumar S. Laminar Burning Velocity of Propane/CO₂/N₂–Air Mixtures at Elevated Temperatures. *Energy & Fuels* 2012;26:5509–18.
- [156] Koutmos P, McGuirk JJ. Isothermal flow in a gas turbine combustor—a benchmark experimental study. *Exp Fluids* 1989;7:344–54.
- [157] PRAVEEN CHU, YADAV AHK. Numerical Simulation of Gas Turbine Can Combustor Engine. *Int J Eng Res Gen Sci* 2015;3:192–201.
- [158] Shih H-Y, Liu C-R. Combustion characteristics of a can combustor with a rotating casing for an innovative micro gas turbine. *J Eng Gas Turbines Power* 2009;131:41501.
- [159] Krieger GC, Campos AP V, Takehara MDB, Da Cunha FA, Veras CAG. Numerical simulation of oxy-fuel combustion for gas turbine applications. *Appl Therm Eng* 2015;78:471–81.
- [160] Gor NH, Pandya MJ. Analysis of Can Type Combustion Chamber—A Review. *Multidiscip. Res. Pract.*, 2014, p. 423–6.
- [161] Alkabie H, McMillan R, Noden R, Morris C. Dual fuel dry low emissions (DLE) combustion system for the ABB Alstom Power 13, 4 MW cyclone gas turbine. *ASME Turbo Expo 2000 Power Land, Sea, Air, American Society of Mechanical Engineers Digital Collection*; 2000.
- [162] Andersson M, Larsson A, Carrera AM. Pentane rich fuels for standard Siemens DLE gas turbines. *Turbo Expo Power Land, Sea, Air*, vol. 54624, 2011, p. 905–16.
- [163] Ghenai C, Janajreh I. Combustion of Renewable Biogas Fuels. *Editor Board Members* 2015:831.

- [164] Ghenai C. Combustion and Emissions Performance of Syngas Fuels Derived from Palm Kernel Shell and Polyethylene (PE) Waste via Catalytic Steam Gasification. *World Acad Sci Eng Technol Int J Mech Aerospace, Ind Mechatron Manuf Eng* 2015;9:1024–30.
- [165] Candel S, Durox D, Ducruix S, Birbaud A-L, Noiray N, Schuller T. Flame dynamics and combustion noise: progress and challenges. *Int J Aeroacoustics* 2009;8:1–56.
- [166] Liu C, Liu F, Yang J, Mu Y, Hu C, Xu G. Experimental investigation of spray and combustion performances of a fuel-staged low emission combustor: effects of main swirl angle. *J Eng Gas Turbines Power* 2017;139.
- [167] Sangl J, Mayer C, Sattelmayer T. Prediction of the NO_x Emissions of a Swirl Burner in Partially and Fully Premixed Mode on the Basis of Water Channel Laser Induced Fluorescence and Particle Image Velocimetry Measurements. *J Eng Gas Turbines Power* 2014;136.
- [168] Shi L, Fu Z, Duan X, Cheng C, Shen Y, Liu B, et al. Influence of combustion system retrofit on NO_x formation characteristics in a 300 MW tangentially fired furnace. *Appl Therm Eng* 2016;98:766–77.
- [169] Vatcha SR. Low-emission gas turbines using catalytic combustion. *Energy Convers Manag* 1997;38:1327–34.
- [170] Miller JA, Bowman CT. Mechanism and modeling of nitrogen chemistry in combustion. *Prog Energy Combust Sci* 1989;15:287–338.
- [171] Naha S, Briones AM, Aggarwal SK. Effect of fuel blends on pollutant emissions in flames 2004.
- [172] Zeng W, Ma H, Liang Y, Hu E. Experimental and modeling study on effects of N₂ and CO₂ on ignition characteristics of methane/air mixture. *J Adv Res* 2015;6:189–201.
- [173] Zhang Y, Huang Z, Wei L, Zhang J, Law CK. Experimental and modeling study on ignition delays of lean mixtures of methane, hydrogen, oxygen, and argon at elevated pressures. *Combust Flame* 2012;159:918–31.
- [174] Zhang Y, Jiang X, Wei L, Zhang J, Tang C, Huang Z. Experimental and

- modeling study on auto-ignition characteristics of methane/hydrogen blends under engine relevant pressure. *Int J Hydrogen Energy* 2012;37:19168–76.
- [175] Jiang X, Pan Y, Sun W, Liu Y, Huang Z. Shock-Tube Study of the Autoignition of n-Butane/Hydrogen Mixtures. *Energy & Fuels* 2018;32:809–21.
- [176] Goswami M, Van Griensven JGH, Bastiaans RJM, Konnov AA, De Goey LPH. Experimental and modeling study of the effect of elevated pressure on lean high-hydrogen syngas flames. *Proc Combust Inst* 2015;35:655–62.
- [177] Mohammad A, Juhany KA. Laminar burning velocity and flame structure of DME/methane+ air mixtures at elevated temperatures. *Fuel* 2019;245:105–14.